5-1996

Integration of Special Sensor Microwave/Imager (SSM/I) and in Situ Data for Snow Studies from Space

Changyi Sun
Utah State University

INTEGRATION OF SPECIAL SENSOR MICROWAVE/IMAGER (SSM/I) AND IN SITU DATA FOR SNOW STUDIES FROM SPACE

by

Changyi Sun

A dissertation submitted in partial fulfillment
of the requirements for the degree

of

DOCTOR OF PHILOSOPHY

in

Watershed Science

UTAH STATE UNIVERSITY
Logan, Utah

1996

ABSTRACT

Integration of Special Sensor Microwave/Imager (SSM/I)

and In Situ Data for Snow Studies from Space

by

Changyi Sun, Doctor of Philosophy

Utah State University, 1996

Major Professors: Drs. Jeffrey J. McDonnell and Christopher M. U. Neale
Department: Forest Resources (Watershed Science Unit)

The Special Sensor Microwave/Imager (SSM/I) radiometer is a useful tool for monitoring snow conditions and estimating snow water equivalent and wetness because it is sensitive to the changes in the physical and dielectric properties of snow. Development and improvement of SSM/I snow-related algorithms is hampered generally by the lack of quantitative snow wetness data and the restriction of a fixed uniform footprint. Currently, there is a need for snow classification algorithms for terrain where forests overlie snow cover.

A field experiment was conducted to examine the relationship between snow wetness and meteorological variables. Based on the relationship, snow wetness was estimated concurrently with SSM/I local crossing time at selected footprints to develop an SSM/I snow wetness algorithm. For the improvement of existing algorithms, SSM/I observations were linked with concurrent ground-based snow data over a study area containing both sparse- and medium-vegetated regions. Unsupervised cluster analysis was applied to separate SSM/I brightness temperature (Tb) data into groups. Six typical SSM/I Tb signatures, based on cluster means of desired snow classes, were identified. An artificial neural network (ANN) classifier was designed to learn the typical Tb patterns

for land-surface snow cover classification. An ANN approximator was trained with the relations between inputs of SSM/I Tb observations and outputs of ground-based snow water equivalent and wetness.

Results indicated that snow wetness estimated from concurrent air temperature could provide the ground-based data needed for the development of SSM/I algorithms. The use of cluster means might be sufficient in ANN supervised learning for snow classification, and the ANN has the potential to be trained for retrieving different snow parameters simultaneously from SSM/I data.

It is concluded that the ANN approach may overcome the drawbacks and limitations of the existing SSM/I algorithms for land-surface snow classification and parameter estimation over varied terrain. This study demonstrated a nonlinear retrieval method towards making the inferences of snow conditions and parameters from SSM/I data over varied terrain operational.

(151 pages)

ACKNOWLEDGMENTS

I express my sincere thanks to Drs. Jeffrey McDonnell and Christopher Neale not only for accepting me as a graduate student, but also for moral and financial support during my graduate study in Watershed Science. To Drs. Robert Gunderson, Michale Jenkins, and Douglas Ramsey, I gratefully thank them for their valuable direction and suggestion on this work.

I would especially like to thank Dr. Heng-Da Cheng for encouraging me to write and publish conference papers. Special thanks also goes to Tracy Nielsen for keeping my office clean and trying not to disturb me while I was working late and sleeping on the desk.

As I worked from nothing to something and from nonsense to sense during my entire Ph.D. study, I was indebted to my friends Chihsin Chien, Shun-Li Huang, Horng-Jer Shieh, Chen-Yuan Wu, and Tzy-Tao Yang for the kind friendship, to my colleagues Xin Qiu and Georghios Vassiliades for the useful discussion of passive microwave remote sensing, and to Rashid Ahmed for the help in ARC/INFO GIS techniques.

This study was funded by the NASA WetNet project under Contract NAG8-897.

Changyi Sun

CONTENTS

LIST OF TABLES

LIST OF FIGURES

CHAPTER 1

GENERAL INTRODUCTION

Snow cover and its eventual melt are major factors controlling the hydrological response of watersheds in mid and high latitudes. Monitoring large-scale snow properties throughout the snow accumulation and melt seasons is essential for understanding regional hydrologic response and global climatic feedbacks. Conventional snow measurements are limited to point or snow course data, and do not permit examination of large-scale seasonal snowpack conditions, which is possible only by the use of remotely sensed data.

Spaceborne passive microwave radiometry is the most useful tool for regional snow property estimations because of: (1) its relative independence of atmospheric conditions such as nonprecipitating cloud cover, (2) its excellent penetration depth into the snowpack, and (3) its sensitive response to the changes in snow physical and dielectric properties.

Beginning in the mid-1970s, several spaceborne radiometers were launched for atmospheric and terrestrial measurements, including (1) the Electrically Scanning Microwave Radiometer (ESMR) instrument flown aboard U.S. satellite Nimbus-5 and Nimbus-6, (2) the Scanning Multichannel Microwave Radiometer (SMMR) on Nimbus-7, and (3) the Special Sensor Microwave/Imager (SSM/I) on the Defense Meteorological Satellite Program (DMSP) F8, F10, and F11 satellites.

Since July 1990, the National Aeronautics and Space Administration (NASA) has maintained the WetNet computer network system, providing workstations and data to science team members from NASA, the National Oceanic and Atmospheric Administration (NOAA), and the university community. The WetNet system involves the acquisition, management, and display of SSM/I satellite imagery and associated data. Using either magneto-optical (MO) disk or Internet networking, SSM/I data can be distributed to the investigator for algorithm development, verification,

intercomparison, and modification. Current SSM/I snow products are the Grody, Goodison, and DMSP Cal/Val snow cover and depth algorithms [1], [2], [3], [4].

The WetNet workstation at Utah State University (USU) is housed in the Biological and Irrigation Engineering Department. The workstation is based on an IBM PS/2 80486 personal computer. An integral part of the workstation is the Man computer Interactive Data Access System for the OS/2 operating system (McIDAS-OS2) developed at the Space Science and Engineering Center at the University of Wisconsin-Madison.

The primary tasks of the USU WetNet project are twofold: (1) improvement of land-surface-type classification algorithms and surface moisture retrieval algorithms and (2) improvement of the snow classification, snow depth, and water equivalent retrieval algorithms. This study represents accomplishments of the second task of the USU WetNet project. Research findings are presented in multiple-paper format in this dissertation.

A. Review of Literature

1) Satellite Microwave Radiometry and Its Limitation: The function of a microwave radiometer is to receive electromagnetic energy radiated by the scene under observation. A radiometer consists of an antenna for collecting the radiation incident upon it, a receiver for measuring the antenna radiometric temperature (T_A), and the microwave switches for determining the source of energy input to the receiver [5], [6].

The apparent temperature (T_{AP}) represents the upwelling radiation collected in a certain direction by the antenna main-lobe and is estimated by applying an antenna pattern correction on T_A. As illustrated in Figure 1.1, T_{AP} consists of three sources of radiation, the atmospheric upward self-emission (T_{UP}), the terrain self-emission, which is the brightness temperature (Tb), and the atmospheric downward self-emission scattered at the terrain surface (T_{SC}). In the case of a clear

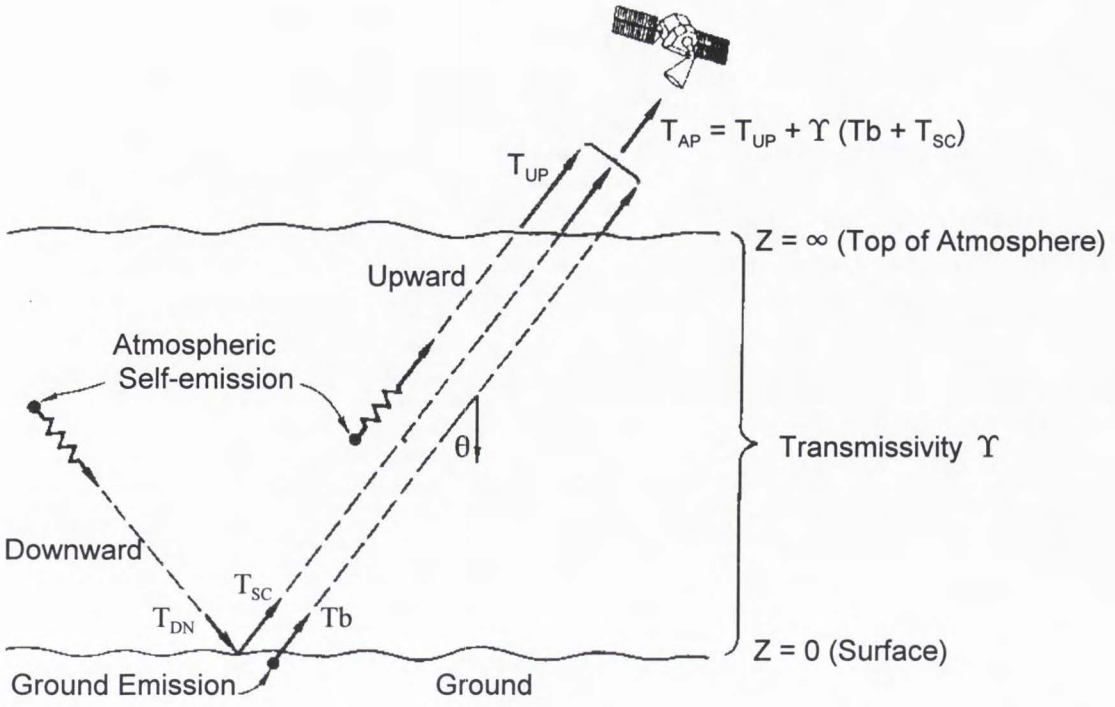

Figure 1.1. Satellite radiometer observing the earth at a nadir angle (from Ulaby *et al.* [7]).

atmosphere, T_{AP} is equal to Tb since the only contribution to T_{AP} is emission from the terrain. Under general atmospheric conditions, T_{AP} is not equal to Tb. The combination of terrain emission and scattering (Tb + T_{SC}) is attenuated in magnitude by the atmosphere between the scene and the antenna. However, T_{AP} is commonly used to describe the Tb of terrain under observation [5], [7], [8].

Polarization describes how the electric (E) field vectors of an electromagnetic (EM) wave are oriented to the plane of incidence, which is defined by the propagation direction of the wave and the normal vector to the interface (e.g., ground surface). In passive microwave radiometry, a wave is horizontally polarized if its E field vector is parallel to the ground surface and is vertically polarized if the E field vector is perpendicular to the surface. Emission and scattering by different

terrain surfaces usually are polarization-dependent. With a view angle different from 0°, vertical polarization always yields higher T_{AP}. The difference between vertical (V) and horizontal (H) polarization occurs because horizontal features of the scene tend to absorb the horizontal component of the E field. Consequently, many spaceborne radiometers have a view angle different from nadir in order to measure the effective T_{AP} difference for scene interpretation [5], [9].

The spatial resolution of a microwave radiometer is often given in terms of the instantaneous field of view (IFOV), which defines the area on the ground covered by the antenna main-lobe. Due to the limited size of current antennas and the very low levels of microwave emission from the earth-atmosphere system, radiation observed by a spaceborne radiometer with a large IFOV has been required to ensure an acceptable signal-to-noise ratio. Typically, the spatial resolution is restricted to the order of 25 to 50 km, depending on different microwave instruments and channels [5]. Although it is expected that the low spatial resolution will be improved in the near future [10], current satellite microwave radiometers already have the capability for remotely monitoring snowpack conditions with reasonable accuracy at large scales [11], [12].

2) Snowpack Properties and Microwave Response: Snowpack or snow cover, which has formed from a number of snowfalls, is defined as the mixture of ice crystals, air, impurities, and liquid water if melting [13]. From the time snow falls until snowmelt occurs, a snowpack undergoes many changes in grain size and shape, called snow metamorphism, which greatly affect the snowpack properties [14], [15].

Snow on the ground can be classified as either dry or wet depending on whether it is below or at its melting temperature [16], [17]. Dry snow is characterized by rounded or faceted crystals at small or large temperature gradient. Wet snow is characterized by clusters of grains at low liquid water content, or by poorly bounded slush at high liquid water content.

The interaction between microwave radiation and snowpack can be described by both emission and extinction process occurring simultaneously [5], [18]. The extinction, involving both volume scattering and absorption process, is governed by ice crystals and liquid water in the snow. Microwave emission at a snowpack surface consists of radiation emitted from the background surface, reduced in magnitude due to extinction by the snow volume, and the radiation emitted and scattered by the snow medium along the propagation path.

In a dry snow layer, the radiation emitted can be scattered on its way to the surface by ice crystals. Larger grain sizes permit more scattering as the grain size approaches the microwave wavelength [11]. Thus the deeper the snow the more the volume scattering, resulting in a lower microwave emission at the snow surface. When snow is wet, the liquid water held by the snow grains causes a significant increase in volume absorption and decrease in volume scattering, by which the snow medium behaves like a blackbody radiator and re-emits the energy absorbed at the surface, causing an increase in the microwave emission [19].

For a given snow layer, as shown in Figure 1.2, an increase in the microwave frequency (i.e., decrease in the microwave wavelength) results in a decrease in brightness temperature when snow is dry or refrozen, but an increase in brightness temperature for wet snow [9], [20], [21]. Thus, the microwave emission of snow is a function of snow depth, grain size, wetness, background conditions, and microwave wavelength.

3) Inversion of Radiometer Measurements: Unlike in situ methods, the passive microwave approach provides an indirect estimate by using parameter retrieval algorithms, with radiometer measurements as input data, to derive information about snow properties. In order to develop the algorithm, either empirical or theoretical interpretations of microwave observations along with ground truth data are required. In the application of the algorithm, the microwave reading is known, and the state of variables is inferred.

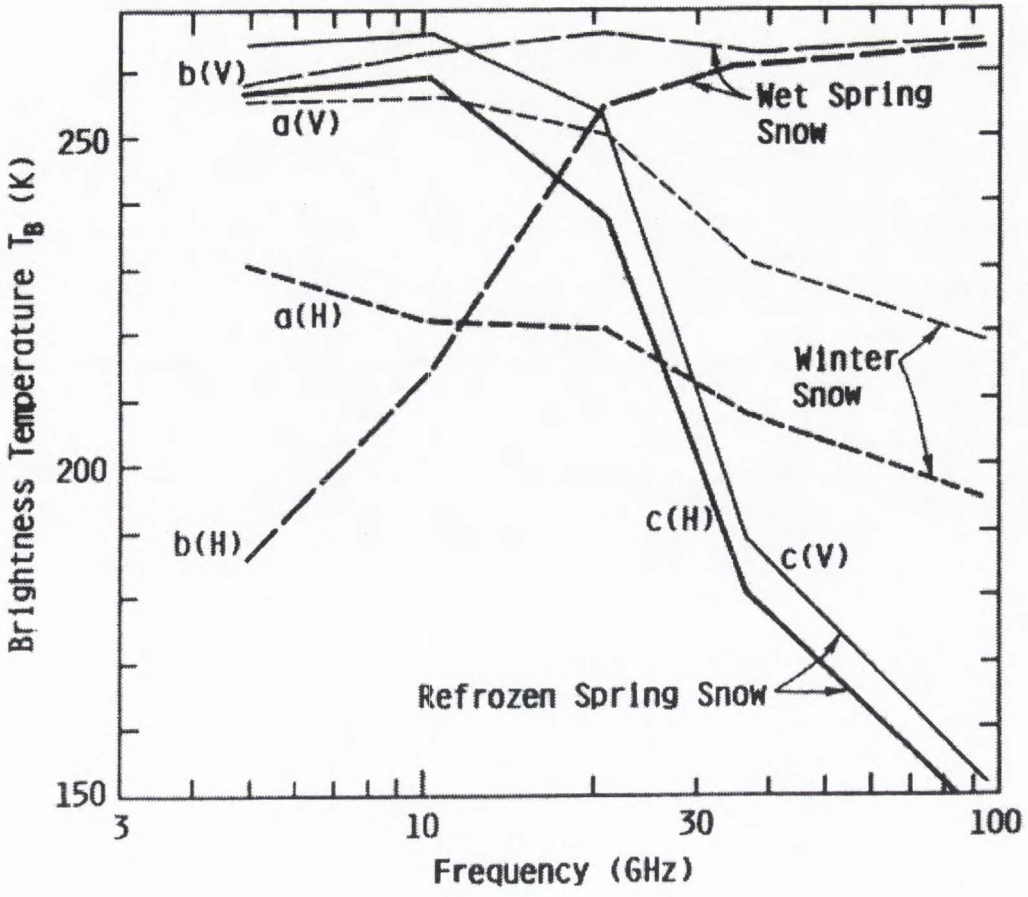

Figure 1.2. Brightness temperature of different snow conditions observed at vertical and horizontal polarization with a 50-degree nadir angle (from Schanda *et al.* [20]).

Previously, the use of passive microwave measurements to derive snow parameters has resulted from the following techniques: (1) regression analysis, (2) theoretical calculations, and (3) pattern recognition. Among these techniques, empirical linear regression analysis has been widely used to link ground truth information with microwave data; the snow retrieval algorithm is the inverted regression equation obtained.

The noncoherent and coherent approaches are the two basic methods used in theoretical calculations of emission and scattering by a surface [5]. In the noncoherent approach, emission is determined only by the surface properties of the snow medium (zero-order), or the surface of each layer in the snow medium (first-order). In the coherent approach, emission is governed by the entire profile of the snow medium.

By treating snow as a dielectric layer containing Rayleigh scatterers, radiative transfer theory has been used extensively for modeling the emission of snow-covered ground [22], [23], [24]. The model parameters used in the theory include the optical thickness of the layer, and the albedo of the snow medium. At a given frequency, the necessary input parameters to specify optical thickness and albedo for dry snow are the snow density, grain size, and the physical temperature of the snow; for wet snow, the snow wetness is also needed [7]. Once a radiative transfer model (RTM) is validated by comparing the simulated data with radiometer measurements for a variety of surface types, it can be inverted to extract the information about snow parameters from known microwave readings over typical spatial footprints.

Since the situations of snow cover are typically complex, there are too many unknown radiative physical parameters that need to be determined by arbitrary assumptions in a RTM. Therefore, it is often helpful to handle this complex problem only with pattern classification techniques [25]. One method is cluster analysis, which classifies passive microwave observations into physically significant categories. Recently, artificial neural networks (ANNs) have been used to classify snow cover from passive microwave data [26], [27], [28]. Studies have indicated that an ANN has the capability to learn complex patterns with no assumptions about the nature of the distribution of the pattern data [29], and performs as well as or better than other classification techniques [28].

4) Satellite Observations of Snow Parameters: The basic hydrologic description of a snowpack is snow water equivalent, which is the amount of water that would be obtained if a column of snow were completely melted. Thus, in order to determine the available water volume in a snow-covered region, measurements of snow extent, depth, and density are essential. In addition, measurements of snow wetness, in terms of percent of free water by volume, can improve estimation of the timing of runoff during the snowmelt period [21], [30]. Significant results and findings of past studies in passive remote sensing of snow properties are briefly summarized below.

a) Snow extent and classification: After the launch of SMMR on Nimbus-7 in 1978 and that of the SSM/I on DMSP-F8 in 1987, the capability of spaceborne radiometers for snow mapping was improved by the use of multichannel radiometer measurements. Using the horizontally polarized brightness temperature from both 37 and 18 GHz SMMR channels, Kunzi *et al.* [12] found a discriminant function with an empirically determined threshold value by which they were able to define the dry snow layer above 5 cm.

Based on statistical analysis of SSM/I data, Neale *et al.* [31] and McFarland and Neale [32] used the NASA CLIPS expert system to develop a land-surface-type classification scheme by which the dry, wet, and refrozen conditions of snow over land could be determined. Fiore Jr. and Grody [2] developed a decision-tree algorithm, using three channels (19V, 22V, and 85V) of data from the SSM/I, for the global classification of snow cover and precipitation over large regions. Lure *et al.* [27], on the other hand, used an ANN approach to classify snow cover and precipitation from SSM/I with some success.

b) Snow depth and water equivalent: For dry snow, most investigations on the determination of snow depth (SD) or snow water equivalent (SWE) have focused on the 37 GHz due to relatively more scattering at that frequency as the wave travels through the snowpack. An inverse relationship (Figure 1.3) is usually found between 37 GHz brightness temperature and SD or SWE

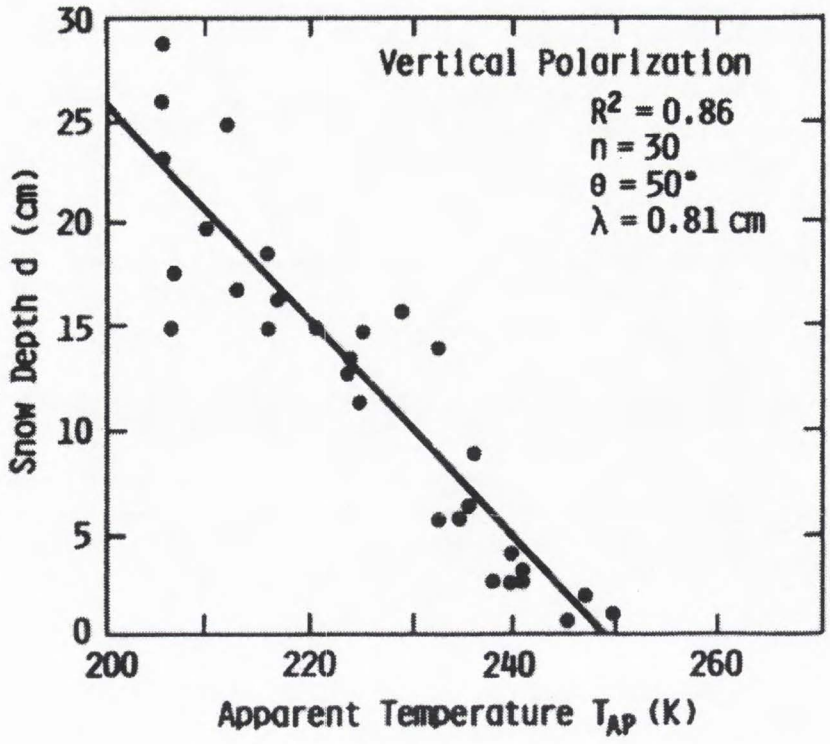

Figure 1.3. Apparent temperature versus snow depth measured at vertical polarization of 37 GHz by Nimbus-6 ESMR (from Rango *et al.* [11]).

[11], [32], [33]. However, Schanda *et al.* [20], in the study of SWE in a winter alpine snowpack, observed a weaker increase of the brightness temperature when SWE ≥ 20 cm (Figure 1.4).

In order to resolve the ambiguity in retrieval algorithms when SWE ≥ 20 cm, the use of multichannel observations has been recommended [7]. Rango *et al.* [34] found a positive linear relationship ($R^2 = 0.78$) between the difference in brightness temperature at two SMMR channels (18 and 37 GHz) and the average SWE in a mountain basin. Kunzi *et al.* [12] evaluated seven different SD or SWE retrieval algorithms for different SMMR channels and combinations of channels; they concluded that the most significant relationship was obtained between the SD/SWE and the difference in brightness temperature at 18 and 37 GHz.

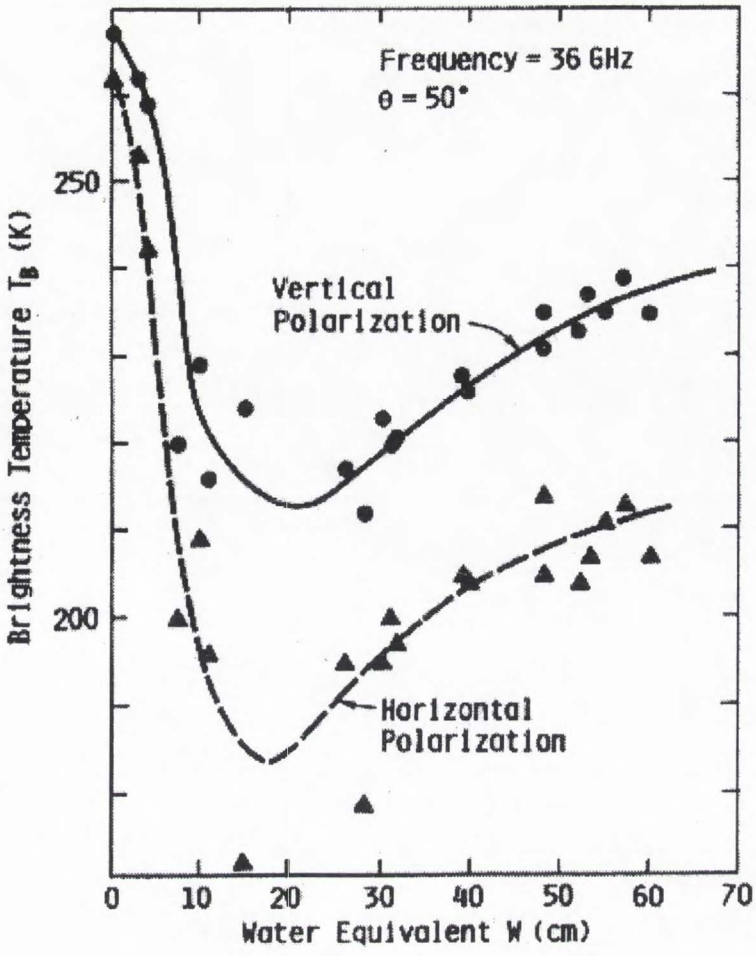

Figure 1.4. Brightness temperature measurements as a function of snow water equivalent of winter snow (from Schanda *et al.* [20]).

For wet snow, Chang *et al.* [35] found that the deeper the SD, the higher the brightness temperature. McFarland *et al.* [36] reported that brightness temperature at SMMR 37 GHz channel increased rapidly with pronounced decreases in SD during the ripening and melting period. Moreover, McFarland *et al.* [36] observed that the polarization difference for the SMMR 18 and 37 GHz brightness temperatures varied significantly, but in general decreased with decreasing in SD.

Chang and Tsang [28] used a backpropagation learning algorithm to train a multiple layered neural network with simulated data generated by a RTM, and used SSM/I brightness temperatures as input to retrieve SWE after the neural network was trained. They found that neural networks were better for SWE estimates in the low (12 cm) and high (> 32 cm) SWE range, while regression methods seemed to perform better in the mid (18 to 24 cm) range.

c) Snow wetness and onset of melt: Generally, brightness temperatures at frequencies above 10 GHz increase rapidly with increasing wetness (up to 4% by volume), which is especially observable at 37 GHz [6], [37]. Figure 1.5 shows that the brightness temperature to snow wetness

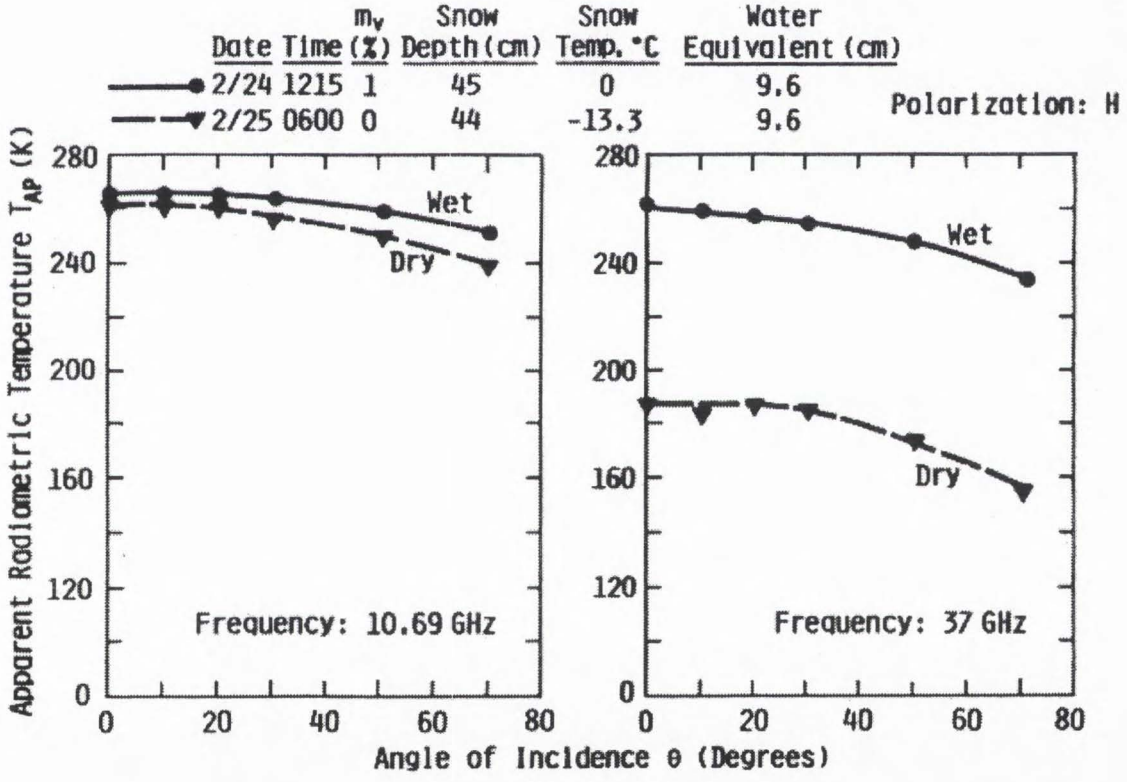

Figure 1.5. Angular response of brightness temperature at 10.69 GHz and 37 GHz to wet and dry snow (from Stiles and Ulaby [37]).

variation is almost insensitive at 10.69 GHz. In contrast, the presence of a 1% of liquid water results in a change of 70°K in brightness temperature at 37 GHz (Figure 1.5).

Prior to melting, a snowpack usually undergoes several wetting and freezing cycles, which result in large fluctuations in microwave brightness temperature. Therefore, temporal analysis of passive microwave observations is the key to the detection of the onset of snowmelt [7].

Kunzi *et al.* [12] identified the onset of snowmelt for individual footprints by checking the frequency gradient (GT) of the brightness temperature between 18 and 37 GHz SMMR channels. Areas showing a change of GT from negative values (dry snow condition) to about zero (wet snow condition) at least once in three consecutive days of satellite overpass were marked snowmelt areas. Armstrong and Hardman [38] interpreted a melting snow surface by monitoring the 37 GHz brightness temperature when values increase by more than 5-10 K between successive SSM/I passes over the same location on the ground.

5) The SSM/I Instruments: The SSM/I is a seven-channel, four-frequency, linearly polarized, passive microwave radiometric system [8], [39]. It is flown on a DMSP Block 5D-2 satellite in a circular sun-synchronous near-polar orbit at an altitude of 833 km (Figure 1.6). The orbit produces 14.1 full orbit revolutions per day and has two local observation times (ascending and descending observations). The scan direction is from the left to the right with the active scene measurements lying ±51.2° about the aft direction, resulting in a swath width of 1400 km (Figure 1.7). The scan angle from nadir is 45.0°, and the incidence angle from nadir is 53.1°.

The SSM/I receives both vertically and horizontally linearly polarized radiations at 19.35, 37.0, and 85.5 GHz and vertical only at 22.235 GHz (Table 1-I) [8], [39]. Radiometer data are sampled over each A- or B-scan, alternately. On each A- or B-scan, 128 uniformly spaced samples of the 85.5 GHz scene data are taken over the 102.4° scan sector. Radiometer data at the remaining frequencies are sampled only on A-scan, with 64 samples over the scan sector.

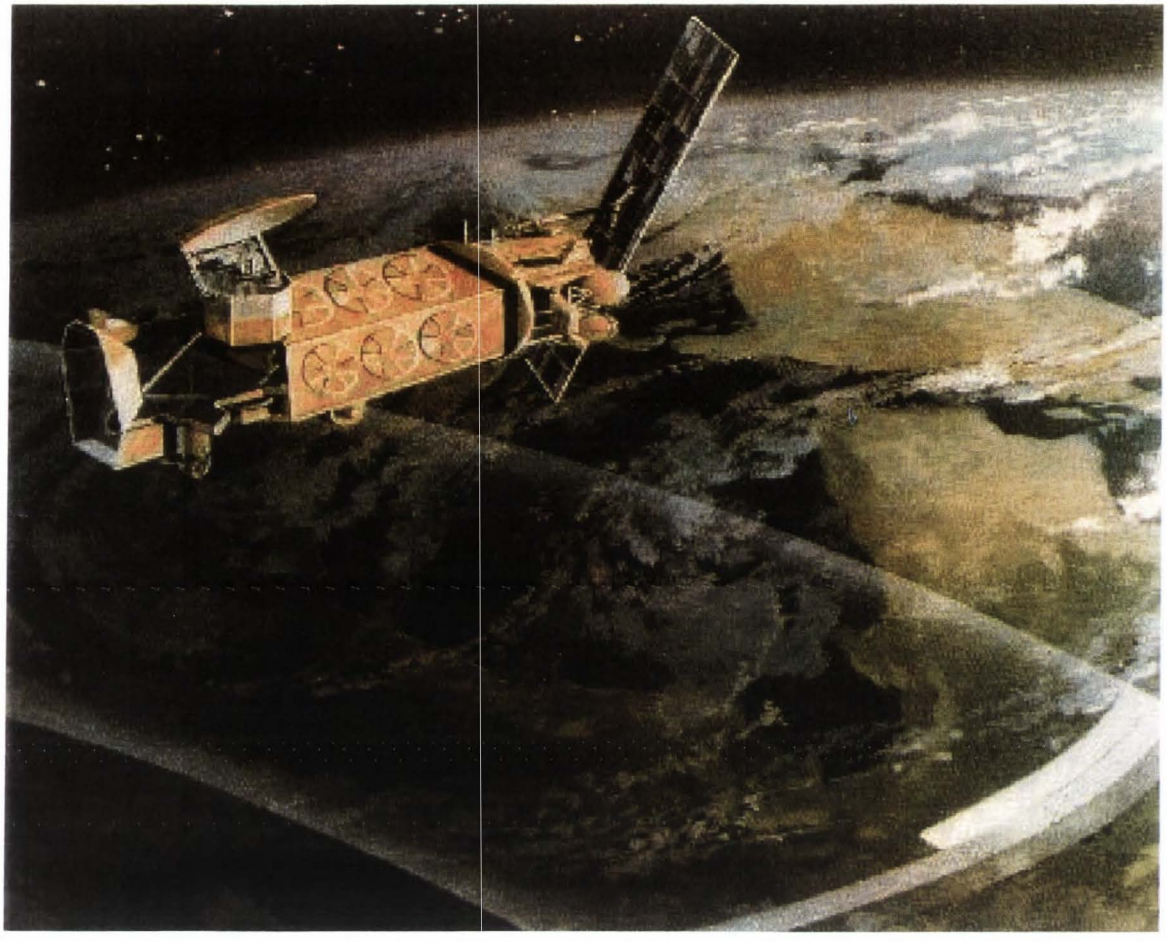

Figure 1.6. Defense Meteorological Satellite Program (DMSP) block 5D-2 satellite with the SSM/I located at the upper left (from Hollinger *et al.* [39]).

TABLE 1-1
SUMMARY OF SSM/I CHANNEL CHARACTERISTICS

Channel	Frequency (GHz)	Polarization	Footprint size (km)
19V	19.35	Vertical	69X43
19H	19.35	Horizontal	69X43
22V	22.235	Vertical	60X40
37V	37.0	Vertical	37X29
37H	37.0	Horizontal	37X29
85V	85.5	Vertical	15X13
85H	85.5	Horizontal	15X13

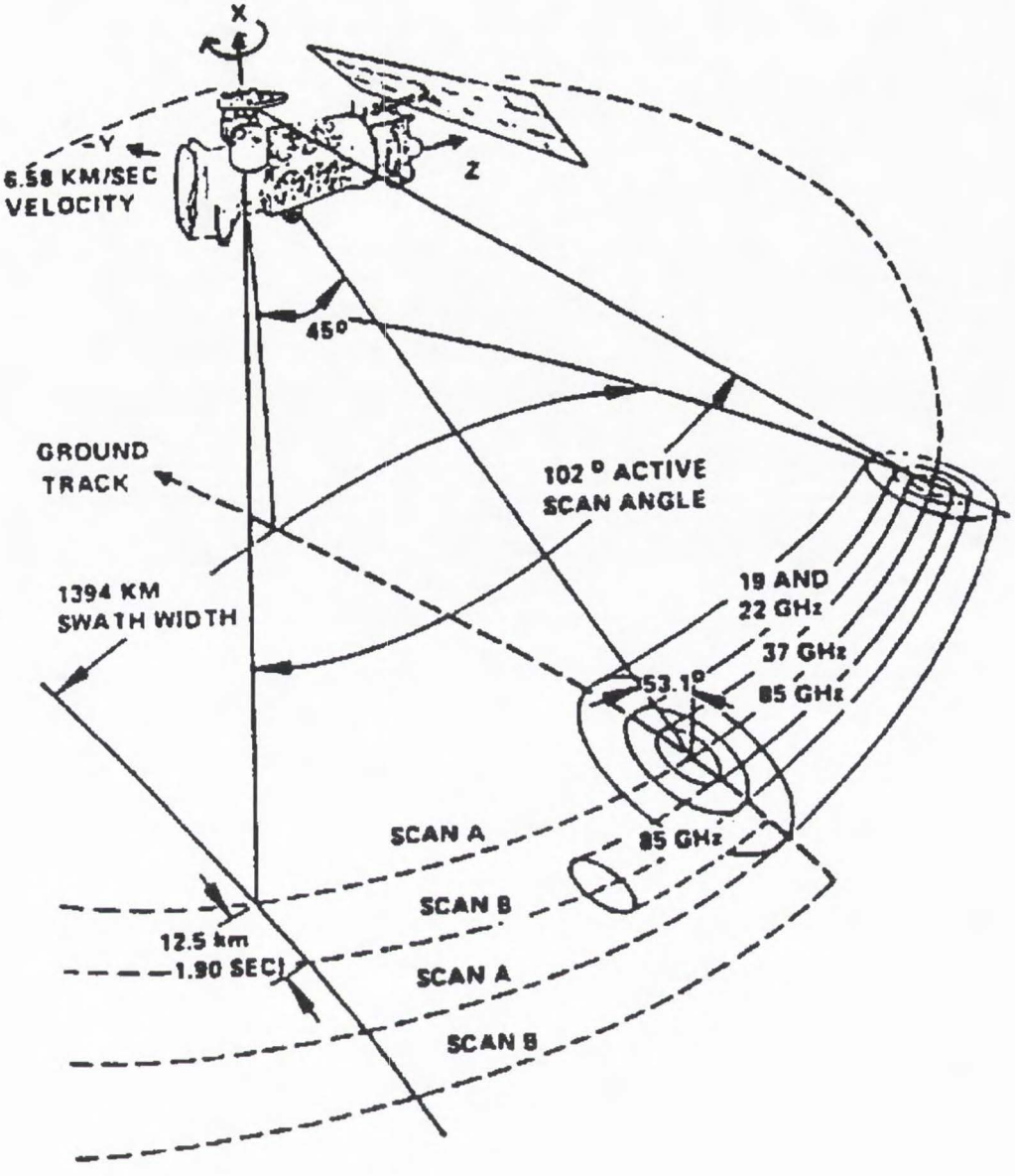

Figure 1.7. SSM/I scan geometry (from Hollinger [8]).

To date, four of the seven SSM/I radiometers have been launched aboard DMSP F8, F10, F11, and F12 satellite in 1987, 1990, 1991, and 1995, respectively. However, the SSM/I on F8 has problems with 85 GHz and that on F12 failed to operate.

B. The Problem and Its Solution

The purpose of this research is to improve existing SSM/I snow retrieval algorithms and develop new algorithms in order to characterize snow properties for varied terrain. Certain problems and their solutions with respect to the accomplishment of the objectives were as follows.

1) The Lack of Quantitative Snow Wetness: From the papers reviewed, it is clear that ground truth information plays an important role in interpreting passive microwave measurements. In order to interpret data more accurately, as indicated by Hall *et al.* [40], a quantitative history and accounting of snow accumulation and metamorphosis must be undertaken, and data must be analyzed in the context of climatological conditions. Nevertheless, the lack of extensive and reliable snow wetness data to provide ground truth information has always been a problem in the development of SSM/I snow wetness algorithms.

It is well known that the snowmelt process is influenced by meteorological variables such as air temperature, solar radiation, vapor pressure, and wind [41]. Among these variables, air temperature and solar radiation data are generally available. However, no empirical relations have been developed for snow wetness estimation directly from the meteorological parameters. Thus, a field experiment with continuous measurements of snow wetness and climatological conditions at corresponding SSM/I footprints would enable the establishment of a relationship between snow wetness and meteorological variables. Consequently, the extensive snow wetness data needed for the development of an SSM/I snow wetness algorithm can be estimated.

2) Objective 1: To develop a snow wetness retrieval algorithm based on field measurements.

3) Task 1: Conduct a field experiment in an area corresponding to an SSM/I footprint with flat nonforested terrain to obtain extensive simultaneous measurements of snow wetness and meteorological variables required for algorithm development. Field data are used to (1) model the snow wetness as a function of the correlated meteorological variables and (2) define the relationship

between the snow wetness estimated from meteorological variables and the concurrent SSM/I brightness temperatures observed at the footprint.

4) The Restriction of Fixed Uniform Footprint and the Effect of Vegation: According to Farrar and Smith [42], the use of SSM/I measurements is impeded by the fact that different phenomena are being sampled by different channels, which results in differing spatial resolutions (footprints) of the scene as observed (Figure 1.8). Therefore, a uniform footprint is desired for multichannel data applications. Because the distance between concentric A-scan footprints is on the order of 1/4° (about 27 km) at midlatitudes, most of the time only one concentric SSM/I footprint was placed in each fixed quarter degree latitude/longitude cell (1/4° box). The 1/4° box has been used as the uniform footprint in SSM/I data applications [31], [43], [44]. In this way, the corresponding ground-based data needed for the development of algorithms are also taken from each 1/4° box. Nevertheless, the geolocations of SSM/I footprints vary with each overpass. The use of a fixed uniform footprint may contribute additional SSM/I geolocation errors, which impose difficulties in the calibration and validation of algorithms.

Accordingly, a new sampling scheme that uses a neighborhood merging method to integrate the multisource data into one database is needed. The merged database could be built by searching the ground truth point or pixel data, either from weather stations or other satellites, which fall within a certain search radius around a particular SSM/I latitude/longitude coordinate. Values of each variable would be averaged to represent the SSM/I footprint. In this way, SSM/I brightness temperatures and ground truth information could be organized thematically as a multisource database for a region of interest. The database can be then analyzed based on the available data at the same SSM/I latitude/longitude coordinates. Thus, the accuracy in retrieving snow parameters from SSM/I algorithms developed from this database could be greatly improved.

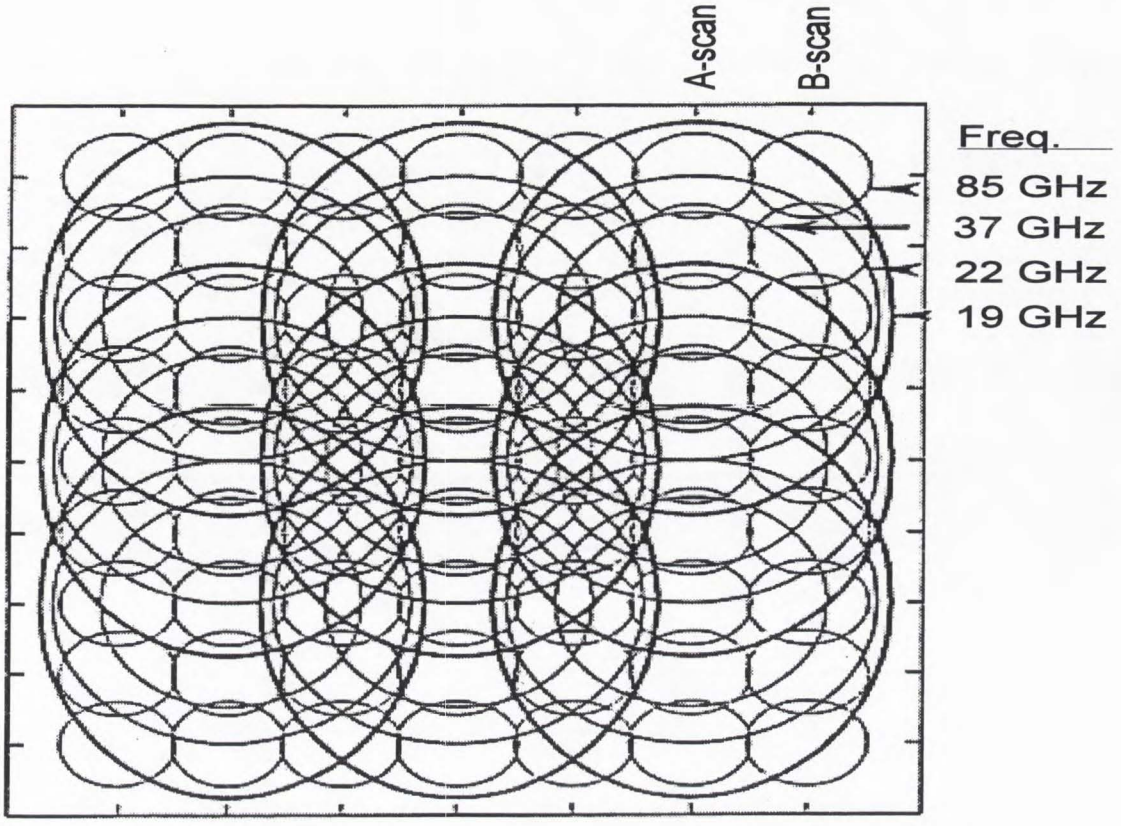

Figure 1.8. Ground footprints overlap of the four SSM/I frequencies (from Farrar and Smith [42]).

Since snow accumulation and melt are different in vegetated and nonvegetated areas, and because vegetation overlying snow affects the passive microwave response of snow, brightness temperatures together with vegetation index could explain most of the variances observed in snow over varied terrain [44]. During the past decade, the normalized difference vegetation index (NDVI) derived from NOAA Advanced Very High Resolution Radiometer (AVHRR) data has been widely used to characterize the seasonal vegetation condition over particular regions [45]. Consequently, a priori knowledge of vegetation cover using NDVI for SSM/I footprints of interest should increase the accuracy in retrieval snow parameters, especially at locations where both evergreen forests and

snow cover are present.

5) Objective 2: To develop a multisource database based on dynamic SSM/I footprint geolocations.

6) Task 2: Integrate Soil Conservation Service (SCS) SNOTEL, NOAA climatic, and NOAA NDVI data with SSM/I brightness temperatures over a large region to develop the multisource database, which is established by using the neighborhood merging method to search the ground truth data that fall within a particular SSM/I footprint.

7) The Need of Robust Snow Classification Algorithms: Previous SSM/I algorithms, such as the land-surface-type classification scheme [31], [32], are based on empirical regression analysis of SSM/I data from major surface types over plains. However, in snow classification, these rules are restricted to land surfaces with uniform snow conditions. Where evergreen forests overlay snowpack, the developed algorithms may mis-identify those forested snow covers with areas of snow-free conditions. As indicated by Hall *et al.* [40], vegetation, especially coniferous trees, tends to raise the microwave brightness temperature, and a dense canopy of trees will mask the microwave emission from the snow below the trees. In such complex situations, empirical regression is unsuitable because there are too many unknown characterizing parameters that makes the problem extremely nonlinear. Consequently, there exists a need for nonlinear retrieval methods to develop a robust snow classification algorithm by which different snow conditions over varied terrain can be determined simultaneously.

According to Staelin [24], the most complex problem can be handled with pattern recognition techniques. Studies have shown that clustering analysis can be used to identify significant passive microwave signatures [25] and that artificial neural networks have potential to learn brightness temperature patterns [46], [47]. Thus, an ANN learned from the significant SSM/I brightness temperature patterns identified by the cluster analysis would be able to improve the snow

classification retrieval accuracy.

8) Objective 3: To improve the existing snow classification scheme using cluster analysis and neural networks.

9) Task 3: Use a cluster analysis to identify the physical significance of clusters in the database developed in Task 2, and prepare the training and test data sets according to the identified clusters to train an artificial neural network, which is able to classify land-surface snow conditions over varied terrain.

10) The Need of Unified Snow Parameter Processing Algorithms: As indicated in [48], with the availability of the multispectral sensor systems on remote-sensing satellites, there exists an opportunity to develop unified processing algorithms in which many geophysical variables could be determined simultaneously. According to [49], the artificial neural network can be regarded as a graphic notation for a large class of algorithms or a function represented by the composition of many basic functions. Studies in [26], [50], using an ANN to invert snow parameters simultaneously from Tb measurements, have shown how a unified SSM/I snow parameters processing algorithm can be developed by the neural network approach.

In previous studies, however, the neural network was trained with simulated data generated by the radiative transfer models (RTMs). Since the situations of snow are typically complex, there are many unknown radiative physics that need to be determined by arbitrary assumptions in a RTM. Although an ANN can learn from the simulated data, its behavior under real situations often remains unknown.

According to [29], the neural network approach is suitable for multichannel data fusion. Consequently, an ANN trained with a priori knowledge of NDVI and Tb patterns and corresponding ground truth of snow parameters in different snow conditions should be able to estimate snow parameters under all terrain and snow conditions from SSM/I footprints of interest.

11) Objective 4: To develop a unified snow parameter processing algorithm using neural networks.

12) Task 4: Use the capability of the developed SSM/I ANN snow classifier in Task 3 to classify snow conditions from SSM/I Tb's in the database, and relate the ground truth snow wetness and water equivalent to the corresponding SSM/I Tb of all classified snow conditions to form a training and test data sets. An ANN approximator, which is able to estimate snow wetness and water equivalent under all snow conditions, was developed by learning from the mapping of the inputs of SSM/I Tb's to the outputs of snow wetness and water equivalent in training data.

C. General Methodology

Figures 1.9 and 1.10 illustrate the flowchart for SSM/I snow wetness algorithm development using regression analysis and that for SSM/I snow classification using pattern recognition, respectively. Key elements of the methodology are described in the subsections.

1) Field Site and Study Area Determination: Three ground-based seasonally snow-covered field sites located in Snowville (41.97°N/112.95°W with an elevation of 1300 m), Logan (41.73°N/111.82°W with an elevation of 1400 m), and Tony Grove (41.88°N/111.57°W with an elevation of 1920 m), Utah were selected for the study of snow wetness (Figure 1.11).

The Logan site was the most accessible from Utah State University for extensive snow wetness measurement; therefore, this site was used primarily to define the relationship between snow wetness and meteorological data. The Snowville field site had both flat, nonforested topography and homogeneous snow distribution; this site was used to link snow wetness with corresponding SSM/I observations for the development of a SSM/I snow wetness retrieval algorithm. The Tony Grove field site represented the complex mountainous terrain; this site was used to check the performance of the derived SSM/I snow wetness retrieval algorithm in mountainous terrain.

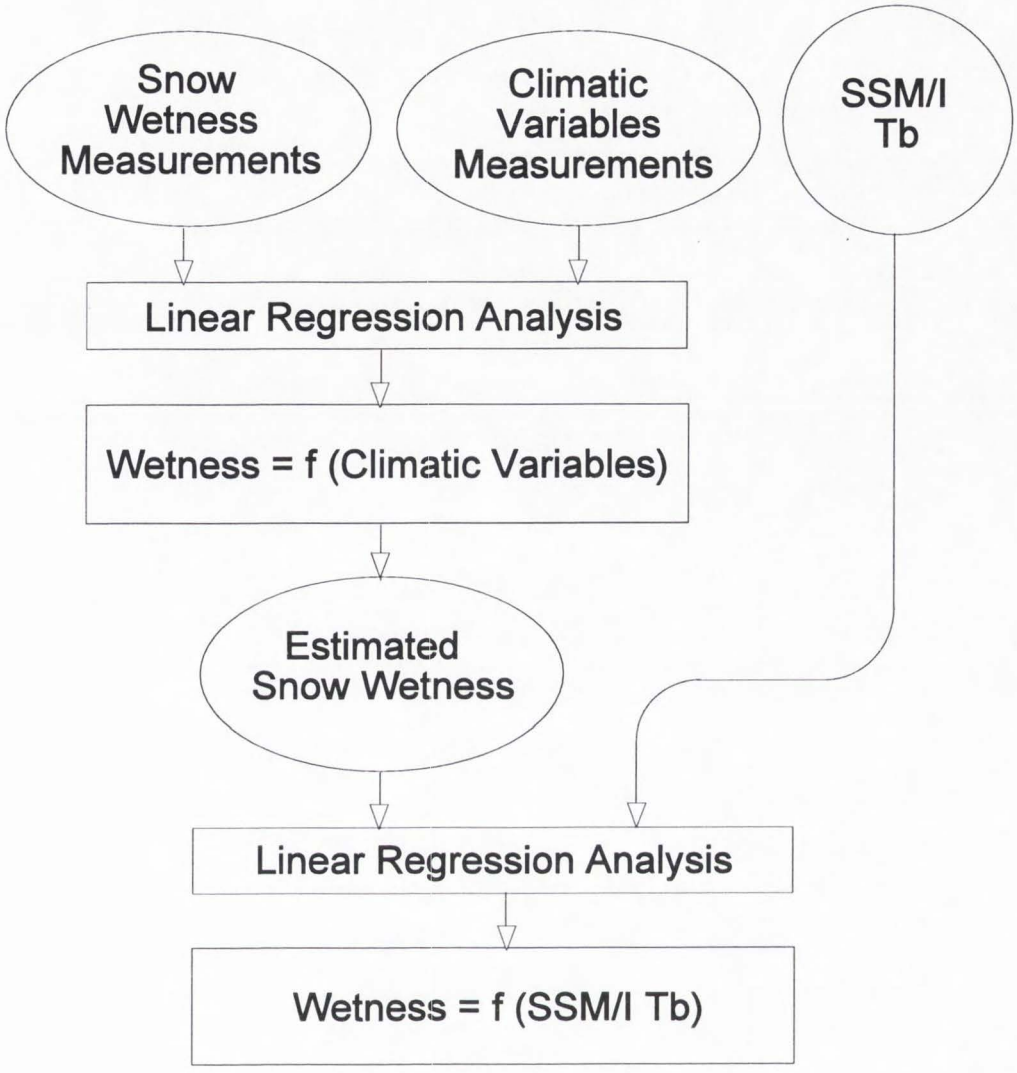

Figure 1.9. Flow chart of the design of the development of SSM/I snow wetness algorithm.

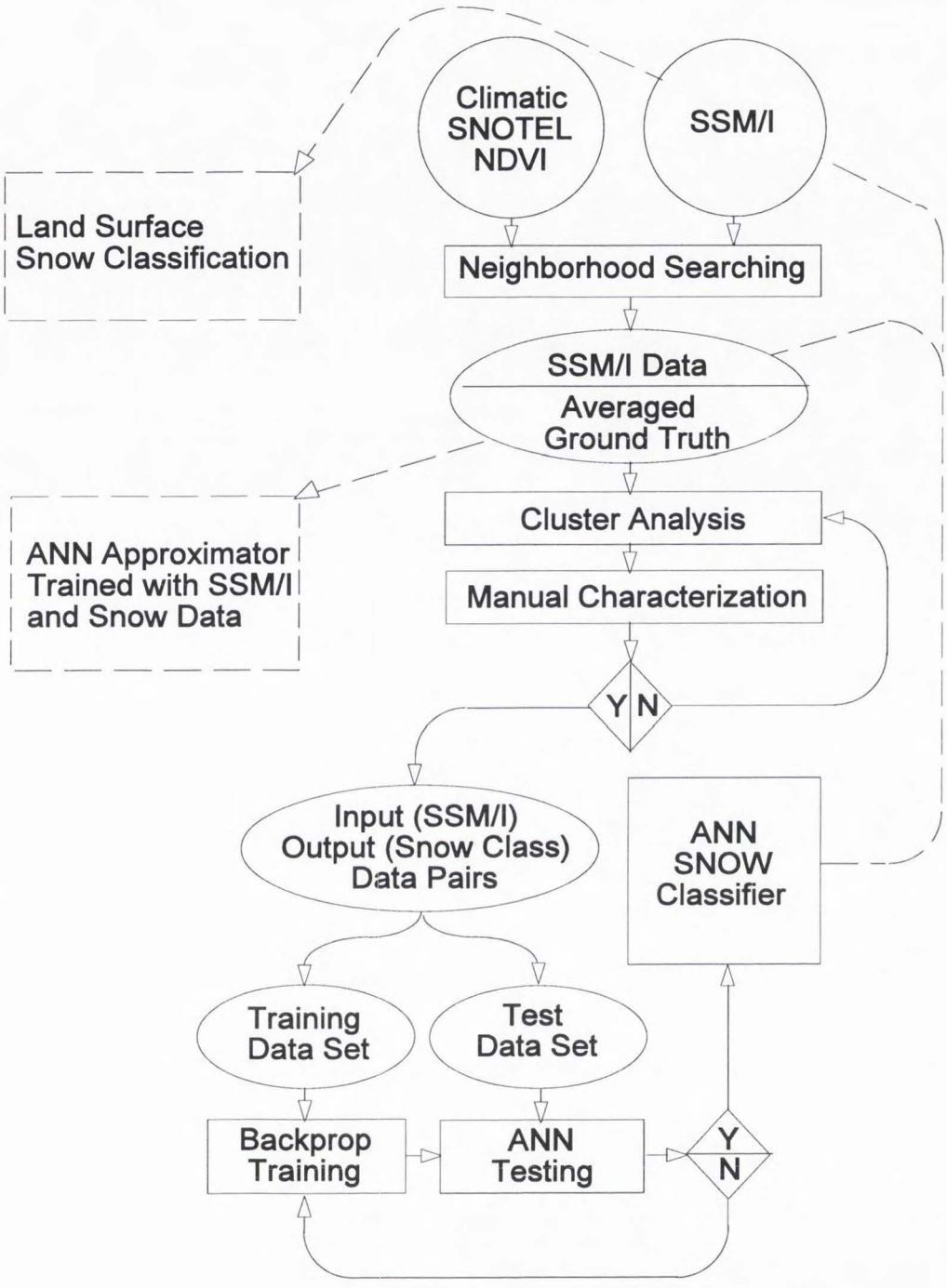

Figure 1.10. Flow chart of the design of the development of SSM/I snow classification and parameter retrieval algorithm using artificial neural networks.

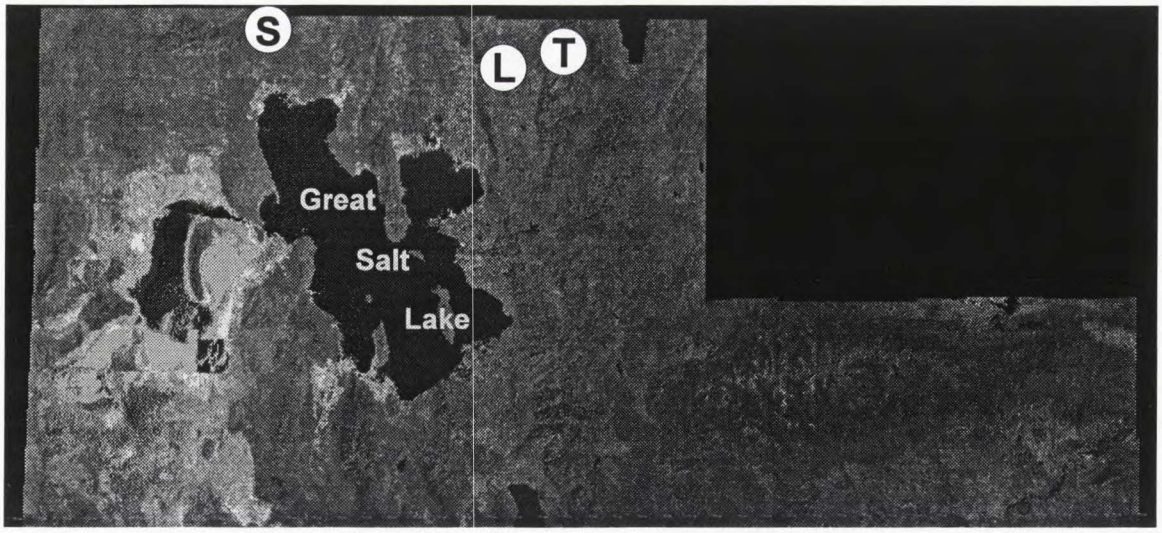

Figure 1.11. Locations of three selected field sites in northern Utah (S – Snowville site; L – Logan site; T – Tony Grove site).

A study area bounded by latitude of 40°N to 45°N and longitude of 100°W to 115°W longitude was selected (Figure 1.12). This area includes both plains and mountain regions for different representative terrains in the western United States. Six hundred seven stations (191 from SCS SNOTEL system and 416 from NOAA climatic network) of the weather data acquisition networks are located in the study area to provide the ground truth information. SSM/I data observed in this area were combined with in situ data to develop the multisource database used for the subsequent study.

2) SSM/I Data Acquisition: a) The Naval Research Laboratory: DMSP-F8 SSM/I data were obtained from the Naval Research Laboratory (NRL) on optical disks in data exchange format (DEF). SSM/I Tb's within the study area were downloaded to disk file using software supplied by NRL for the VAX VMS operation system. The data were then submitted to a set of computer programs that removed header records and prepared the data for the integration with ground truth data (Figure 1.10).

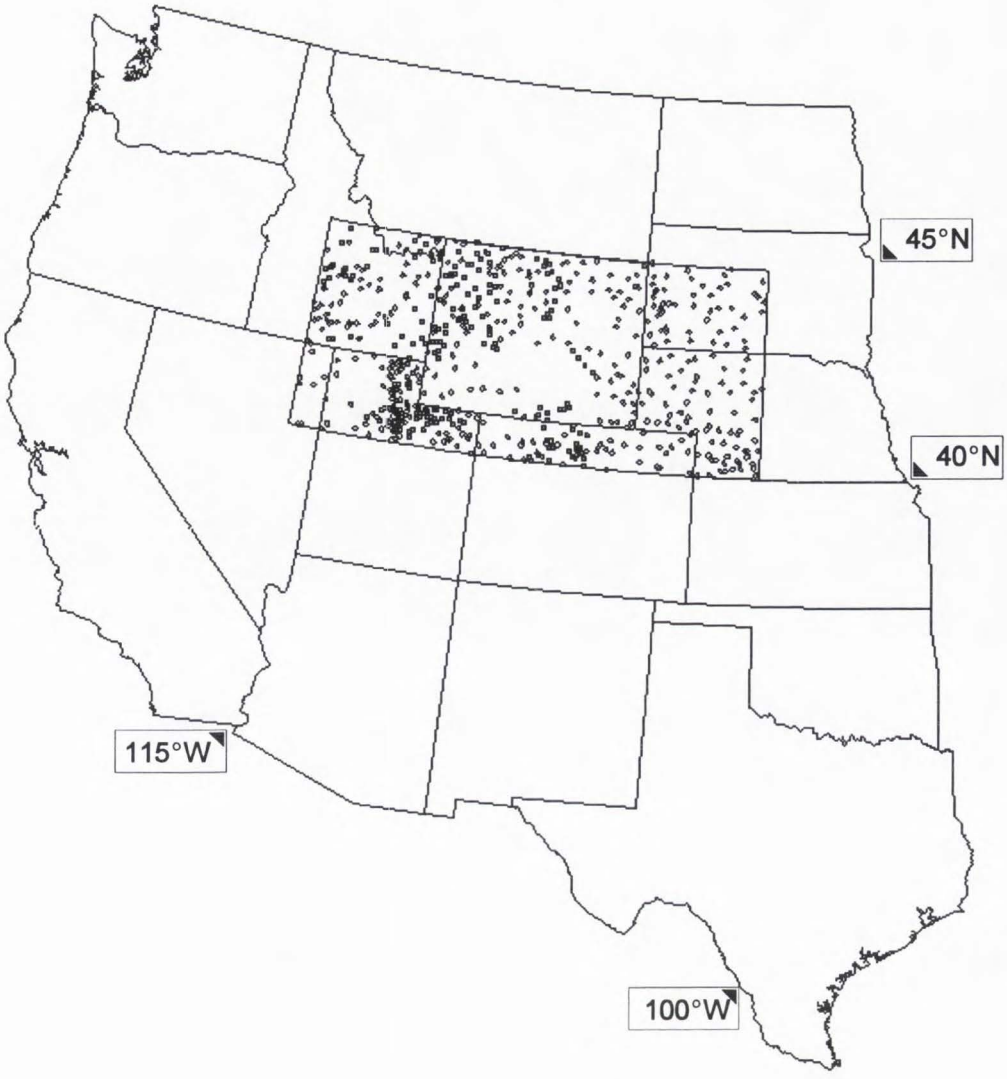

Figure 1.12. Boundary of the study area in western United States and the ground truth weather stations within the area.

b) The USU WetNet station: DMSP-F11 SSM/I data were derived from WetNet computer system [51] at Utah State University, which is maintained by NASA for the acquisition, management, and display of SSM/I satellite imagery and associated data. The integral part of the system is the Man computer Interactive Data Access System (McIDAS) for the OS/2 operating system. Each 14-day-period WetNet database, which contains the browse (reduced resolution) and the full resolution data,

is placed onto magneto-optical disk and mailed to WetNet users. An overnight broadcast of the browse products was retrieved through the Internet networking distribution.

Under the WetNet environment, SSM/I data can be accessed through McIDAS either by selecting from a menu, or by typing commands, or both. With the menu mode of the WetNet system, SSM/I data, separated by different frequency and polarization, are transferred as seven graphic frames, which can be viewed on the screen one frame at a time.

SSM/I Tb's observed at the corresponding browse and full resolution footprints during the field experiment or within the study area were downloaded from the database.

3) Field Measurements: Data were collected between Mar. 8 and Mar. 19, 1993 at the Snowville site, between Feb. 18 and Feb. 25, 1994 at the Logan site, and between Mar. 6 and Mar. 20, 1994 at the Tony Grove site. An automatic climatological data recording system, mounted on a tripod (e.g., Figure 1.13), was set up at each site. Net radiation (W/m^2) and air temperature (°C) were measured at 1.5 m above snow surface using a net radiometer (Radiation Energy Balance System,model Q-6) and temperature probe (Campbell Scientific, Model HMP35C), respectively. Data were recorded at 10-minute intervals in a datalogger (Campbell Scientific, type 21X). In addition, net radiation (JK/m^2) at the base of 24, 12, and 6 hours before snow sampling, and minimum, maximum, and average air temperatures within 24 hours prior to field measurement were also determined.

Snow parameters were sampled based on irregular time intervals during daytime. At each time when the snow was sampled, one randomly selected snow pit (e.g., Figure 1.14) was dug at each site. Snow density, and wetness at 10 cm intervals through the snow profile were measured. Snow density (g/cm^3) was obtained with the Strong Stitch Snow Density Gage. With the snow density data as input, a dielectric probe, made by LEAS Inc. in France, was used for quickly measuring snow liquid water content in percent (%) by volume.

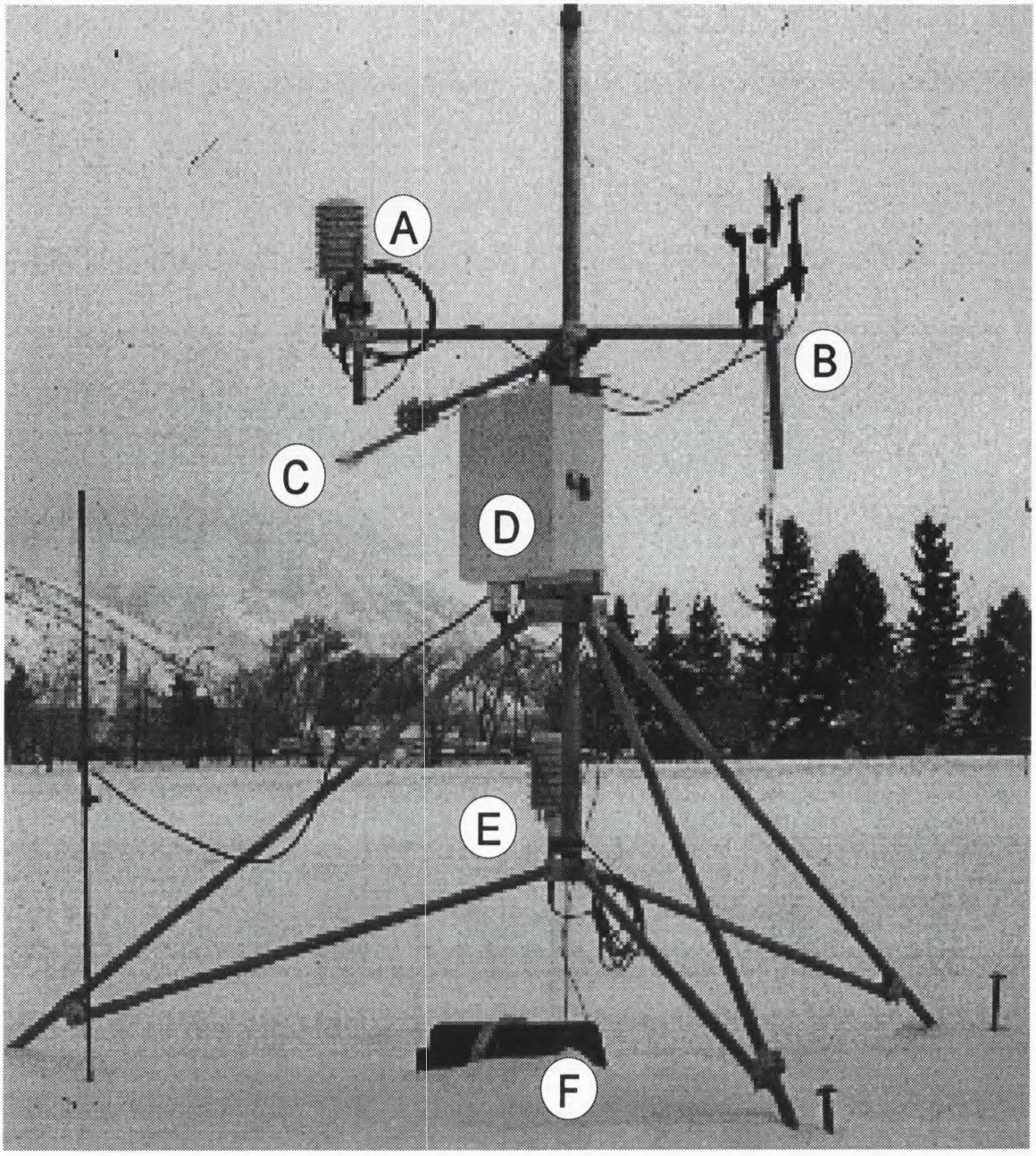

Figure 1.13. The weather station set up at the Logan site (A,E – temperature probe at different height; B – anemometer; C – net radiometer; D – enclosure with 21X datalogger for data recording; F – enclusure with battery).

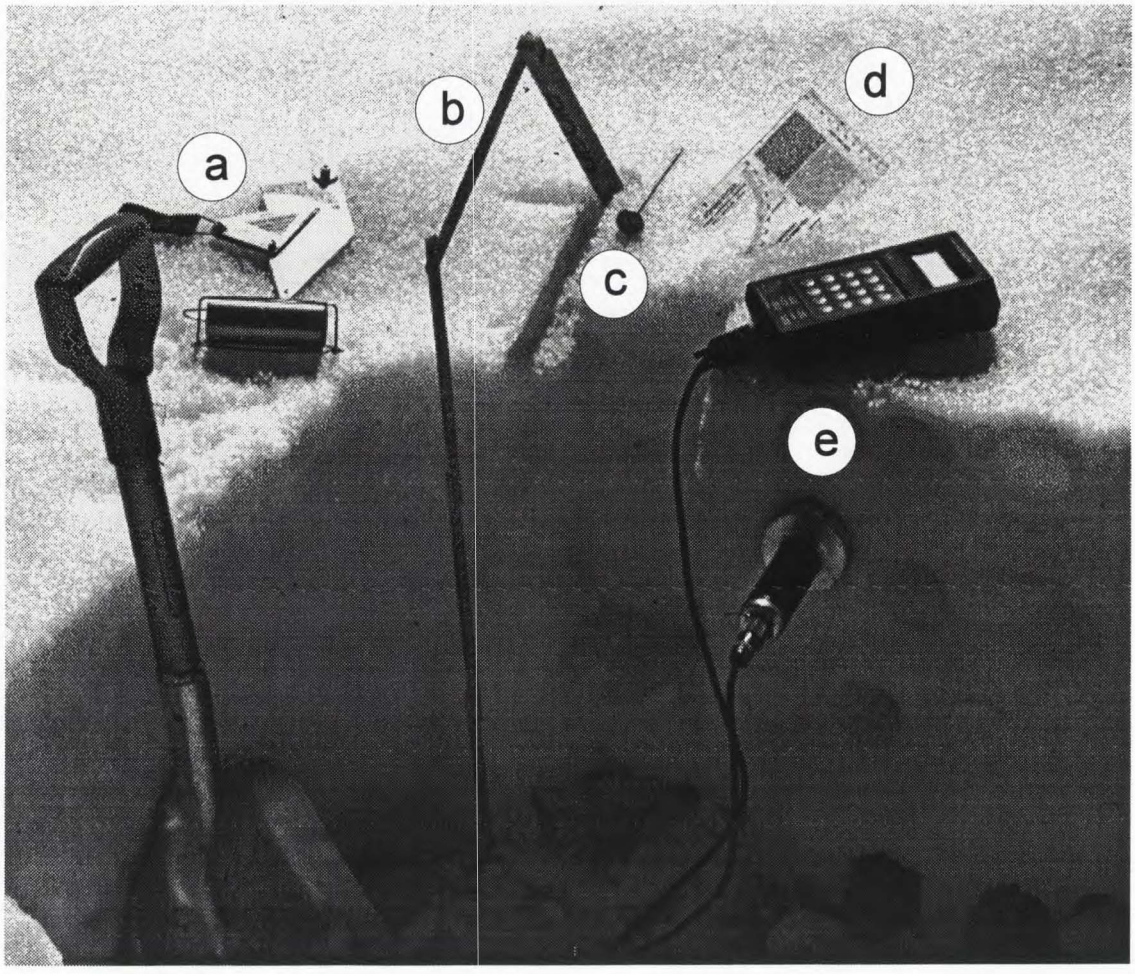

Figure 1.14. Snow pit measurement of snow parameters (a – snow density gage; b – folding ruler; c – snow thermometer; d – snow crystal card; e – snow wetness probe).

4) Ground Truth Information Acquisition: a) The SCS SNOTEL data: The Soil Conservation Service (SCS) installs, operates, and maintains an extensive, automated system, called SNOTEL (SNOwpack TELemetry), to collect snowpack and related climatic data in the western United States. There are currently 642 SNOTEL sites in 11 states. Snow water equivalent, precipitation, and air temperature (i.e., maximum, mean, and minimum) are recorded every 15 minutes and reported on a daily basis via meteor burst telemetry to the SCS master stations [52].

Since the SNOTEL stations are generally located in remote high-mountain meadows, SNOTEL data were used as the main source of ground truth information for mountainous areas in the western United States.

SNOTEL daily data of the 191 stations in the study area (Figure 1.12), formatted into a 1990 water-year period database, were obtained from the SCS West National Technical Center (WNTC) in Portland, Oregon. A set of programs was used to arrange the SNOTEL data into ASCII data files, which contained the latitude/longitude coordinates of each station, the date, and the corresponding snow data. The rearranged SNOTEL data were then merged with SSM/I data to form the multisource database.

b) The NOAA climatic data: The NOAA National Climatic Data Center (NCDC) operates a large cooperative network of weather stations that collect daily climatic data in the continental United States. These climatic data, containing daily maximum and minimum temperature, precipitation, and snow depth, are available from the NCDC Climatic tapes. Due to the dense distribution of weather stations in the central plains, these climatic data were used to represent the reliable snow cover information of flat terrains.

The climatic data of the 416 stations for 1990 water year in the study area (Figure 1.12) were download from tapes to computer disk, using software developed at Texas A&M University for the VAX VMS operating system. Daily climatic data at each station was combined with corresponding SSM/I data to constitute the multisource database.

c) The NOAA NDVI data: The NDVI is calculated from the difference of AVHRR near-infrared and visible radiances divided by the sum of the two. It has a valid greenness value range from 110 to 160; the higher value is associated with greater density and greenness of the plant canopy [53].

Monthly maximum scaled NDVI data of 1990 water year for the study area (Figure 1.12)

were used for the vegetation evaluation. These data were computed by taking the maximum values of biweekly NDVIs for each approximate month, then reprojecting the original Mercator-projected data to a 10-minute latitude/longitude grid as the Global View CD-ROM products available from the NOAA National Geophysical Data Center (NGDC) [54].

5) Development of Snow Wetness Algorithm: Regression analysis was performed for modeling the snow wetness as a function of the correlated meteorological variables (Figure 1.9). A correlation coefficient matrix was computed to measure the degree of linear associations among pairs of variables. Cook's distance method [55], a measure of the influence of an observation, was employed to detect the possible outliers for improving the fit of the regression models.

Correlation coefficients based on daytime series were plotted to examine the variations between snow wetness and related variables. Collinearity of the predictors was also examined for the selection of significant predictors in a multiple regression model. Methods of the variance inflation factor (VIF), the condition number (CN), and the variance proportions were used to quantify the degree of collinearity [56].

After selecting the predictor variables, multiple correlation coefficients were determined to examine the relationship of all combinations of variables to snow wetness. R^2, a measure of the strength of linear relationship, and Mallows' Cp [57], a measure of total squared error, were used for the best model selection in defining regression models.

The study focused on the SSM/I 19.35 and 37.0 GHz channels due to the sensitivity of Tb to snow wetness [7]. Time series of 37.0 GHz observations and Tb differences in the 19.35 and 37.0 GHz channels full resolution footprints in the Snowville area were examined. Based on the best regression model, snow wetness at the Snowville footprint, concurrent with the SSM/I local passing time, was estimated. With the available data of SSM/I and snow wetness, regression analyses were applied to develop the SSM/I snow wetness retrieval algorithm. The developed algorithm was tested

on the Tony Grove footprint by comparing the snow wetness estimated from the best meteorology-based model to that estimated from the SSM/I algorithm to see the agreements in both data.

6) Development of Multisource Database: The neighborhood searching method was used to integrate the SSM/I Tb's at each footprint with the ground truth of SNOTEL, climatic, and NDVI data into one database (Figure 1.10). This became the multisource database with the SSM/I seven Tb's and corresponding ground truth data.

Neighborhood searching was conducted by first calculating the great circle distance (z) between latitude/longitude coordinates of each weather station or AVHRR pixel and those of a particular SSM/I footprint (e.g., lat1/lon1 and lat2/lon2, respectively) defined by [58]:

$$z = 6370.997 * \arccos(\sin(lat1) * \sin(lat2) + \cos(lat1) * \cos(lat2) * \cos(|lon1 - lon2|))$$

where 6370.997 is the approximate radius of the earth's sphere in km, and latitude/longitude coordinates are in radians. The latitude/longitude coordinates of the weather station or AVHRR pixels that fell within a 15-km search radius around each SSM/I latitude/longitude location (approximately the size of a 3-dB 37.0 GHz footprint) were then searched. Finally, the average value or dominating condition of the searched points or pixels was taken to represent the ground truth information of the SSM/I footprint.

7) Cluster Analysis and Manual Characterization: Cluster analysis was employed to classify the SSM/I data into physically significant categories (Figure 1.10). Manual characterization was then performed to assign the hypothetical true snow class to each cluster using knowledge of microwave responses of snowpack defined in the literature [5], [7], [32]. The SSM/I snow classification rules from research findings and the known ground truth information at each SSM/I footprint were also used to characterize the SSM/I response to each cluster. By doing this, the possibility of inaccuracies in the ground truth data with respect to a possible true cluster were

reduced. The results were effectively the collection of input (SSM/I Tb's) and output (snow class) data pairs suitable for training of the artificial neural network in input/output patterns (Figure 1.10).

8) Design of Artificial Neural Network (ANN): A single-hidden-layer ANN (e.g., Figure 1.15), which consists of one input layer, one hidden layer, and one output layer, was employed. Each layer contained several nodes, and nodes of adjacent layers were fully connected with different weights. The error backpropagation (backprop) learning algorithm [59], which allowed forward feeding node outputs through layers and backward propagating mapping errors to adjust connection weights between layers, was used for training the neural network. This method requires that both input (i.e., SSM/I Tb's) and corresponding output (i.e., snow classes or snow parameter values) data pairs be applied during the training procedures.

As illustrated in Figure 1.15, the main mechanism in a backprop ANN training is first to allow inputs to flow forward through a hidden layer to the output layer by calculating the node outputs in each layer with a nonlinear transfer function (either hyperbolic tangent (tanh) or logistic). Training or mapping error between the calculated output and the desired output is measured at the output layer. Measured error is then propagated backward from the output layer to the input layer to adjust connection weights using a gradient descent optimization method. This method changes the weight in a direction that minimizes the error, so that the calculated output is more like the desired output. Thus, a backprop ANN is determined by its connection weights, the function applied to calculate each node output, and the learning rule used for the weight updates.

In this study, the connection weights were randomly initialized with a range around ±0.1 before training. The inputs (x_j) were scaled between −1 and 1 if tanh function was used or between 0 and 1 if logistic function was used. These scaled inputs were passed directly as mapping outputs (m_j) through connection weights to the hidden layer. However, each node in the hidden and output layers determined its output by calculating the net, which was the sum of all of its incoming

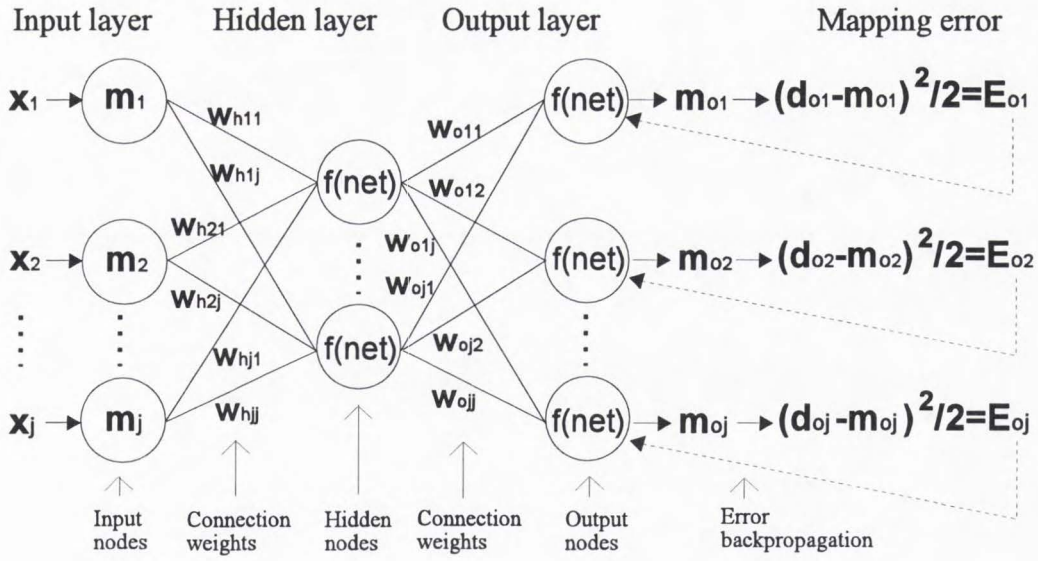

Figure 1.15 Single-hidden-layer backprop artificial neural network.

connection weights (w_j) multiplied by the mapping outputs (m_j) from the previous layer:

$$net^S = \sum_j m_j^{S-1} w_j \tag{1}$$

where S denotes the state of the current layer. Then, the net was passed through the tanh transfer function to give a mapping output between −1 and 1:

$$m^S = f(net^S) = \frac{\exp(net^S) - \exp(-net^S)}{\exp(net^S) + \exp(-net^S)} \tag{2}$$

or through the logistic function to give an mapping output between 0 and 1:

$$m^S = f(net^S) = 1/(1+\exp(-net^S)) \tag{3}$$

After calculating mapping outputs in the output layer, mapping error between desired output (d_o) and mapping output (m_o) for a single node were measured according to the delta learning rule:

$$E_o^S = \frac{1}{2}(d_o^S - m_o^S)^2 = \frac{1}{2}(d_o^S - f(net_o^S))^2 \tag{4}$$

The factor of 1/2 in Eq. (3) was used for convenience in calculating the derivative used in obtaining

the error gradient which was propagated back to adjust the weights connected to each output node:

$$\nabla E_o^s = -\partial E_o^s / \partial w_{oj} = (\partial E_o^s / \partial m_o^s)(\partial m_o^s / \partial w_{oj})$$
$$= -(d_o^s - m_o^s)\, f'(net_o^s)\, m_j^{s-1} \quad (5)$$

Since the error minimization required the weight adjustment to be in the negative gradient direction, the gradient component for a single weight update was specified as:

$$\Delta w_{oj} = -\eta\, \nabla E_o^s = \eta (d_o^s - m_o^s)\, f'(net_o^s)\, m_j^{s-1} \quad (6)$$

where η is the learning rate constant, typically less than 1.0. Once the gradient component was found, each connection weight to the output layer was updated in the following way:

$$w_{oj}^t = w_{oj}^{t-1} + \Delta w_{oj} + \alpha\, \Delta w_{oj}^{t-1} \quad (7)$$

where t is the time when the weight was updated, and α is the momentum term [60]. Since the derivative of hyperbolic tangent function in Eq. (2) can be expressed in terms of itself:

$$f'(net^s) = (1 + f(net^s))\ (1 - f(net^s)) \quad (8)$$

and the derivative of logistic function in Eq. (3) can be expressed as:

$$f'(net^s) = f(net^s)\ (1 - f(net^s)) \quad (9)$$

Thus, with the tanh function, the weight update equation in Eq. (7) can be modified to:

$$w_{oj}^t = w_{oj}^{t-1} + \eta (d_o^s - m_o^s)(1 + m_o^s)(1 - m_o^s) m_j^{s-1} + \alpha\, \Delta w_{oj}^{t-1} \quad (10)$$

or, with the logistic function, modified to:

$$w_{oj}^t = w_{oj}^{t-1} + \eta (d_o^s - m_o^s) m_o^s (1 - m_o^s) m_j^{s-1} + \alpha\, \Delta w_{oj}^{t-1} \quad (11)$$

Because there is no desired output for hidden layers, Eq. (10) or Eq. (11) cannot be used to adjust the connection weights to those layers. Backprop ANN implements the training process by propagating back a weighted sum of error gradients from the previous layer to each node in the hidden layer for error computation:

$$E_h^s = \sum_j w_j^{s+1}\, \nabla E_j^{s+1} \quad (12)$$

Then, the error gradient for weight adjustment was determined by:

$$\nabla E_h^s = -E_h^s \, f'(net_h^s) \, m_j^{s-1} \tag{13}$$

This error gradient was then used to adjust the connection weights in that hidden layer by:

$$w_{hj}^t = w_{hj}^{t-1} + \eta \, \nabla E_h^s \, m_j^{s-1} + \alpha \, \Delta w_{hj}^{t-1} \tag{14}$$

which can be revised to:

$$w_{hj}^t = w_{hj}^{t-1} + \eta \left(\sum_j w_j^{s+1} \nabla E_j^{s+1}\right) (1 + m_h^s)(1 - m_h^s) m_j^{s-1} + \alpha \, \Delta w_{hj}^{t-1} \tag{15}$$

if tanh function was used, or revised to:

$$w_{hj}^t = w_{hj}^{t-1} + \eta \left(\sum_j w_j^{s+1} \nabla E_j^{s+1}\right) m_h^s (1 - m_h^s) m_j^{s-1} + \alpha \, \Delta w_{hj}^{t-1} \tag{16}$$

if logistic function was used.

Training epoch, which involved forward feeding node outputs through layers, backward propagating mapping errors, adjusting the connection weights, and calculating the root-mean-square (RMS) error after all input/output data pairs were processed, repeated until a given RMS threshold was reached. The RMS error was calculated as:

$$RMS = \sqrt{\frac{1}{n \, q} \sum_n \sum_q (d_o - m_o)^2} \tag{17}$$

where n is the number of input/output data pairs in the training data set and q is the number of nodes in the output layer.

9) Development of ANN Classifier: A single-hidden-layer backprop ANN was used to develop the ANN classifier. In the input layer, the number of nodes was determined by SSM/I Tb's. For the hidden layer, nodes were chosen by trial and error. The nodes in the output layer were decided by the number of snow classes. In addition, a bias node, functioning similar to a constant in a regression, was connected to hidden and output layers.

The training and independent test data sets, containing the inputs of SSM/I data and the

corresponding outputs of snow classes, were prepared from the input and output data pairs (Figure 1.10). After training, the neural network was expected to be able to predict snow properties with input of SSM/I observations. The performance and limitations of the neural network were examined by comparing the results between ANN's with different settings (i.e., learning rate, momentum term, RMS tolerance). The final step was to determine the ANN classifier that was the most accurate in classifying the test data set.

10) Development of ANN Approximator: SSM/I Tb data of the multisource database were reclassified by the developed ANN classifier. Snow ground truth information and the SSM/I Tb's of each reclassified snow condition were used to define snow water equivalent or snow wetness as a nonlinear function of SSM/I Tb's. A single-hidden-layer backprop ANN was applied to inverse the nonlinear relationship of the dependent variables (i.e., snow parameters) to the independent variables (i.e., remotely sensed data) by learning the mapping of inputs (SSM/I Tb's patterns) to outputs (snow wetness and water equivalent). After training, the neural network was expected to be able to estimate snow wetness and water equivalent simultaneously with input of SSM/I Tb observations.

D. Significance of the Study

To date, no single existing algorithm has been able to identify land-surface snow conditions or estimate snow parameters over varied terrain. The use of artificial neural networks may overcome the drawbacks and limitations of the traditional methods for classifying land-surface snow types and estimating snow wetness and water equivalent under the circumstances that vegetation overlays snowpack. This study may suggest a nonlinear snow retrieval method, which is more useful to snow related applications at large scale, such as detecting the onset of snowmelt, mapping the snow conditions, and estimating the snow accumulation.

In snow hydrology, one of the major applications of remote sensing is for inputs of spatial

and temporal data to the global hydrological analysis. Monitoring SSM/I Tb observations throughout snow season may provide the timing of the onset of snowmelt. In addition, with the land-surface snow conditions determined from the SSM/I ANN classifier and the snow wetness and water equivalent estimated by the SSM/I ANN approximator, the database of snow extent, snow accumulation, and snowmelt runoff needed for the global analysis could be established.

E. References

[1] N. C. Grody, "Classification of snow cover and precipitation using the Special Sensor Microwave Imager," *J. Geophys. Res.*, vol. 96, no. D4, pp. 7423-7435, 1991.

[2] J. V. Fiore Jr. and N. C. Grody, "Classification of snow cover and precipitation using SSM/I measurements: case studies," *Int. J. Remote Sens.*, vol. 13, no. 17, pp. 3349-3361, 1992.

[3] B. E. Goodison, A. E. Walker, and F. W. Thirkettle, "Determination of areal snow water equivalent on the Canadian prairies using near real-time passive microwave data," in *Proc. Workshop on Applications of Remote Sensing in Hydrology*, 1990, pp. 297-316.

[4] J. P. Hollinger, "DMSP Special Sensor Microwave/Imager calibration/validation," Naval Research Laboratory, Washington, DC, Final Report, vol. II, 1991.

[5] F. T. Ulaby, R. K. Moore, and A. K. Fung, *Microwave Remote Sensing: Active and Passive*, Vol. I, *Microwave Remote Sensing Fundamentals and Radiometry*. Norwood, MA: Artech House, 1981.

[6] J. L. Foster, D. K. Hall, A. T. C. Chang, and A. Rango, "An overview of passive microwave snow research and results," *Rev. Geophys. Space Phys.*, vol. 22, no. 2, pp. 195-208, 1984.

[7] F. T. Ulaby, R. K. Moore, and A. K. Fung, *Microwave Remote Sensing: Active and Passive*, Vol. III, *from Theory to Applications*. Norwood, MA: Artech House, 1986.

[8] J. P. Hollinger, "DMSP Special Sensor Microwave/Imager calibration/validation," Naval Research Laboratory, Washington, DC, Final Report, vol. I, 1989.

[9] P. Y. Bernier, "Microwave remote sensing of snowpack properties: potential and limitations," *Nordic Hydrol.*, vol. 18, no. 1, pp. 1-20, 1987.

[10] F. Carsey, "Remote sensing of ice and snow: review and status," *Int. J. Remote Sens.*, vol. 13, no. 1, pp. 5-11, 1992.

[11] A. Rango, A. T. C. Chang, and J. L. Foster, "The utilization of spaceborne microwave radiometers for monitoring snowpack properties," *Nordic Hydrol.*, vol. 10, no. 1, pp. 25-40, 1979.

[12] K. F. Kunzi, S. Patil, and H. Rott, "Snow-cover parameters retrieved from Nimbus-7 scanning multichannel microwave radiometer (SMMR) data," *IEEE Trans. Geosci. Remote Sens.*, vol. GE-20, no. 4, pp. 452-467, 1982.

[13] D. H. Brooks, *Hydrology and the Management of Watersheds*. Ames, IA: Iowa State University Press, 1991.

[14] D. H. Male, "The seasonal snowcover," in *Dynamics of Snow and Ice Masses*, S. C. Colbeck, Ed. New York: Academic Press, 1980, pp. 305-395.

[15] S. C. Colbeck, "An overview of seasonal snow metamorphism," *Rev. Geophys. Space Phys.*, vol. 20, no. 1, pp. 45-61, 1982.

[16] S. C. Colbeck, "A review of the metamorphism and classification of seasonal snow cover crystals," in *Avalanche Formation, Movement and Effects (Proceedings of the Davos Symposium, September 1986)*. IAHS Publ., no. 162, Wallingford, Oxfordshire, UK: IAHS Press, 1987, pp. 3-34.

[17] S. C. Colbeck, "Snow-crystal growth with varying surface temperatures and radiation penetration," *J. Glaciology*, vol. 35, no. 119, pp. 23-29, 1989.

[18] A. T. C. Chang, J. L. Foster, and D. K. Hall, "Microwave snow signatures (1.5 mm to 3 cm) over Alaska," *Cold Regions Sci. Tech.*, vol. 13, no. 2, pp. 153-160, 1987.

[19] T. J. Schmugge, "Microwave approaches in hydrology," *Photogramm. Eng. Remote Sens.*, vol. 46, no. 4, pp. 495-507, 1980.

[20] E. Schanda, C. Matzler, and K. Kunzi, "Microwave remote sensing of snow cover," *Int. J. Remote Sens.*, vol. 4, no. 1, pp. 149-158, 1983.

[21] A. T. C. Chang, J. L. Foster, D. K. Hall, A. Rango, and B. K. Hartline, "Snow water equivalent estimation by microwave radiometry," *Cold Regions Sci. Technol.*, vol. 5, no. 3, pp. 259-267, 1982.

[22] A. K. Fung, "A review of volume scatter theories for modeling applications," *Radio Sci.*, vol. 17, no. 5, pp. 1007-1017, 1982.

[23] H. J. Eom, K. K. Lee, and A. K. Fung, "Microwave emission from an irregular snow layer," *Remote Sens. Environ.*, vol. 13, no. 5, pp. 423-437, 1983.

[24] D. H. Staelin, "Progress in passive microwave remote sensing: nonlinear retrieval techniques," in *Remote Sensing of Atmospheres and Oceans*, A. Deepak, Ed. San Diego, CA: Academic Press, 1980, pp. 259-274.

[25] S. R. Rotman, A. D. Fisher, and D. H. Staelin, "Analysis of multiple-angle microwave observations of snow and ice using cluster-analysis techniques," *J. Glaciology*, vol. 27, no. 95, pp. 89-97, 1981.

[26] L. Tsang, Z. Chen, S. Oh, R. J. Marks II, and A. T. C. Chang, "Inversion of snow parameters from passive microwave remote sensing measurements by a neural network trained trained with a multiple scattering model," *IEEE Trans. Geosci. Remote Sens.*, vol. 30, no. 5, pp. 1015-1024, 1992.

[27] Y. M. F. Lure, N. C. Grody, H. Y. M. Yeh, and J. S. J. Lin, "Neural network approaches to

classification of snow cover and precipitation from spectral sensor microwave/imager (SSM/I)," presented at *8th Int'l Conf. Interactive Info. Proces. Sys. (IIPS) Meteorol., Oceano., and Hydrol.*, Atlanta, GA, 1992.

[28] A. T. C. Chang and J. Tsang, "A neural network approach to inversion of snow water equivalent from passive microwave measurements," *Nordic Hydrol.*, vol. 23, no. 3, pp. 173-182, 1992.

[29] M. F. Augusteijn and A. S. Dimalanta, "Feature detection in satellite images using neural network technology," in *Proc. 1992 Goddard Conference on Space Applications of Artificial Intelligence*, 1992, pp. 123-136.

[30] W. H. Stiles, F. T. Ulaby, and A. Rango, "Microwave measurements of snowpack properties," *Nordic Hydrol.*, vol. 12, no. 3, pp. 143-166, 1981.

[31] C. M. U. Neale, M. J. McFarland, and K. Chang, "Land-surface-type classification using microwave brightness temperatures from the Special Sensor Microwave/Imager," *IEEE Trans. Geosci. Remote Sens.*, vol. 28, no. 5, pp. 829-838, 1990.

[32] M. J. McFarland and C. M. U. Neale, "Land parameter algorithms validation and calibration," in "*DMSP Special Sensor Microwave/Imager calibration/validation,*" J. P. Hollinger, Ed. Naval Research Laboratory, Washington, DC, Final Report, vol. II, 1991, pp. 1-108.

[33] D. K. Hall, J. L. Foster, and A. T. C. Chang, "Nimbus-7 SMMR polarization response to snow depth in the Mid-Western U.S.," *Nordic Hydrol.* vol. 15, no. 1, pp. 1-8, 1984.

[34] A. Rango, J. Martinec, A. T. C. Chang, J. L. Foster, and V. F. Van Katwijk, "Average areal water equivalent of snow in a mountain basin using microwave and visible satellite data," *IEEE Trans. Geosci. Remote Sens.*, vol. GE-27, no. 6, pp. 740-745, 1989.

[35] A. T. C. Chang, J. L. Foster, M. Owe, D. K. Hall, and A. Rango, "Passive and active microwave studies of wet snowpack properties," *Nordic Hydrol.*, vol. 16, no. 2, pp. 57-66, 1985.

[36] M. J. McFarland, G. D. Wilke, and P. H. Harder, III, "Nimbus 7 SMMR investigation of snowpack properties in the northern Great Plains for the winter of 1978-1979," *IEEE Trans. Geosci. Remote Sens.*, vol. GE-25, no. 1, pp. 35-46, 1987.

[37] W. H. Stiles, and F. T. Ulaby, "The active and passive microwave response to snow parameters 1. wetness," *J. Geophys. Resear.*, vol. 85, no. C2, pp. 1037-1044, 1980.

[38] R. L. Armstrong and M. Hardman, "Monitoring global snow cover," in *Proc. Western Snow Conf.*, 1991, pp. 103-108.

[39] J. P. Hollinger, J. L. Peirce, and G. A. Poe, "SSM/I instrument evaluation," *IEEE Trans. Geosci. Remote Ses.*, vol. 28, no. 5, pp. 781-790, 1990.

[40] D. K. Hall, M. Sturm, C. S. Benson, A. T. C. Chang, J. L. Foster, H. Garbeil, and E. Chacho, "Passive microwave remote and in situ measurements of Arctic and Subarctic snow cover in Alaska," *Remote Sens. Environ.*, vol. 38, no. 3, pp. 161-172, 1991.

[41] J. F. Zuel and L. M. Cox, "Relative importance of meteorological variables in snowmelt," *Water Resour. Res.*, vol. 11, no. 1, pp. 174-176, 1975.

[42] M. R. Farrar and E. A. Smith, "Spatial resolution enhancement of terrestrial features using deconvolved SSM/I microwave brightness temperatures," *IEEE Trans. Geosci. Remote Sens.*, vol. 30, no. 2, pp. 349-355, 1992.

[43] B. G. Gérard, "*Development of surface moisture algorithms using Special Sensor Microwave/Imager (SSM/I) signatures.*" M.S. Thesis, Utah State University, Logan, UT, 1990.

[44] A. T. C. Chang, J. L. Foster, A. Rango, and E. G. Josberger, "The use of microwave

radiometry for characterizing snow storage in large river basins," in *Snow, Hydrology and Forests in High Alpine Areas (Proceedings of the Vienna Symposium, August 1991)*, IASH Pub., no. 205, Wallingford, Oxfordshire, UK: IAHS Press, 1991, pp.73-80.

[45] G. G. Gutman, "Vegetation indices from AVHRR: an update and future prospects," *Remote Sens. Environ.*, vol. 35, no. 2&3, pp. 121-136, 1991.

[46] D. T. Davis, Z. Chen, L. Tsang, J. Hwang, and A. T. C. Cheng, "Retrieval of snow parameters by iterative inversion of a neural network," *IEEE Trans. Geosci. Remote Sens.*, vol. 31, no. 4, pp. 842-852, 1993.

[47] J. Key, J. A. Maslanik, and A. J. Schweiger, "Classification of merged AVHRR and SMMR Arctic data with neural networks," *Photogramm. Eng. Remote Sens.*, vol. 55, no. 9, pp. 1331-1338, 1989.

[48] NOAA and NASA, *Space-Based Remote Sensing of the Earth.* Washington, DC: U.S. Government Printing Office, 1987.

[49] T. Poggio and F. Girosi, "Networks for approximation and learning," *Proc. IEEE*, vol. 78, no. 9, pp. 1481-1497, 1990.

[50] D. T. Davis, Z. Chen, L. Tsang, J. Hwang, and A.T.C. Chang, "Retrieval of snow parameters by iterative inversion of a neural network," *IEEE Trans. Geosci. Remote Sens.*, vol. 31, no. 4, pp. 842-852, 1993.

[51] NASA, *WetNet User's Manual.* Huntsville, AL: NASA Marshall Space Flight Center, 1991.

[52] SCS, *Snow Survey and Water Supply Products Reference.* Portland, OR: USDA SCS West National Technical Center, 1988.

[53] K. B. Kidwell, *Global Vegetation Index User's Guide.* Washington, DC: NOAA National Geophysical Data Center, Satellite Data Services Division, 1994.

[54] A. M. Hittelman, L. W. Row, J. J. Kineman, R. E. Habrmann, and D. A. Hastings, *Global*

View CD-ROMs and User's Manual. Boulder, CO: NOAA National Geophysical Data Center, 1994.

[55] R. D. Cook, "Detection of influential observations in linear regression," *Technometrics*, vol. 19, no. 1, pp. 15-18, 1977.

[56] D. A. Belsley, E. Kuh, and R. E. Welsch, *Regression Diagnostics*. New York: John Wiley & Sons, 1980.

[57] C. L. Mallows, "Some comments on Cp," *Technometrics*, vol. 15, no. 4, pp. 661-675, 1973.

[58] D. H. Maling, *Coordinate Systems and Map Projections*. Elmsford, NY: Pergamon Press, 1991.

[59] J. M. Zurada, *Introduction to Artificial Neural Systems*. St. Paul, MN: West Publishing Co., 1992.

[60] D. E. Rumelhart, G. E. Hinton, and R. J. Williams, "Learning internal representations by error propagation," in *Parallel Distributed Processing: Explorations in the Microstructure of Cognition*, Vol. 1, *Foundations*, J. A. Feldman, P. J. Hayes, and D. E. Rumelhart, Eds. Cambridge, MA: MIT Press, 1986, pp. 318-362.

CHAPTER 2

ON THE ESTIMATION OF SNOW WETNESS FROM SSM/I DATA

A. Abstract

The development of satellite-based snow wetness retrieval algorithm has been impeded by the lack of an adequate ground-based snow wetness measurement network. A field experiment was conducted to examine the relationship between snow wetness and meteorological variables. Net radiation, air temperature at 1.5 m above the snow surface, and snow wetness at depth of 0.1 m below the surface were measured at three study sites. Regression analysis showed that concurrent air temperature, TAIR (°C), was significantly related to ground-based measurement of snow wetness, WETNESS (% by volume), by the linear model ($R^2 = 0.71$), WETNESS = 1.0285 + 0.5708(TAIR). Special Sensor Microwave/Imager (SSM/I) observations, in terms of brightness temperature (Tb), were collected for one of the sites. Concurrent with SSM/I local crossing time, snow wetness was estimated by the air-temperature-based model. Regression analysis was applied to extrapolate empirical relationships between SSM/I Tb and snow wetness. Results indicated that snow wetness varied inversely as the first-, second-, and third-power of SSM/I Tb difference, between vertical polarization at 19.35 GHz (T19V) and horizontal at 37.0 GHz (T37H). An SSM/I snow wetness retrieval algorithm ($R^2 = 0.95$) was developed: WETNESS = $-4.75 + 339.53(TD)^{-1} - 6159.53(TD)^{-2} + 40112.00(TD)^{-3}$, where TD = T19V - T37H. Due to the depolarization effect of vegetation on the SSM/I Tb, the algorithm is not applicable to areas where forests overlie snow cover. Improvement is expected if an empirical relationship between SSM/I Tb and snow wetness can be developed for a specific region and applied only to those similar geographic areas.

B. Introduction

Snow wetness, the liquid or free water content in snow cover, is an important parameter in

estimating the timing of snowmelt [1] and assessing the snowpack avalanche potential [2]. Because the snow wetness has a significant effect on the microwave emission at the snowpack surface, monitoring large-scale snow wetness is possible through satellite microwave radiometry [3],[4].

The Special Sensor Microwave/Imager (SSM/I), flown on the Defense Meteorological Satellite Program (DMSP) satellites [5], is a useful tool in estimating snow properties because it is sensitive to the changes in snow physical and dielectric properties. Unlike in situ methods, the SSM/I provides an indirect estimate by using parameter retrieval algorithms, with measurements of brightness temperatures (Tb's) as inputs, to derive information about snow properties. In order to develop the algorithm, either empirical or theoretical interpretations of microwave observations along with ground truth data are required. In the application of the algorithm, the microwave reading is known, and the state of variables is inferred. Thus, conventional snow measurements have always played an important role in the development of snow parameter retrieval algorithms.

Although techniques for the measurement of snow wetness in field or laboratory are well addressed [6], [7], conventional observation of snow wetness through ground-based network system has not been established. The development of satellite-based snow wetness retrieval algorithms has been impeded by the lack of sufficient ground-based snow wetness data.

As indicated in [8], the snowmelt process is strongly influenced by meteorological variables such as air temperature, solar radiation, vapor pressure, and wind. Among these meteorological variables, air temperature and solar radiation data are generally available. However, no empirical equations have been developed to estimate snow wetness directly from these available parameters.

This study links ground-based snow wetness measurements with air temperature and solar radiation and develops a relationship by which the snow wetness data needed for a passive microwave approach can be estimated. A retrieval algorithm for the SSM/I was then developed and test with in situ filed observations of snow wetness.

C. Methods

1) Field Experiments: Three sites were selected in northern Utah, representing different terrain and vegetation complexes. The Snowville site was situated at latitude/longitude coordinates of 41.97°N/112.95°W with an elevation of 1300 m, and has a flat, nonforested terrain with sparse vegetation. This site was selected because of its usually homogeneous snow distribution. The Tony Grove site was at 41.88°N/111.57°W with an elevation of 1920 m, and represented a forested mountainous terrain. The Logan site, located in the Logan City cemetery at an open grass area, was at 41.73°N/111.82°W with an elevation of 1400 m. The selection of the Logan site was for the convenience of collecting sufficient snow wetness measurements.

Data were collected between Mar. 8 and Mar. 19, 1993 at Snowville, between Feb. 18 and Feb. 25, 1994 at Logan, and between Mar. 6 and Mar. 20, 1994 at Tony Grove. An automated weather station was set up at each site. Net radiation (W/m^2) and air temperature (°C) were measured at 1.5 meters above the snow surface using a net radiometer (Radiation Energy Balance Systems, Model Q-6) and temperature probe (Campbell Scientific, Model HMP35C), respectively. Data were recorded at 10-minute intervals for the sampling duration and processed to include data of net radiation at 24, 12, and 6 hours before snow sampling. Data of minimum, maximum, and average air temperatures within the 24-hour period prior to field measurement were also determined.

Snow parameters were sampled at irregular time intervals during the daytime. Each time the snow was sampled, one randomly selected snow pit was dug at each site. Snow density and wetness were measured at 10-cm intervals with the snow profile. Snow density (g/cm^3) was obtained with the Strong Stitch Snow Density Gage. Snow wetness (% by volume) was measured using a dielectric probe (LEAS Inc.).

2) SSM/I Data Acquisition: The SSM/I is a seven-channel, four-frequency, linearly polarized, passive microwave radiometric system. It measures both vertically (V) and horizontally

(H) linearly polarized Tb's, at 19.35, 37.0, and 85.5 GHz and only vertical polarization at 22.235 GHz [5]. DMSP-F11 SSM/I data were derived from the WetNet computer system at Utah State University. The integral part of the system is the Man computer Interactive Data Access System (McIDAS) for the OS/2 operating system [9]. Under the McIDAS environment, SSM/I Tb data are in the format of full and browse resolutions. The full and browse resolutions are all gridded in the global rectilinear projection with fixed latitude/longitude coordinates. The full resolution is at the size of 1/4° box (0.25°latitude × 0.25°longitude cell) , whereas the browse is at the size of 1/2° box.

In this study, SSM/I Tb's observed at the corresponding footprint of full resolution, located at 42.01°N/112.87°W, and that of browse resolution, located at 42.00°N/113.03°W, during the field experiment period were downloaded from the WetNet system.

3) Modeling Snow Wetness as a Function of Meteorological Variables: From the perspective of passive microwave remote sensing, wet snow means snow whose surface layer contains water in liquid form [10]; therefore, only snow wetness data measured in the surface layer were taken into account in the study. A correlation coefficient matrix was computed to measure the degree of linear associations among pairs of sampled variables (i.e., snow wetness, concurrent temperature, maximum temperature, minimum temperature, average temperature, net radiation, 6-hour net radiation, 12-hour net radiation, and 24-hour net radiation). Regression analysis was performed for modeling the snow wetness as a function of the correlated meteorological variables. Cook's distance method, a measure of the influence of an observation [11], was employed to detect the possible outliers in data and improve the fit of the regression model.

After eliminating the outliers, correlation coefficients based on daytime series were plotted to examine the variations between snow wetness and related meteorological variables. The collinearity among the predictor variables was examined for the selection of significant predictors in the multiple regression model. The variance inflation factor (VIF), the condition number (CN),

and the variance proportions [12] were used to quantify the degree of collinearity.

Multiple correlation coefficients were determined to examine the relationship of all combinations of selected variables to snow wetness. Stepwise regression [13] was used for the model selection. R^2, a measure of the strength of linear relationship; Mallows' Cp, a measure of total squared error [14]; and MSE, a measure of the mean square error, were used to define the best regression model.

4) SSM/I Snow Wetness Algorithm Development: The SSM/I snow wetness algorithm development was restricted to the 19.35 and 37.0 GHz channels due to the sensitivity of Tb at these frequencies to snow wetness [10]. Time series of 37.0 GHz observations and Tb differences in the 19.35 and 37.0 GHz channels for the Snowville footprint were examined to determine microwave response to changes in snow condition, including liquid water content. Based on the best regression model, snow wetness was estimated at the Snowville footprint, concurrent with the SSM/I local passing time. With the available data of SSM/I and snow wetness, regression analyses were applied to develop the SSM/I snow wetness retrieval algorithm. The developed algorithm was tested on the Tony Grove footprint and compared with the snow wetness estimated by a developed meteorology-based model to compare the agreements in varied terrain.

D. Results and Discussion

1) Relations Between Snow Wetness and Meteorological Variables: The correlation matrix (Tables 2-I and 2-II) showed that the highest positive correlation coefficient ($r = 0.65$) was found between snow wetness and concurrent air temperature. Accordingly, a linear relationship ($R^2 = 0.42$) between snow wetness and concurrent air temperature was defined. Based on this relationship, possible outliers among observations were evaluated by Cook's distance method (Figure 2.1). After checking the corresponding field conditions, it was found that the statistically defined outliers had

TABLE 2-I
CORRELATION MATRIX OF SNOW WETNESS AND RADIATION

Variable	Snow Wetness, %	Net Radiation, W/m^2	6-hour Net Radiation, $JK/m^2/6h$	12-hour Net Radiation, $JK/m^2/12h$	24-hour Net Radiation, $JK/m^2/24h$
Snow Wetness	1.000	0.461	0.586	0.512	0.266
Net Radiation		1.000	0.230	0.067	0.078
6-hour Net Radiation			1.000	0.895	0.279
12-hour Net Radiation				1.000	0.412
24-hour Net Radiation					1.000

TABLE 2-II
CORRELATION MATRIX OF SNOW WETNESS AND AIR TEMPERATURES

Variable	Snow Wetness, %	Concurrent Temp., °C	Min. Temp., °C	Max. Temp., °C	Avg. Temp., °C
Snow Wetness	1.000	0.650	0.427	0.505	0.593
Concurrent Temperature		1.000	0.225	0.787	0.629
Minimum Temperature			1.000	0.329	0.842
Maximum Temperature				1.000	0.716
Average Temperature					1.000

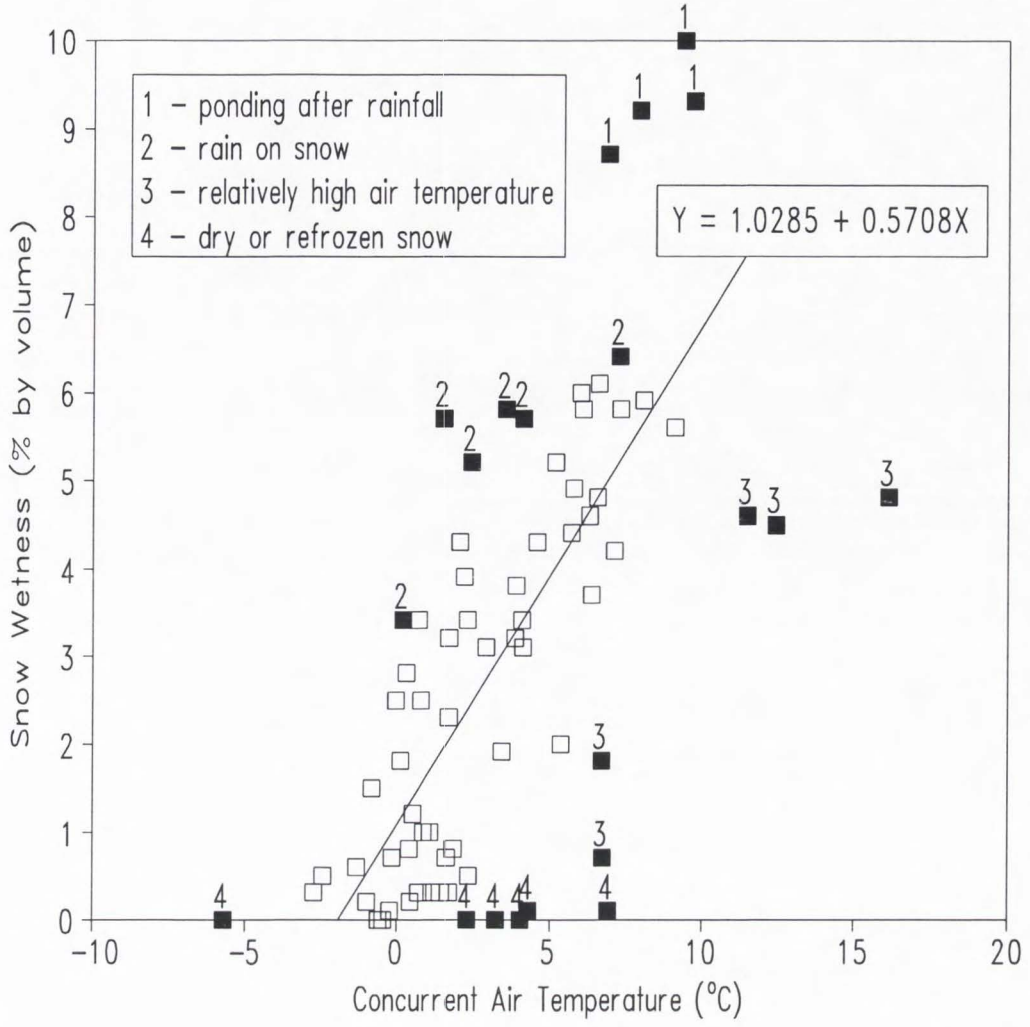

Figure 2.1. Plot of snow wetness versus concurrent air temperature and the linear regression model ($R^2 = 0.71$) derived from the data. Filled squares with labels are the possible outliers defined by Cook's distance method.

resulted from extremely wet snow due to ponding after rainfall (label 1 on Figure 2.1) or rain on snow (label 2), from wet or moist (label 3) snow with relatively high air temperature, and from dry or refrozen snow (label 4). After discarding these uncertain data of extreme cases, a better linear relationship ($R^2 = 0.71$) was obtained.

The correlation time series (Figure 2.2) showed a diurnal variation in the relation between snow wetness and different meteorological variables. Snow wetness was highly correlated with the minimum air temperature in the morning, and maximum air temperature in the afternoon. High correlations were also found in response to the net radiation at noon, the 24-hour net radiation in the morning, and the 12-hour net radiation at 10 am and 4 pm. However, the concurrent air temperature was the most significant variable in relation to snow wetness throughout the day. These findings further confirmed that the concurrent air temperature was the most important predictor in modeling snow wetness as shown in Tables 2-I and 2-II.

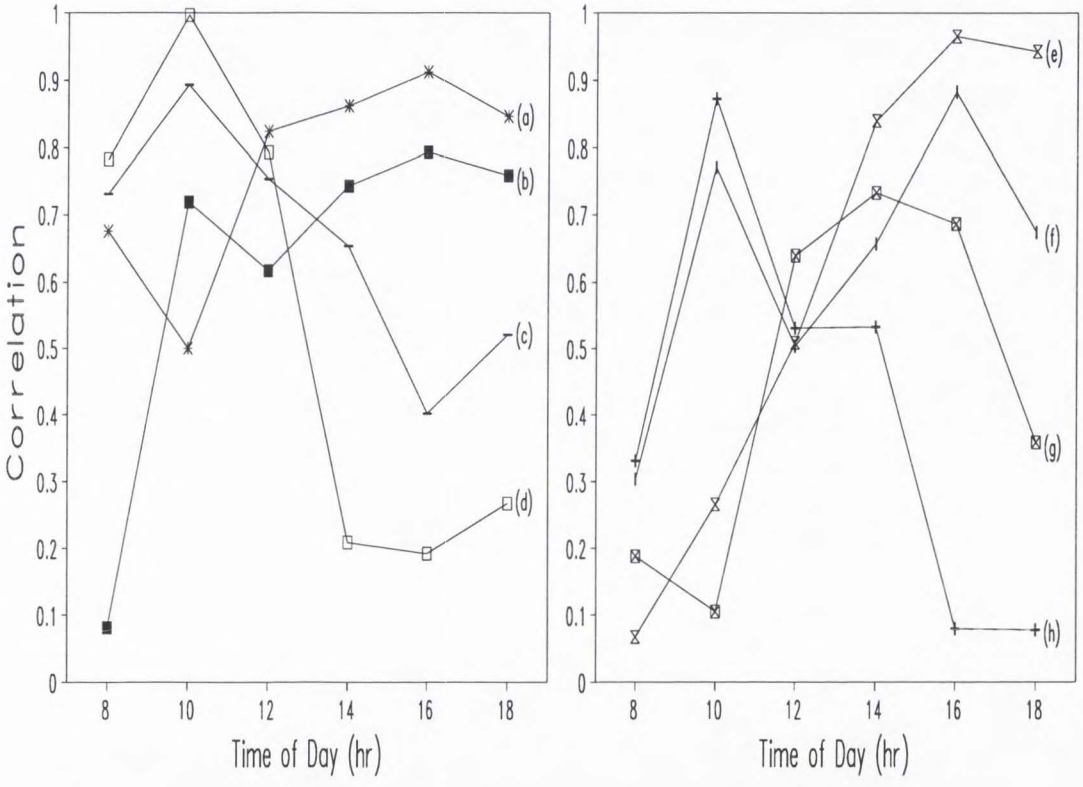

Figure 2.2. Correlations between snow wetness and (a) concurrent air temperature, (b) maximum air temperature, (c) average air temperature, (d) minimum air temperature, (e) 6-hour net radiation, (f) 12-hour net radiation, (g) net radiation, and (h) 24-hour net radiation at the daytime series.

According to [12], a CN level of 10.0 suggests the presence of mild to moderate collinearity and a level of 30.0 or greater indicates a moderate to severe problem among the predictors. This study had a CN level of 16.1 with respect to all measured meteorological variables (Table 2-III). This suggested that a potential problem existed among the set of available meteorological data. The larger a variable's VIF, the more troublesome the variable. After eliminating variables with a VIF greater than 6.0, the CN level dropped to 4.8 for the set of remaining variables (Table 2-IV). This collinearity reduction further confirmed the selection of concurrent air temperature, concurrent net radiation, 12-hour net radiation, and 24-hour net radiation as the predictors in the snow wetness estimation.

TABLE 2-III
COLLINEARITY DIAGNOSTICS FOR ALL PREDICTORS

Variable	CN	Intercept	TAIR	TMIN	TMAX	TAVG	QNET	QN6	QN12	QN24
		Variance proportions								
1	1.0	0.00	0.00	0.00	0.00	0.00	0.01	0.00	0.00	0.01
2	1.6	0.00	0.00	0.01	0.00	0.01	0.00	0.00	0.00	0.02
3	2.3	0.00	0.01	0.00	0.00	0.00	0.13	0.00	0.04	0.07
4	2.6	0.01	0.02	0.00	0.00	0.00	0.00	0.02	0.02	0.34
5	3.7	0.09	0.00	0.00	0.02	0.01	0.28	0.00	0.01	0.14
6	6.9	0.05	0.86	0.01	0.00	0.00	0.38	0.10	0.02	0.18
7	8.4	0.16	0.00	0.00	0.03	0.00	0.17	0.63	0.73	0.12
8	8.9	0.45	0.10	0.20	0.20	0.05	0.00	0.14	0.06	0.11
9	16.1	0.22	0.00	0.77	0.73	0.92	0.03	0.10	0.11	0.01
			Variance inflation factor (VIF)							
			4.18	9.70	6.40	19.09	2.34	6.14	5.80	1.90

TAIR, concurrent air temperature in °C; TMIN, minimum air temperature in °C; TMAX, maximum air temperature in °C; TAVG, average temperature in °C; QNET, net radiation in W/m^2; QN6, net radiation in $KJ/m^2/6h$; QN12, net radiation in $KJ/m^2/12h$; QN24, net radiation in $KJ/m^2/24h$.

TABLE 2-IV
COLLINEARITY DIAGNOSTICS FOR SELECTED PREDICTORS

Variable	CN	Intercept	TAIR	QNET	QN12	QN24
		Variance proportions				
1	1.0	0.04	0.02	0.02	0.03	0.03
2	1.7	0.01	0.01	0.09	0.09	0.32
3	2.2	0.00	0.02	0.08	0.25	0.48
4	2.5	0.93	0.04	0.10	0.03	0.01
5	4.8	0.02	0.91	0.69	0.60	0.17
			Variance inflation factor (VIF)			
			2.72	2.09	2.00	1.27

TAIR, concurrent air temperature in °C; QNET, net radiation in W/m^2; QN12 net radiation in $KJ/m^2/12h$; QN24, net radiation in $KJ/m^2/24h$.

Multiple correlation coefficients (Table 2-V) showed that concurrent air temperature was the best predictor if only one meteorological variable was available for snow wetness prediction. None of the net radiation related variables could explain the variation in snow wetness. However, the addition of air temperature to one or more net radiation related variables greatly raised the total explained variation. In comparison, no significant improvement could be achieved by using those combinations rather than air temperature alone in relation to snow wetness.

Table 2-VI shows the valid models selected using the criterion of R^2 greater than 0.70 and Cp less than 5.00. According to [15], if the correct model is considered, the value of Cp is expected to be close to p+1, where p is the number of predictors in model. Thus, model 3 and model 7 in Table 2-VI were the two candidates that followed this criteria. Model 3, which includes concurrent air temperature (TAIR) and 12-hour net radiation (QN12), had the smallest MSE and was selected as the best model. However, because the TAIR is the most available variable from climatic data network, the simplest model, model 1 (Table 2-VI), appears to be more practical in the estimation of snow wetness.

TABLE 2-V

SELECTED METEOROLOGICAL VARIABLE COMBINATIONS IN RELATION TO SNOW WETNESS

Number of Variable	Variable Combinations	Multiple Correlation	Standard Error
4	TAIR,QNET,QN12,QN24	0.859311	0.038156
3	TAIR,QN12,QN24	0.858713	0.038396
	TAIR,QNET,QN24	0.854841	0.039274
	TAIR,QNET,QN12	0.854780	0.039289
	QNET,QN12,QN24	0.730503	0.068026
2	TAIR,QN24	0.854757	0.039295
	TAIR,QN12	0.852910	0.039755
	TAIR,QNET	0.843225	0.040464
	QNET,QN12	0.729813	0.068173
	QNET,QN24	0.538661	0.103541
	QN12,QN24	0.518686	0.106622
1	TAIR	0.841222	0.040937
	QN12	0.518296	0.106681
	QNET	0.431655	0.113937
	QN24	0.217458	0.138967

TAIR, concurrent air temperature in °C; QNET, net radiation in W/m^2; QN12, net radiation in KJ/m^2/12hr; QN24, net radiation in KJ/m^2/24hr.

TABLE 2-VI

REGRESSION MODELS BASED ON R^2 AND C_p SELECTION FOR SNOW WETNESS ESTIMATION BY DIFFERENT COMBINATION OF PREDICTORS

				Parameter Estimates				
m	#	R^2	Cp	Intercept	TAIR	QNET	QN12	QN24
1	1	0.7077	3.6494	1.0285	0.5708	-	-	-
2	2	0.7306	2.2830	0.9444	-	-	-	0.000106
3	2	0.7275	2.8014	0.9975	0.5223	-	0.00027	-
4	3	0.7374	3.1688	0.9439	0.5313	-	0.00018	0.000081
5	3	0.7308	4.2594	0.9479	0.5684	-0.00058	-	0.000107
6	3	0.7306	4.2767	0.9714	0.4798	0.00300	0.00032	-
7	4	0.7384	5.0000	0.9331	0.5056	0.00176	0.00022	0.000074

m, model number; #, number of variable in model, TAIR, concurrent air temperature in °C; QNET, net radiation in W/m^2; QN6, net radiation in KJ/m^2/6hr; QN24, net radiation in KJ/m^2/24hr.

2) Time Series Interpretation of SSM/I Observations: Time series of SSM/I T37V observations (Figure 2.3-a) showed that winter dry snow was characterized by 220K<T37V<250K. As indicated in [16], the decrease in Tb was partly due to the volume scattering and partly due to the decreased physical temperature of the snow and underlying soil. As is seen in Figure 2.3-a, the large fluctuations in the T37V series may imply the microwave response with respect to the depletion or accumulation of the snowpack among snow storms, whereas the lagged curves may indicate the change of Tb in relation to the effect of snow metamorphism.

During the spring, the onset of the snow melting and refreezing processes was identified by an observable diurnal variation of T37V between 265K and 200K (Figure 2.3-a). The melting and refreezing processes resulted in melt-freeze crystals or ice layers [17]. As snow refreezes, these polycrystalline particles of solid ice or ice layers caused additional scattering at lower microwave frequencies (i.e., 22 and 19 GHz) and further lowered the Tb's. As a result, a larger Tb difference between T19V and T37H was detected in the time series of Figure 2.3-b. While snow was melting, the increase in liquid water content at snow surface caused an increase in Tb at 37 GHz, and resulted in a smaller Tb difference between T19V and T37H.

As noted above, these interpretations provide the physical reasons of using SSM/I T19V and T37H channel observations in the development of snow wetness algorithm. Accordingly, the increase in Tb differences may indicate a decrease in snow wetness. More specifically, the range of the T19V−T37H difference from 10K to 15K may suggest wet snow, from 15K to 30K moist snow, from 30K to 45K dry snow, and over 45K refrozen snow.

3) The SSM/I Algorithm and Its Application: In the development of the SSM/I snow wetness algorithm, the simplest air-temperature-based model (model 1 in Table 2-VI), WETNESS = 1.0285 + 0.5708(TAIR), was applied to estimate the snow wetness at the time of the SSM/I overpass at Snowville. Based on the estimated WETNESS and concurrent full resolution SSM/I

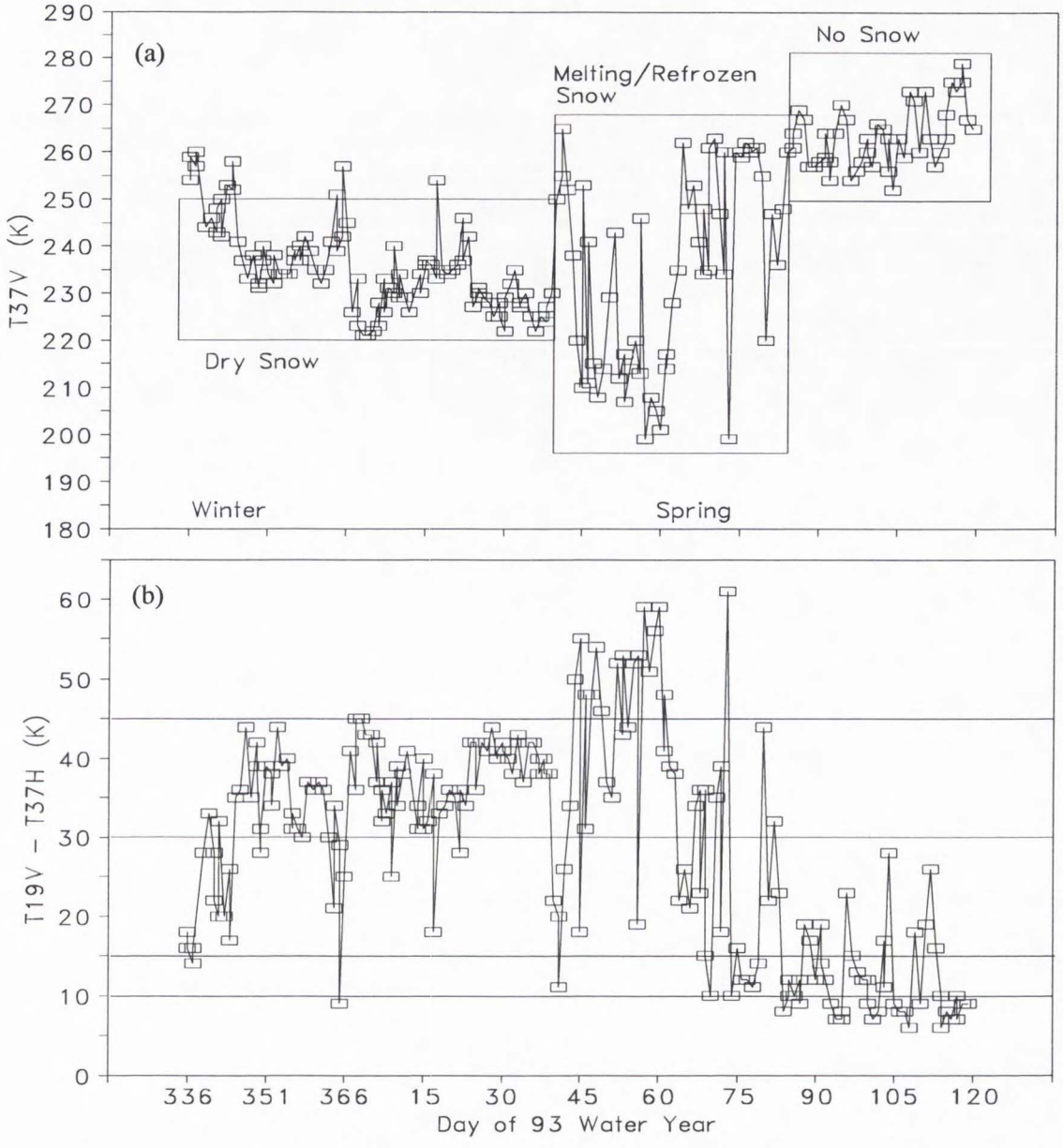

Figure 2.3. Time series of (a) SSM/I T37V observations and (b) T19V–T37H differences for the full resolution footprint at Snowville site.

T19V-T37H data, results indicated that snow wetness varied inversely as the first-, second-, and third-power of SSM/I Tb difference, TD (K), between T19V and T37H. Thus, an SSM/I snow wetness retrieval algorithm ($R^2 = 0.95$) is:

$$WETNESS = -4.75 + 339.53(TD)^{-1} - 6159.53(TD)^{-2} + 40112.00(TD)^{-3}$$

where TD = T19V - T37H.

If browse SSM/I data are included in the relationship, 70% of the total variation can be explained by the regression model (Figure 2.4). Since the algorithm was developed based on the SSM/I full resolution data, the drop in R^2 (i.e., from 0.95 to 0.70) may reflect certain unexplained variation introduced by the browse resolution data. However, significant agreement is obtained in estimating snow wetness at browse resolution footprints.

In comparison with the field snow wetness measurements at Snowville in 1993 (Figure 2.5), the application of the SSM/I algorithm showed some underestimations in snow wetness. Since the wetness was not measured at the concurrent SSM/I crossing time (i.e., 5 am for the descending overpass and 5 pm for the ascending), the snow wetness measured at 8 am could be higher than that at 5 am due to a higher air temperature. In fact, the wetness measured at 6 pm, which was close to the SSM/I ascending crossing time, showed a better agreement with the SSM/I prediction line. Due to the limitations in field snow wetness measurement, these findings indicate the importance of the air-temperature-based snow wetness model in relation to the development of the SSM/I snow wetness algorithm.

Since Feb. 1994, the DMSP-F11 satellite has only had two (of the four) operational recorders. This resulted in a blackout of data over northern Utah at most of the time during field works. Only eight SSM/I descending (6 am local sun time) Tb observations at the Tony Grove footprint were obtained for the algorithm testing.

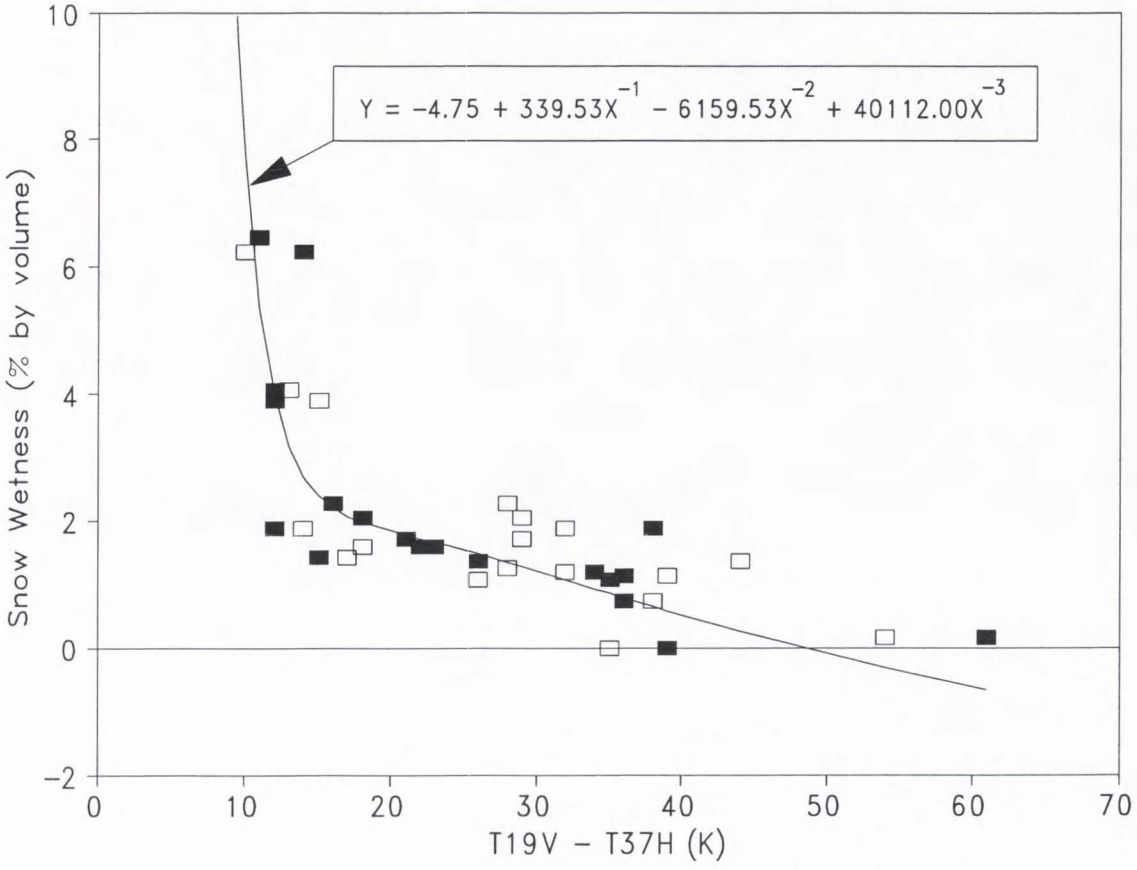

Figure 2.4. Snow wetness varies inversely as the first-, second-, and third-power of SSM/I T19V-T37H difference ($R^2 = 0.95$). Filled squares are values of snow wetness estimated from air temperatures at corresponding full resolution footprint, whereas empty squares are values in response to T19V−T37H differences at browse resolution.

Results showed an overestimation in snow wetness predicted by the SSM/I algorithm at the Tony Grove footprint (Figure 2.5), compared to those estimated from concurrent air temperature using the air-temperature-based model. Since the Tony Grove footprint is located in forested mountains, one possible explanation is that evergreen forests overlying the snowpack depolarized the Tb and resulted in a smaller T19V−T37H Tb difference, causing the estimation of wetness in snowpacks with actually dry or refrozen conditions.

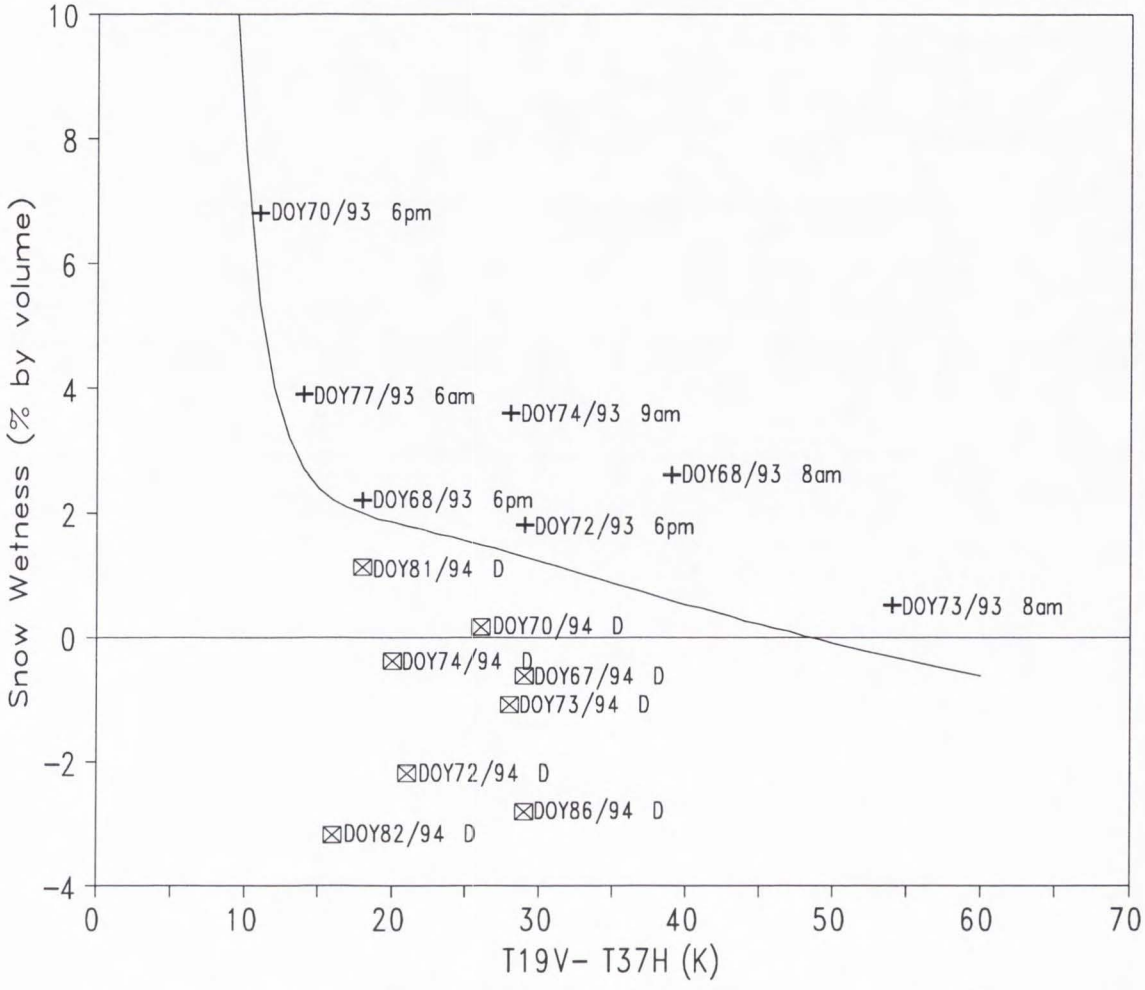

Figure 2.5. Plot of snow wetness measured at Snowville site at different local time (+) and estimated by the air-temperature-based model at Tony Grove site at SSM/I local descending crossing time (⊠) versus the SSM/I Tb difference with respect to the regression line (solid curve) predicted by the SSM/I snow wetness algorithm.

E. Conclusions

Air temperature appears to be the most important factor controlling snow wetness. This study showed that snow wetness estimated from concurrent air temperature measurement can contribute the necessary data for the development of the SSM/I snow wetness retrieval algorithm. Although

abnormal weather conditions (e.g., heavy rain on wet snow) may introduce errors in the use of air temperature alone as a dependant variable in a predictive equation, the simplest air-temperature-based model provides an accessible way for concurrent snow wetness estimation.

Microwave emissions from dry, wet, and refrozen snow are distinct. Monitoring SSM/I Tb throughout the snow season may provide the timing of distinct snow conditions. With increasing liquid water content in a snowpack, the Tb increases significantly, especially at 37.0 GHz, resulting in a decrease in the T19V-T37H Tb difference. These changes allow for the detection of the onset snowmelt and the use of the SSM/I snow wetness retrieval algorithm.

Nonetheless, the SSM/I Tb observed at an area where evergreen forests overlie the snowpack is quite different from those in the plains where vegetation cover is sparse. The vegetation cover tends to depolarize the Tb, resulting a smaller T19V-T37H Tb difference, which causes an overestimation in snow wetness from the SSM/I snow wetness retrieval algorithm. Improvement is expected if an empirical relationship between SSM/I Tb and snow wetness can be developed for a specific region and applied only to those similar geographic areas.

F. References

[1] W. I. Linlor, F. D. Clapp, D. J. Angelakos, J. L. Smith, N. Berg, and J. Bergman, "Snow wetness measurements and runoff forecasting," in *Proc. Western Snow Conf.*, 1981, pp. 1-12.

[2] E. Brun, "Investigation on wet-snow metamorphism in respect of liquid-water content," *Annals Glaciology*, vol. 13, pp. 22-26, 1989.

[3] W. H. Stiles and F. T. Ulaby, "The active and passive microwave response to snow parameters 1. Wetness," *J. Geophys. Res.* vol. 85, no. C2, pp. 1037-1044, 1980.

[4] R. L. Armstrong, and M. Hardman, "Monitoring global snow cover," in *Proc. Western Snow*

Conf., 1991, pp. 103-108.

[5] J. P. Hollinger, J. L. Peirce, and G. A. Poe, "SSM/I instrument evaluation," *IEEE Trans. Geosci. Remote Sens.*, vol. 28, no. 5, pp. 781-790, 1990.

[6] R. Kattelmann, "Methods of estimating liquid water storage in snow," in *Proc. Western Snow Conf.*, 1987, pp. 158-161.

[7] H. S. Boyne and D. Fisk, "A comparison of snow cover liquid water measurement techniques," *Water Resour. Res.*, vol. 23, no. 10, pp. 1833-1836, 1987.

[8] J. F. Zuzel and L. M. Cox, "Relative importance of meteorological variables in snowmelt," *Water Resour. Res.*, vol. 11, no. 1, pp. 174-176, 1975.

[9] NASA, *WetNet User's Manual*, Marshall, AL: NASA Marshall Space Flight Center, 1991.

[10] F. T. Ulaby, R. K. Moore, and A. K. Fung, "Emission behavior of snow," in *Microwave Remote Sensing: Active and Passive*, Vol. III, *from Theory to Applications*. Norwood, MA: Artech House, 1986, pp. 1603-1634.

[11] R. D. Cook, "Detection of influential observations in linear regression," *Technometrics*, vol. 19, no. 1, pp. 15-18, 1977.

[12] D. A. Belsley, E. Kuh, and R. E. Welsch, *Regression Diagnostics*, New York: John Wiley & Sons, 1980.

[13] SAS Institute Inc., *SAS/STAT Users Guide, Release 6.03 Edition*, Cary, NC: SAS Institute Inc., 1988.

[14] C. L. Mallows, "Some comments on Cp," *Technometrics*, vol. 15, no. 4, pp. 661-675, 1973.

[15] D. G. Kleinbaum, L. L. Kupper, and K. E. Muller, *Applied Regression Analysis and Other Multivariable Methods*. Boston, MA: PWS-KENT Publishing, 1988.

[16] M. J. McFarland and C. M. U. Neale, "Land parameter algorithms validation and calibration," in "*DMSP Special Sensor Microwave/Imager calibration/validation,*" J. P.

Hollinger, Ed. Naval Research Laboratory, Washington, DC, Final Report, vol. II, 1991, pp. 1-108.

[17] S. C. Colbeck, "An overview of seasonal snow metamorphism," *Rev. Geophys. Space Phys.*, vol. 20, no. 1, pp. 45-61, 1982.

CHAPTER 3

MONITORING LAND-SURFACE SNOW CONDITIONS FROM SSM/I DATA USING AN ARTIFICIAL NEURAL NETWORK CLASSIFIER

A. Abstract

The Special Sensor Microwave/Imager (SSM/I) radiometer is a useful tool for monitoring snow-covered land surfaces because it is sensitive to the changes in snow physical and dielectric properties. Previously developed SSM/I snow classification algorithms have limitations and do not work properly for terrain where forests overlie snow cover. Unsupervised cluster analysis was applied to separate SSM/I brightness temperatures (Tb's) into groups. Six desired snow classes were identified; both sparse- and medium-vegetated region scene classes were assessed. Typical SSM/I Tb signatures, based on cluster means of each snow class, were determined by calculating the mean Tb's of the corresponding cluster. A single-hidden-layer artificial neural network (ANN) classifier was designed to learn the typical Tb patterns. The error backpropagation training algorithm was applied to train the ANN. After training, the winner-takes-all method was used to determine the snow classification from the outputs of the ANN classifier with inputs of Tb observations. Classification error rates were as small as 2.4%. This study demonstrates the potential of cluster means in ANN supervised learning, and suggests a nonlinear retrieval method towards making the inferences of snow classes from SSM/I data over varied terrain operational.

B. Introduction

Snow cover is a dominant factor controlling the hydrological response of watersheds in mid and high latitudes. Monitoring large-scale snow conditions throughout the snow accumulation and melt seasons is essential for understanding regional hydrologic response and global climatic feedbacks. Generally, land-surface snow cover can be classified as dry, wet, or refrozen depending

on its internal temperature and physical properties. Dry snow is characterized by rounded grains or faceted crystals at small or large temperature gradient. Wet snow is characterized by clusters of grains at low liquid water content, or by poorly bounded slush at high liquid water content. Refrozen snow is characterized by rounded polycrystals when water in veins freezes.

The Special Sensor Microwave/Imager (SSM/I) radiometer, flown on the Defense Meteorological Satellite Program (DMSP) satellites, is a useful tool for monitoring snow-covered land surface because it is sensitive to the changes in snow physical and dielectric properties. The SSM/I is a seven-channel, four-frequency, linearly polarized, passive microwave radiometric system; it measures both vertically (V) and horizontally (H) linearly polarized brightness temperatures (Tb's), at 19.35, 37.0, and 85.5 GHz and only vertical polarization at 22.235 GHz [1].

In a dry or refrozen snow layer, the radiation emitted from the underlying ground surface is scattered on its way to the snow surface by ice crystals, resulting in a decrease in brightness temperature (Tb) observed by the SSM/I. When snow is wet, the liquid water held in the snow grains causes a large increase in volume absorption by which more radiation is reemitted, following an increase in SSM/I Tb. Thus, large-scale characterization of seasonal snowpack conditions is possible through utilization of passive microwave remote sensing.

Many SSM/I snow classification algorithms have been developed, e.g., Neale *et al.* [2]; McFarland and Neale [3] developed a land-surface-type classification scheme by which the dry, wet, and refrozen conditions of snow over land could be determined, and Fiore Jr. and Grody [4] developed a decision-tree algorithm for the global classification of snow cover and precipitation over large regions. In general, these methods employed statistical linear relationships of polarization information, in terms of thresholds of certain Tb's or Tb combinations, between different land surface features to form the classification rules. However, in snow classification, these rules are restricted to land surfaces with uniform snow conditions. Where evergreen forests overlie snowpack, the

developed algorithms may misidentify those forested snow covers with areas of snow-free conditions. As indicated in [5], vegetation (especially coniferous trees) will mask the microwave emission from the snow below, resulting in a higher microwave brightness temperature and making the classification rules uncertain.

In such complex terrain situations, statistical regression is often unsuitable because there are too many random variables involved in the characterization of microwave response, making the problem extremely nonlinear. Consequently, there exists a need for nonlinear retrieval methods to develop a robust snow classification algorithm by which different snow conditions over varied terrain can be determined simultaneously.

According to [6], some of the most complex remote sensing problems can be handled with unsupervised cluster analysis, which separates the observed data vectors into groups. Cluster analysis has the advantage of making no a priori assumptions about the possible classes, and providing objective indications of the information imbedded in multidimensional data sets. The study of [7] shows that typical Tb signatures for a variety of snow classes can be distinguished from the mean Tb values of each desired cluster (cluster means).

Recently, the use of an artificial neural network (ANN) with supervised learning to retrieve snow properties from passive microwave data has been addressed (e.g., [8], [9],[10]). Studies have shown that ANNs have the potential to learn Tb patterns, where previously, the complexity and nonlinearity of random variables made them difficult to define using empirical regression approaches.

In neural computing, error backpropagation (backprop) training [11] is the most widely used leaning method in the development of an ANN classifier. This method requires that during training, when the input is applied, the corresponding output has to be provided; therefore, the selection of training samples is essential to the success in ANN generalization. Generally, it is claimed that more, rather than fewer, training samples in each class are best. Following [12], however, an ANN trained

from only cluster means has shown a reliable generalization capability in pattern classification.

Therefore, a possible research framework would be to take typical SSM/I Tb signatures of desired snow classes interpreted from unsupervised cluster analysis, and use them as a prelude to supervised leaning in an ANN classifier. In this way, the ANN learns only the central idea of the clusters, in terms of geophysical significance of the snow classes, instead of all random information from the data. Consequently, the purpose of this study was to explore the above concept towards making the inference of snow classes from SSM/I data over varied terrain operational. Two clustering methods (average linkage and centroid method) and a single-hidden-layer ANN were used to accomplish this task.

C. Methods

1) SSM/I and Ground Truth Data: A study area bounded by latitude of 40°N to 45°N and longitude of 100°W and 115°W, which contained both plains and mountainous region in the western United States, was selected to represent a variety of sparse- and medium-vegetated terrain. SSM/I Tb's, normalized difference vegetation index (NDVI) data, and ground-based snow measurements were obtained for the area for the period Oct. 1, 1989 to May 30, 1990.

The SSM/I Tb's from the DMSP-F8 satellite were obtained from the Naval Research Laboratory. Due to the increase in noise level of both SSM/I 85.5 GHz channels on DMSP-F8 satellite during 1988, only five Tb's of the lower frequency channels, denoted as T19V, T19H, T22V, T37V, and T37H, were used in this study.

The NDVI, calculated from the visible and near-infrared reflectance values from NOAA Advanced Very High Resolution radiometer (AVHRR), is a useful tool for characterizing the vegetation condition over large regions [13]. These data have a valid greenness value range from 110 to 160, whereas values less than 110 indicate nonvegetated surface features [14]. A monthly

maximum scaled NDVI data set, available from the NOAA National Geophysical Data Center [15], was obtained. These latter data, however, served mainly as a reference in the study.

Ground truth data of daily snow water equivalent (SWE), and maximum, minimum, and average air temperature over mountainous terrain were obtained from the Soil Conservation Service (SCS) SNOTEL (SNOwpack TELemetry) system [16]. Daily snow depth (SD), maximum and minimum air temperature, and air temperature at the observing time in the plains data were derived from the NOAA weather observing network [17].

2) Ground-Based Snow Classification: Daily snow condition of each SNOTEL or NOAA weather station with respect to DMSP-F8 local crossing time (at either 6 am or 6 pm) was further flagged as: (1) snow-free (if SWE or SD was equal to zero), (2) dry snow (while SWE or SD was accumulated from previous time and the concurrent air temperature was below 3.5°C by which the snow wetness was assumed to be less than 3% by volume according to the linear relationship between snow wetness and concurrent air temperature defined in [18]), (3) wet snow (as SWE or SD was not equal to zero and the concurrent air temperature was large than or equal to 3.5°C), or (4) refrozen snow (if the concurrent air temperature was below freezing point and the snow condition of previous time was either wet or refrozen).

Accordingly, for SNOTEL stations, the concurrent air temperature at 6 am and 6 pm were set to be the daily minimum and average air temperature, respectively. For NOAA weather stations, the concurrent air temperature at 6 am or 6 pm was set to be the air temperature at the observing time if the time was between 4 am and 7 am or between 4 pm and 7 pm, respectively; otherwise, the concurrent air temperature at 6 am was equal to the minimum air temperature and that at 6 pm was extrapolated by assuming the maximum air temperature was at 2 pm and linearly decreased to the temperature at observing time, which was after 2 pm or the maximum air temperature of previous day decreased to the air temperature at observing time, which was before 2 pm.

Since the latitude/longitude coordinates of the SSM/I footprints change with each overpass, a neighborhood merging method was employed to merge the multisource data into one database. The database was then built by searching the AVHRR pixels and ground weather stations, which fell within a 15-km search radius around a particular SSM/I latitude/longitude coordinates (i.e., approximately the size of a 37.0 GHz footprint). NDVI values and SWE values were then averaged for that SSM/I footprint, respectively.

According to [18], Tb difference of T19V-T37H at each SSM/I footprint was determined as an additional surface wetness index (SWI), in which the range of the SWI from 10K to 15K may suggest wet snow, from 15K to 30K moist snow, from 30K to 45K dry snow, and over 45K refrozen snow. Moreover, flooding or precipitation condition at each SSM/I footprint was checked and data were discarded from the database if the value of T22V-T19V for the footprint was larger than 4K or T19V was greater than 268K [2], respectively. Consequently, only data of SSM/I footprints with snow-covered land surface (i.e., only if averaged SWE was larger than zero) were considered as the valid elements in the database.

3) Cluster-Analysis-Based Snow Classification: Two clustering methods (average linkage and centroid method [19]) were used to explore the possible clusters with respect to 5 SSM/I Tb's variables (T19V, T19H, T22V, T37V, and T37H). The cubic clustering criterion (CCC) [20], [21] was examined in each method to obtain the possible number of clusters in the data. Clusters for each suggested number were examined from the lowest number of possible clusters until all the desired snow classes were distinguished. Five mean Tb values (typical Tb signature), mean NDVI, and mean SWI for each cluster were calculated. A hypothetical true snow condition was then assigned to each cluster according to its typical Tb's signature (cluster means) and the values of NDVI and SWI in relation to the emission behavior of snow. The clusters in question, if they existed, were discarded. By doing so, the possibility of an uncertain cluster with respect to a possible true snow condition was

reduced. Only data of the six most representative clusters [i.e., dry snow with sparse (DsSv) or medium (DsMv) vegetation, wet snow with sparse (WsSv) or medium (WsMv) vegetation, and refrozen snow with sparse (RsSv) or medium (RsMv) vegetation] were selected for ANN training. Consequently, a data set of input (5 Tb's) and output (6 snow classes) data pairs was created.

4) Training, Validation, and Test Data: The training data set was created using the Tb signatures of the desired snow classes in the form of input and output data pairs. Based on the number of data elements in each snow class, the validation data set was formed by including either all data in the class if the number of elements was less than 101, or the upper and lower quartiles [22] of the data in the class if the number of elements was larger than 100. The validation data set was used as a pseudo test set to evaluate the performance of each ANN during training.

Ideally, an unknown test data set is used to measure the performance of an ANN; therefore it should be completely different from the data sets used for ANN training and validation. Consequently, Tb observations of SSM/I orbit footprints in a geographic region between latitude of 30°N and 50°N over the United States from Jan. 21-26, 1990 were collected as the test data set.

5) ANN Topology and Learning Factors: A single-hidden-layer ANN was created. It consisted of an input layer of five nodes representing the inputs of SSM/I Tb's, and an output layer of six nodes representing the land-surface snow conditions. For the hidden layer, the number of nodes was chosen by trial and error. Given the number of nodes in each layer from input to output as a sequence, the ANN topology used was represented as 5-N-6, where N is the number of nodes in hidden layer.

The error backpropagation (backprop) algorithm [11] was applied to train each ANN. This method allows forward feeding node outputs through layers and backward propagating mapping errors to adjust connection weights between layers. According to [23], having a larger learning rate at hidden layer than that at output layer can decrease learning time. Learning rate at the hidden was

set up as twice the rate at the output layer. Learning rates were determined at 0.05 for hidden layer and 0.025 for the output layer in the training process. The momentum method [24] (i.e., adding the current weight adjustment with a proportion of the previous weight change) was applied to accelerate the learning process. The momentum term was set at 0.90 in this study.

6) ANN Training and Validation: The activation function applied to the net input of nodes in the hidden and output layers was a hyperbolic tangent (tanh), which maps the net output into the range between −1 and 1. Thus, the input data were normalized and rescaled into the range from −1 to 1 to represent the input attributes in the ANN. Land-surface snow conditions were coded as (0.8, −0.8, −0.8, −0.8, −0.8, −0.8) for DsSv, (−0.8, 0.8, −0.8, −0.8, −0.8, −0.8) for DsMv, (−0.8, −0.8, 0.8, −0.8, −0.8, −0.8) for WsSv, (−0.8, −0.8, −0.8, 0.8, −0.8, −0.8) for WsMv, (−0.8, −0.8, −0.8, −0.8, 0.8, −0.8) for RsSv, and (−0.8, −0.8, −0.8, −0.8, −0.8, 0.8) for RsMv to represent the six desired outputs in the ANN.

The root-mean-squared (RMS) error, computed after each training cycle (epoch), was used as the stopping criterion. Five runs were conducted for each ANN. In each run, the training process started by randomly initializing all connection weights between −0.1 and 0.1, and then repeated the error backpropagation training algorithm until the specified RMS tolerance was reached. RMS error was set between 0.1 and 0.3 by trial and error.

After each training run, the validation data set was applied to evaluate the classification performance of the resulting ANN. The winner-takes-all method [25] (i.e., the network output with the highest value designates the class) was applied to determine the classification of snow conditions. Classification result, in terms of error rate (%), was calculated after each run. An ANN with the minimum error rate was eligible for the SSM/I ANN snow classifier. A two-way contingency table, in terms of a two-way crosstabulation [19], was used to show the generalization performance of the qualified ANN on validation data.

7) ANN Testing: Since the ANN classifier was trained only from the desired snow

conditions, it is not applicable to other surface types. Accordingly, existing land-surface-type classification rules for water bodies or flooding (if T22V-T19V>4.0), and precipitation (if T19V>268.0 and T37V-T19V<-3.0) from [2], [3], and ocean (if T19V-T19H>40.0), and snow-free (if T37V<T19V) from [26] were used as a pretreatment procedure to eliminate the snow-free conditions in data before the application of the ANN classifier.

In the examination of ANN performance with the test data set, classified SSM/I footprints were gridded into 1/4° latitude/longitude boxes as a raster data set and displayed as color images (Table 3-I) using the ERDAS Geographic Information System (GIS) software. These ANN classified images were then compared to those by McFarland and Neale's snow classification rules [3].

D. Results and Discussion

1) Cluster Analysis: After eliminating the possible conditions of precipitation, flooding, or water bodies with respect to SSM/I Tb observations, 6486 elements remained in the database for cluster analysis. In determining the number of clusters in SSM/I Tb data, the average linkage showed

TABLE 3-I
COLOR SCHEME FOR RASTER IMAGE DISPLAY OF SSM/I FOOTPRINTS ON TEST DATA

Land-Surface-Class	Color	RGB Colors		
		Red	Green	Blue
Dry snow with sparse vegetation (DsSv)	White	255	255	255
Dry snow with medium vegetation (DsMv)	Gray	127	127	127
Wet snow with sparse vegetation (WsSv)	Rose	255	85	85
Wet snow with medium vegetation (WsMv)	Pink	255	160	140
Refrozen snow with sparse vegetation (RsSv)	Cyan	127	127	127
Refrozen snow with medium vegetation (RsMv)	Aqua	0	255	255
Water body or Flooding	Blue	0	0	255
Precipitation	Yellow	255	255	0
Snow-free	Tan	160	100	40

CCC peaks at 6, 9, 19, 29, 35, and 43 clusters and centroid method suggested 6, 12, 21, 30, 39, 43 or 49 clusters in data (Figure 3.1).

Table 3-II shows the cluster means of six land-surface snow conditions found at different suggested cluster partitions by the two cluster methods. Generally, data of medium-vegetated snow conditions (i.e., DsMv, WsMv, and RsMv) were distinct at a higher number of cluster partitions and a larger data set than those of sparse-vegetated (i.e., DsSv, WsSv, and RsSv). This may imply complexity and nonlinearity among microwave responses of medium-vegetated snow cover, by which the embedded geographical and conditional information of different snow conditions failed to appear in the clusters at the lower CCC number (Figure 3.1). On the other hand, the relatively large data size in clusters of medium-vegetated snow conditions reveals the significant influence of vegetation in characterizing the emission behavior of SSM/I footprints in the western and central United States.

Clusters of wet snow conditions (i.e., WsSv and WsMv) were the most difficult to be separated, as evidenced by the highest number of cluster partitions associated with those wet snow classes (Table 3-II). This could be due to the fact that the effect of both overlying vegetation and liquid water content depolarized the Tb difference between vertical and horizontal polarization in similar microwave signatures.

The mean monthly NDVI values of the selected clusters were all below 110 (Table 3-II), indicating a nonvegetated area according to [14]. This implies that the vegetation cover in most of the SSM/I footprints in the study area was not homogeneous since the NDVIs were integrated from AVHRR high spatial resolutions (1 km) to SSM/I low resolutions. However, relatively higher values were all associated with the medium-vegetated snow classes, suggesting the six resulted Tb signatures are representative for characterizing microwave responses of different vegetated snow conditions.

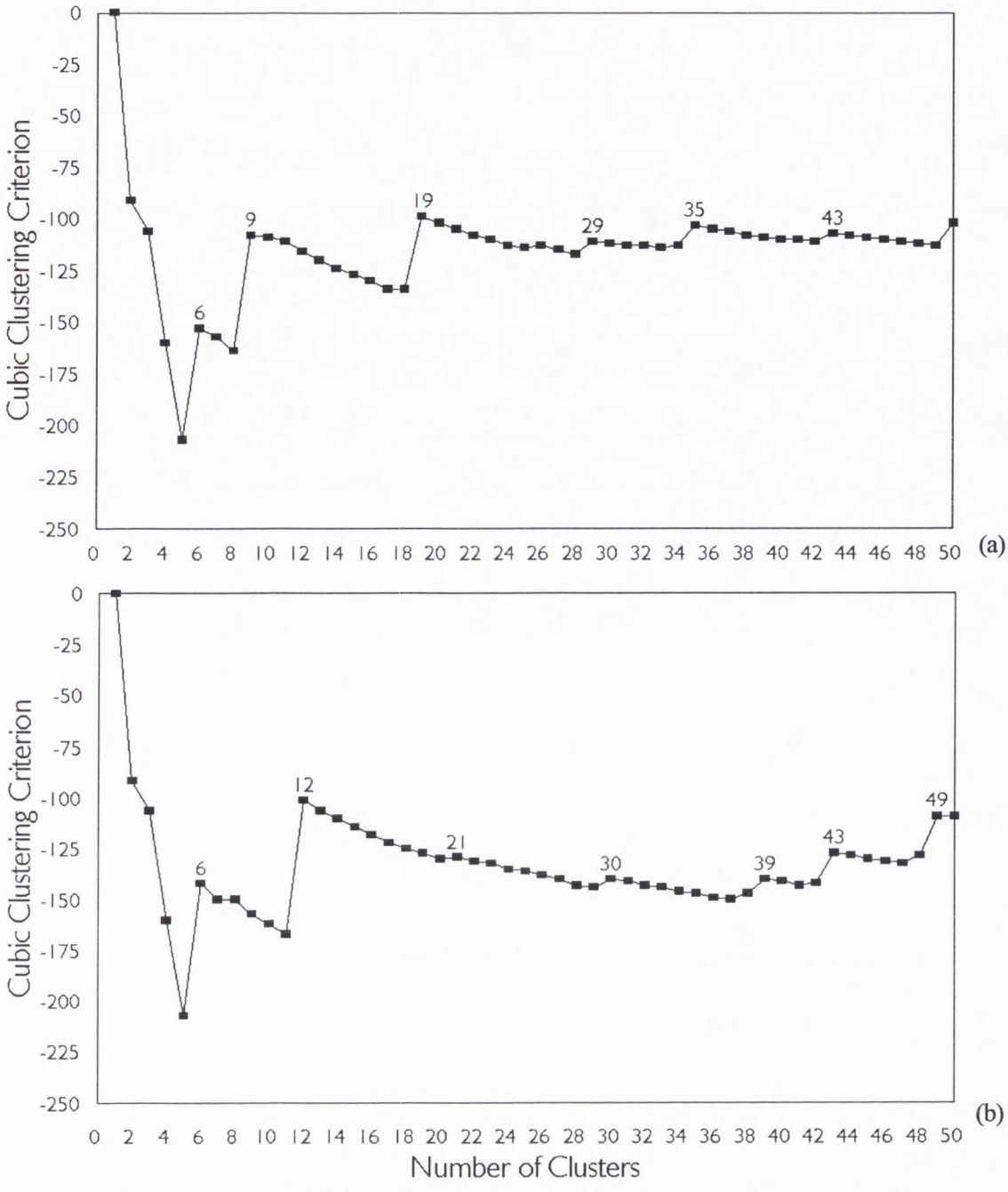

Figure 3.1. Number of clusters in SSM/I observations suggested by cubic clustering criterion with (a) average linkage and (b) centroid method.

TABLE 3-II
CLUSTER MEANS OF SIX LAND-SURFACE SNOW CONDITIONS BY TWO CLUSTERING METHODS

Method	Snow Condition (n)[§]	Mean Brightness Temperature (K) T37V	T37H	T22V	T19V	T19H	NDVI	SWI	# of Cluster Partition
Average Linkage	DsSv (237)	245.97	234.64	252.95	255.21	241.98	90	21	29
	DsMv (1608)	252.03	245.90	258.53	260.57	252.76	105	15	35
	WsSv (93)	259.77	250.71	261.44	261.39	247.39	103	11	43
	WsMv (1123)	259.23	253.74	263.12	264.71	257.40	108	11	43
	RsSv (19)	208.68	200.04	237.61	244.39	228.43	52	44	9
	RsMv (213)	231.97	225.92	248.25	252.32	243.27	93	26	43
Centroid Method	DsSv (216)	245.27	234.53	252.43	254.75	242.03	91	20	39
	DsMv (1112)	250.85	244.37	257.61	259.73	251.48	102	15	49
	WsSv (24)	259.31	250.40	260.45	259.61	243.91	107	9	43
	WsMv (741)	260.07	254.24	264.12	265.62	257.87	109	11	43
	RsSv (19)	208.68	200.04	237.61	244.39	228.43	52	44	12
	RsMv (167)	230.63	223.76	247.70	252.01	241.97	87	28	43

[§] (n): number of data elements in cluster.

With respect to the sparse-vegetated snow conditions, the mean SWI of 11 and 9 for wet snow, 21 and 20 for dry, and 44 and 44 for refrozen snow from the average linkage and centroid method, respectively, agreed with the range for these values found by [18]. In the dry and refrozen snow, high SWIs were associated with sparse-vegetated snow conditions and low SWIs were related to the medium-vegetated snow conditions. This may suggest the depolarization effect of vegetation on the decrease of SWI in medium-vegetated snow conditions. However, there was no significant SWI differences between sparse-vegetated and medium-vegetated wet snow conditions.

Table 3-III shows that the maximum SWI value of the wet snow clusters was larger than 13, which corresponded to a snow wetness less than 3% by volume [18], suggesting some similar Tb signatures other than wet snow might be embedded in this class data. According to [27], the SSM/I Tb signatures of heavy vegetation, frozen ground, and wet snow are similar. Therefore, the signatures with higher SWI (e.g., SWI > 13) may indicate frozen ground conditions. On the other hand, the minimum SWI values less than 9 could indicate the depolarization effect due to vegetation cover, causing the confusion in the identification vegetation cover from wet snow condition.

Figures 3.2 and 3.3 show the typical SSM/I Tb signatures of the 6 snow classes in terms of cluster means (Table 3-II), using the average linkage and centroid method, respectively. Generally, both clustering methods yielded similar Tb patterns for each snow class. Depolarization effects were

TABLE 3-III
MINIMUM AND MAXIMUM OF THE SWI FOUND IN WET SNOW CLUSTERS

Clustering Method	Wet Snow with Sparse Vegetation		Wet Snow with Medium Vegetation	
	Min.	Max.	Min.	Max.
Average Linkage	3.42	17.34	3.28	25.06
Centroid Method	2.98	16.24	3.28	28.64

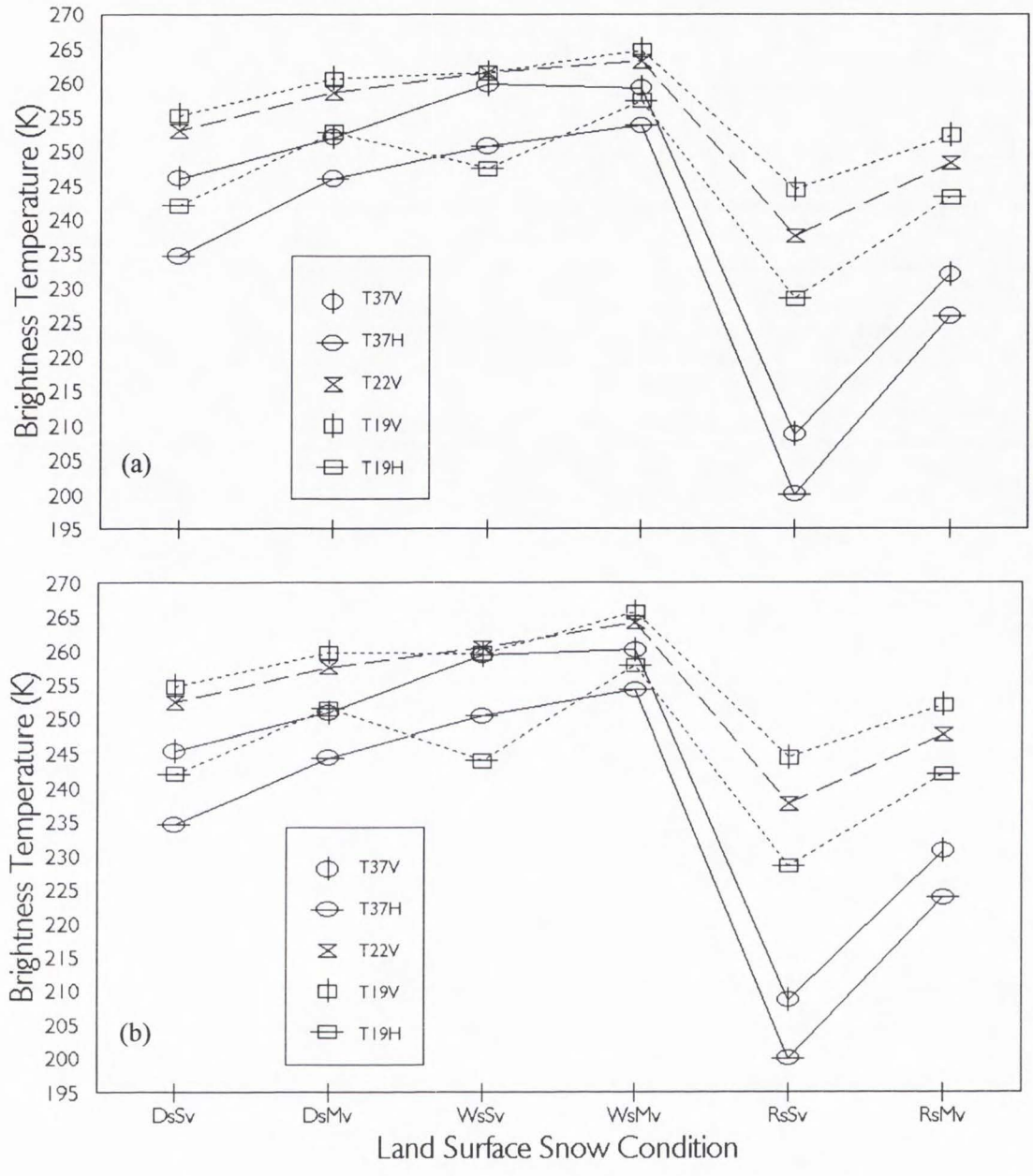

Figure 3.2. SSM/I cluster mean brightness temperatures for six land-surface snow conditions defined by (a) average linkage and (b) centroid method in cluster analysis with variables of five SSM/I lower frequencies observations.

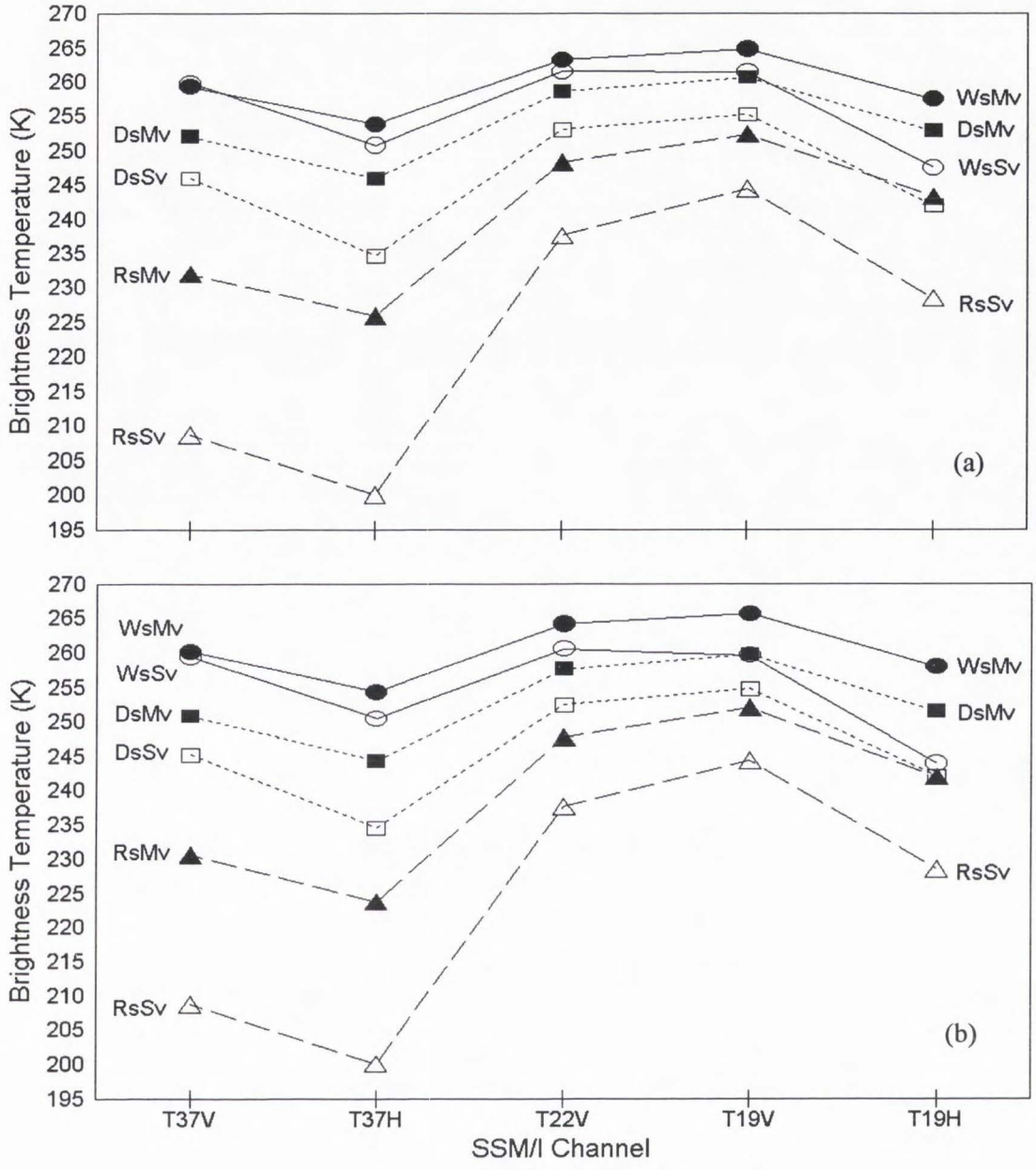

Figure 3.3. Six typical SSM/I Tb signatures of land-surface snow conditions defined by the cluster means from (a) average linkage and (b) centroid method in cluster analysis with variables of five SSM/I lower frequencies observations.

distinct between sparse- and medium-vegetated snow covers of dry, wet, and refrozen conditions, respectively. Evidently, SSM/I Tb's of medium-vegetated snow class were higher than that of spase-vegetated. These results confirm the fact that overlying vegetation tends to increase the Tb [5].

A smaller polarization difference at 37 GHz rather than at 19 GHz was seen in sparse-vegetated wet snow (WsSv) in Figure 3.2. This microwave behavior is due to a rapidly increasing Tb at 37 GHz horizontal polarization with an increase in liquid water content in snowpack [28]. For refrozen snow, more scattering and consequently much lower Tb's were observed at 37 GHz than at 19 GHz, because the melting and refreezing results in larger snow crystals which scatter the shorter wavelengths at 37 GHz [28].

Disagreement was found in certain snow classes defined by the cluster analysis in comparison with the ground-based snow classification (Table 3-IV). Since the ground-based snow condition was derived by averaging the ground-based point snow measurements within each SSM/I footprint in the study area, snow classification using this integration method may not be truly representative for the SSM/I footprint where the point data were less and the snow conditions varied spatially. Moreover, the ground-based snow conditions were determined by arbitrary assumptions in the estimation of concurrent air temperature. Error could be introduced due to the temporal variability of air temperature, causing different ground-based snow conditions related to SSM/I footprints of similar Tb signatures.

Table 3-V shows the mean brightness temperatures (in terms of interaction class means) of SSM/I footprints with the same snow condition found in both ground-based and cluster-analysis-based snow classification events (Table 3-IV). Results of the *t* test [19] showed that 49 out of the 60 interaction class means were not significantly different from those cluster means in Table 3-II. In addition, the means of significant difference were all associated with the medium-vegetated snow conditions. Such differences could be due to the depolarization effect of vegetation, which made

certain SSM/I Tb signatures of different snow conditions similar and clustered together.

As noted above, these interpretations provide the theoretical and statistical basis for using the six cluster-analysis-defined SSM/I Tb signatures as the appropriate inputs in ANN supervised training.

TABLE 3-IV
COMPARISON BETWEEN GROUND-BASED AND CLUSTER-ANALYSIS-BASED SNOW CLASSIFICATION

Clustering Method	Snow Cluster	Data Elements in Ground-Based Snow Class[§]			Data Elements in Snow Cluster
		Dry	Wet	Refrozen	
Average Linkage	DsSv	(112)	12	113	237
	DsMv	(1005)	72	531	1608
	WsSv	37	(26)	30	93
	WsMv	592	(150)	381	1123
	RsSv	9	3	(7)	19
	RsMv	156	5	(52)	213
Centroid Method	DsSv	(111)	11	94	216
	DsMv	(710)	40	362	1112
	WsSv	9	(8)	7	24
	WsMv	336	(121)	284	741
	RsSv	9	3	(7)	19
	RsMv	123	5	(39)	167

[§] Number in () represents the data elements of the interaction of both classification events.

TABLE 3-V

MEAN BRIGHTNESS TEMPERATURES OF THE INTERACTION OF BOTH GROUND-BASED AND CLUSTER-ANALYSIS-BASED SNOW CLASSIFICATION EVENTS AND THE PROBABILITY LEVEL FOR TESTING THE NULL HYPOTHESIS THAT THE INTERACTION CLASS MEANS ARE EQUAL TO THE CLUSTER MEANS WITH RESPECT TO DIFFERENT SNOW CONDITIONS BY TWO CLUSTERING METHODS

Clustering Method	Snow Condition (n)†	Mean Brightness Temperature (K)				
		T37V (Prob>|T|)‡	T37H (Prob>|T|)	T22V (Prob>|T|)	T19V (Prob>|T|)	T19H (Prob>|T|)
Average Linkage	DsSv (112)	245.50 (0.1482)	234.61 (0.9293)	252.58 (0.0855)	254.85 (0.0741)	241.95 (0.9324)
	DsMv (1005)	251.99 (0.7027)	245.96 (0.5846)	258.28 (0.0008)*	260.29 (0.0002)*	252.75 (0.8990)
	WsSv (26)	260.57 (0.1084)	250.74 (0.9540)	261.66 (0.5345)	261.67 (0.5015)	247.61 (0.6625)
	WsMv (150)	260.25 (0.0000)*	253.54 (0.4727)	263.62 (0.0014)*	265.12 (0.0029)*	256.15 (0.0000)*
	RsSv (7)	208.01 (0.7971)	198.26 (0.6005)	238.35 (0.3990)	245.34 (0.3158)	229.69 (0.1908)
	RsMv (52)	232.54 (0.1908)	226.60 (0.1902)	248.51 (0.3432)	252.48 (0.5235)	243.37 (0.7528)
Centroid Method	DsSv (111)	244.89 (0.2668)	234.60 (0.8616)	252.18 (0.1893)	254.49 (0.1555)	242.12 (0.7610)
	DsMv (710)	250.82 (0.7790)	244.57 (0.0989)	257.58 (0.5837)	259.66 (0.2580)	251.80 (0.0192)*
	WsSv (8)	259.58 (0.7509)	249.04 (0.2516)	260.25 (0.7275)	260.28 (0.2929)	244.68 (0.2103)
	WsMv (121)	260.79 (0.0107)*	253.93 (0.4191)	264.28 (0.2294)	265.68 (0.5894)	256.47 (0.0001)*
	RsSv (7)	208.01 (0.7971)	198.26 (0.6005)	238.35 (0.5552)	245.34 (0.3990)	229.69 (0.3158)
	RsMv (39)	230.83 (0.6126)	222.79 (0.1005)	248.59 (0.0308)*	252.95 (0.0121)*	241.92 (0.9005)

† (n), number of data elements in the interaction of both classification events.

‡ (Prob>|T|), the probability of a greater absolute value of *t* statistic under the null hypothesis.

* Means are significantly different at 0.05 level.

2) ANN Training and Validation Performances: Table 3-VI summarizes the training and validation performance of the ANNs with different topologies. Although all training processes converged at the designated RMS tolerance, there is no evidence to show that a smaller RMS tolerance may ensure a better ANN classification performance. The increases in error rates as RMS tolerances decreased could be a sign of overtraining, by which the ANN becomes too specific to the

TABLE 3-VI
RESULTS OF TRAINING EPOCHS AND ERROR RATE OF THE ANNS

Clustering Method	ANN Topology	ANN Learning Factor			Training Epoch	Error Rate (%)
		Learning Rate	Momentum Term	RMS Tolerance		
Average Linkage	5-5-6	0.05	0.9	0.215	1743	10.9
				0.200	2908	3.9
				0.185	7772	4.6
	5-10-6	0.05	0.9	0.300	1159	3.4
				0.200	5243	2.4*
				0.190	4329	6.6
	5-20-6	0.05	0.9	0.230	1708	8.7
				0.215	2597	5.6
				0.200	2603	6.0
	5-30-6	0.05	0.9	0.240	1998	10.1
				0.230	2552	7.2
				0.220	2098	16.9
Centroid Method	5-5-6	0.05	0.9	0.225	1984	5.5
				0.200	1989	4.9
				0.170	3271	5.5
	5-10-6	0.05	0.9	0.250	1440	6.7
				0.200	2268	5.5
				0.190	2247	6.1
	5-20-6	0.05	0.9	0.170	2920	9.8
				0.165	2269	8.0
				0.155	13224	14.7
	5-30-6	0.05	0.9	0.195	2785	7.4
				0.180	2191	6.1
				0.160	4440	6.7

* The best ANN found after training.

training data rather than learning the general patterns for a useful generalization ability [29].

The smallest error rate (2.4%) was reached by the ANN of 5-10-6 (Table 3-VI) trained with cluster means from the average linkage clustering method. Similar results were found in the 5-5-6 ANN using training data from the centroid clustering method. Regarding the number of nodes in the hidden layer, there was no evidence that more nodes in the hidden layer improved ANN performance. The best ANN (i.e., the 5-10-6 with 2.4% error rate) resulted from a number of training runs by trial and error.

The two-way contingency table (Table 3-VII) summarizes the classification accuracy of the best ANN applied to the validation data. Error rates (err%) were 3.8% (2/52) for DsSv, 2.9% (3/102) for DsMv, 3.2% (3/93) for WsSv, 0.0% (0/73) for WsMs, 0.0% (0/19) for RsSv, and 2.7% (2/75) for classified as either DsMv or WsSv conditions. Such misclassification could be due to the

TABLE 3-VII
TWO-WAY CONTINGENCY TABLE OF SNOW CLASSIFICATION BY THE ANN CLASSIFIER AND THE AVERAGE LINKAGE METHOD

Class from ANN	Cluster from Average Linkage Method						
	DsSv	DsMv	WsSv	WsMv	RsSv	RsMv	Total (err%)
DsSv	50	1	1	0	0	0	52 (3.8)
DsMv	0	99	0	3	0	0	102 (2.9)
WsSv	0	0	90	3	0	0	93 (3.2)
WsMv	0	0	0	73	0	0	73 (0.0)
RsSv	0	0	0	0	19	0	19 (0.0)
RsMv	1	0	0	0	1	73	75 (2.7)
Total (err %)	51 (2.0)	100 (1.0)	91 (1.1)	79 (7.6)	20 (5.0)	73 (0.0)	414 (2.4)

depolarization effect caused by the vegetation, which made the SSM/I Tb patterns similar. Overall, the results indicate that the ANN is useful in classifying snow conditions.

3) Application of the ANN Classifier to Case Images: Since the ANN classifier was trained to classify six snow conditions, a pretreatment using existing classification rules (from [2] and [26]) to remove the nonsnow cover classes (i.e., water body, flooding, and precipitation) was used in same case SSM/I overpasses. However, as indicated in [27], the Tb signatures of heavy vegetation, refrozen ground, and wet snow were almost the same. Thus, a posttreatment was needed to check possible heavy vegetation and frozen ground conditions embedded in vegetated wet snow conditions from the ANN classifier.

As shown in this study (Table 3-III), the SWI value (T19V-T37H) larger than 13 in the cluster of wet snow condition might indicate a frozen ground condition. Therefore, an SWI of 13 or 12 was used to remove the possible frozen ground conditions that might be embedded in the sparse- or medium-vegetated wet snow (WsSv and WsMv), classified by the ANN. In addition, SWI of WsSv or WsMv less than 10 or 9, respectively, was treated as snow-free according to [18]. The lower SWI value of 12 and 9 was selected because of the possible depolarization effect of vegetation in WsMv class. Consequently, as shown in Figure 3.4, the use of the ANN snow classifier for SSM/I image classification was accomplished by using pre- and posttreatment classification of the SSM/I data with other rules.

Figures 3.5 and 3.6 (A-1 to A-6) show the images of SSM/I footprints with ANN-based snow classification in a time series from the 21st day of the year (DOY) to the 26th DOY, 1990 in the western and central United States. For the comparison, images of the SSM/I footprints with rules-based snow classification [3] (Figures 3.5 and 3.7, B-1 to B6) and ground-based snow data (Figure 3.8, C-4 to C-6) were illustrated. In addition, images of vegetation cover, in terms of NDVIs, at SSM/I footprints were also represented in Figure 3.9 (D-4 to D-6).

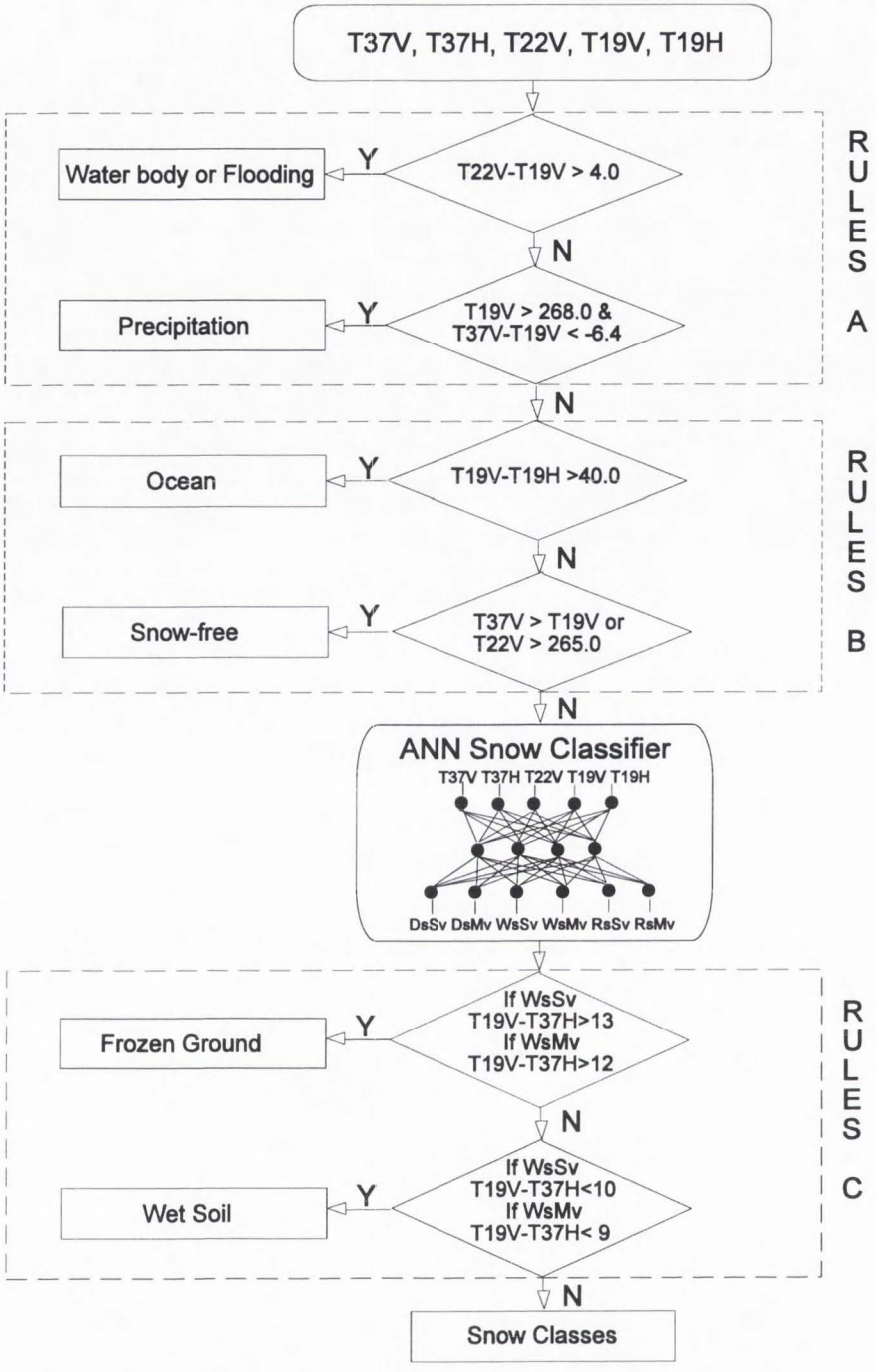

Figure 3.4. Flowchart of the application of the ANN snow classifier, accomplished with pretreatment by rules A from Neale *et al.* [2] and rules B from Grody and Basist [26], and posttreatment by rules C according to Sun *et al.* [18].

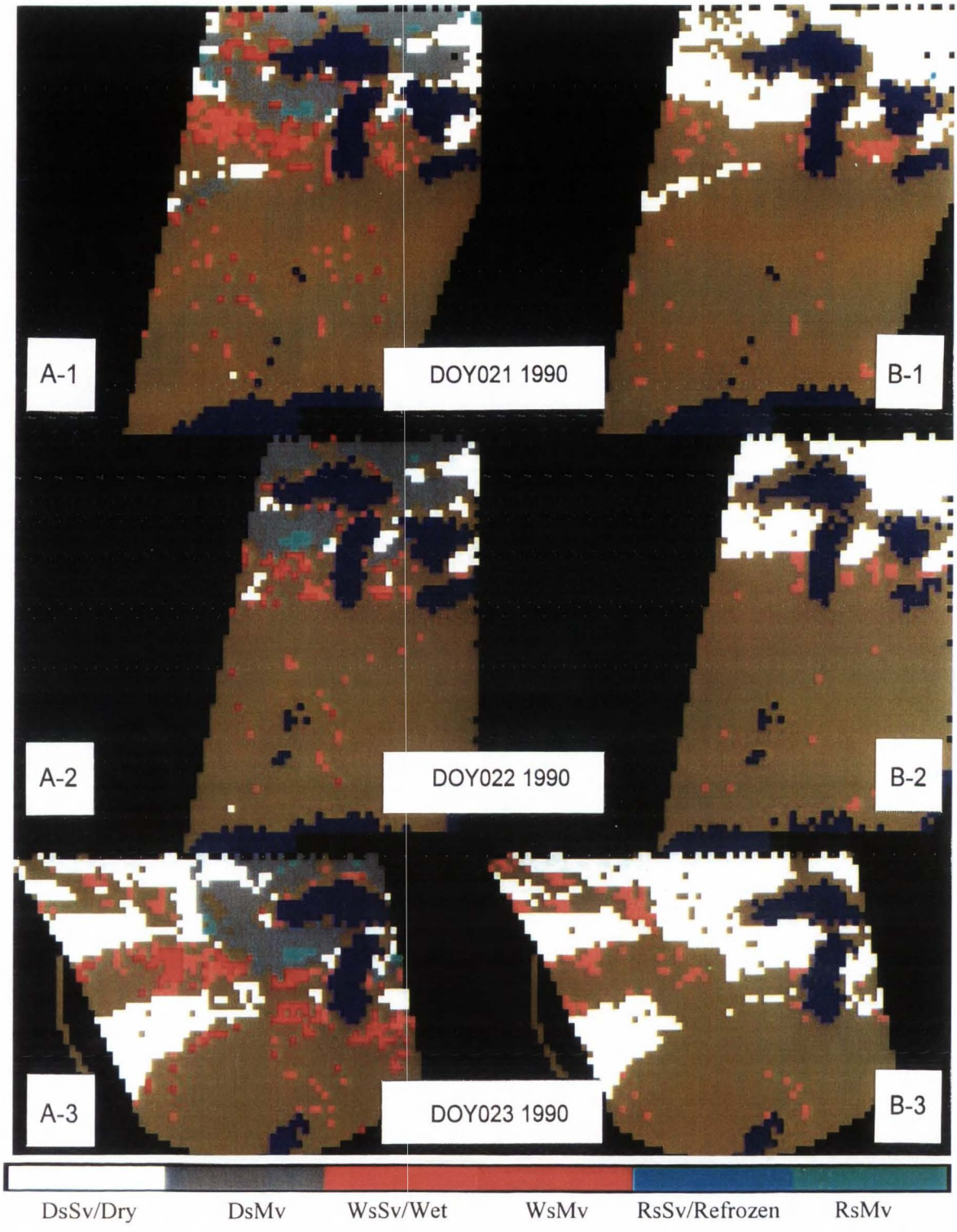

Figure 3.5. Images of the SSM/I footprints with snow conditions defined by the ANN classifier (in A series) and by the snow classification rules [3] (in B series) on DOY 21-23, 1990.

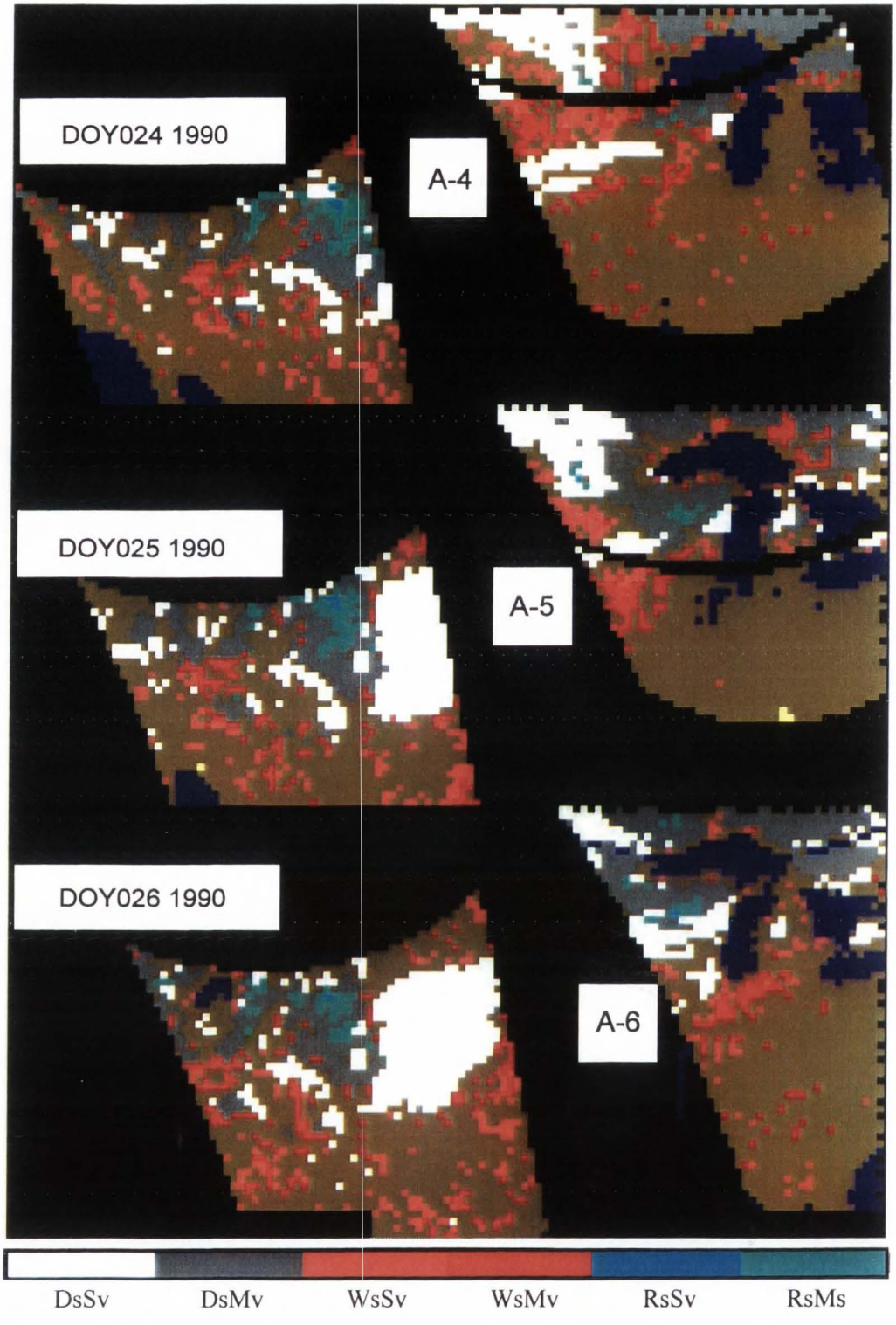

Figure 3.6. Images of SSM/I footprints with snow conditions defined by the ANN classifier on DOY 24-26, 1990.

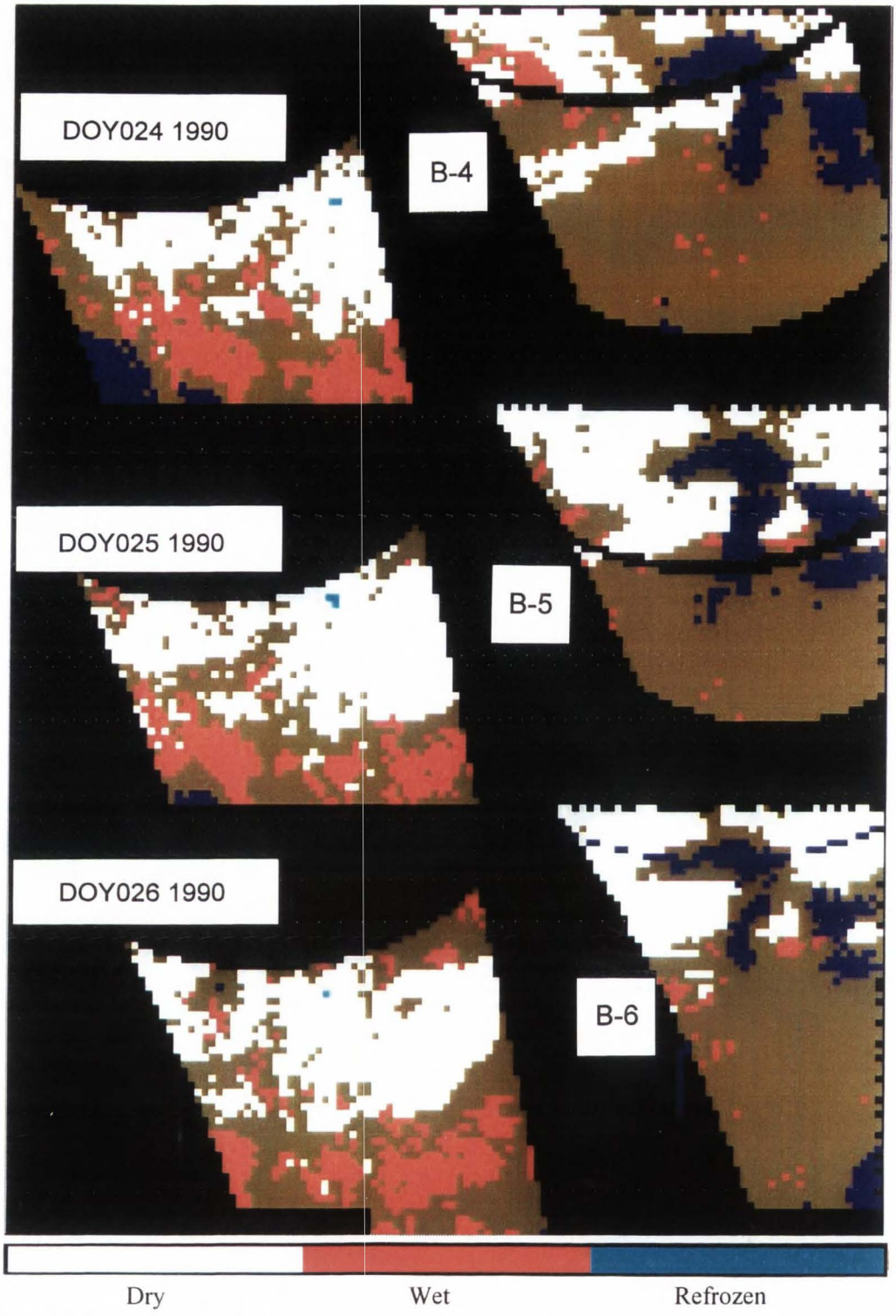

Figure 3.7. Images of SSM/I footprints with snow conditions defined by the snow classification rules [3] on DOY 24-26, 1990.

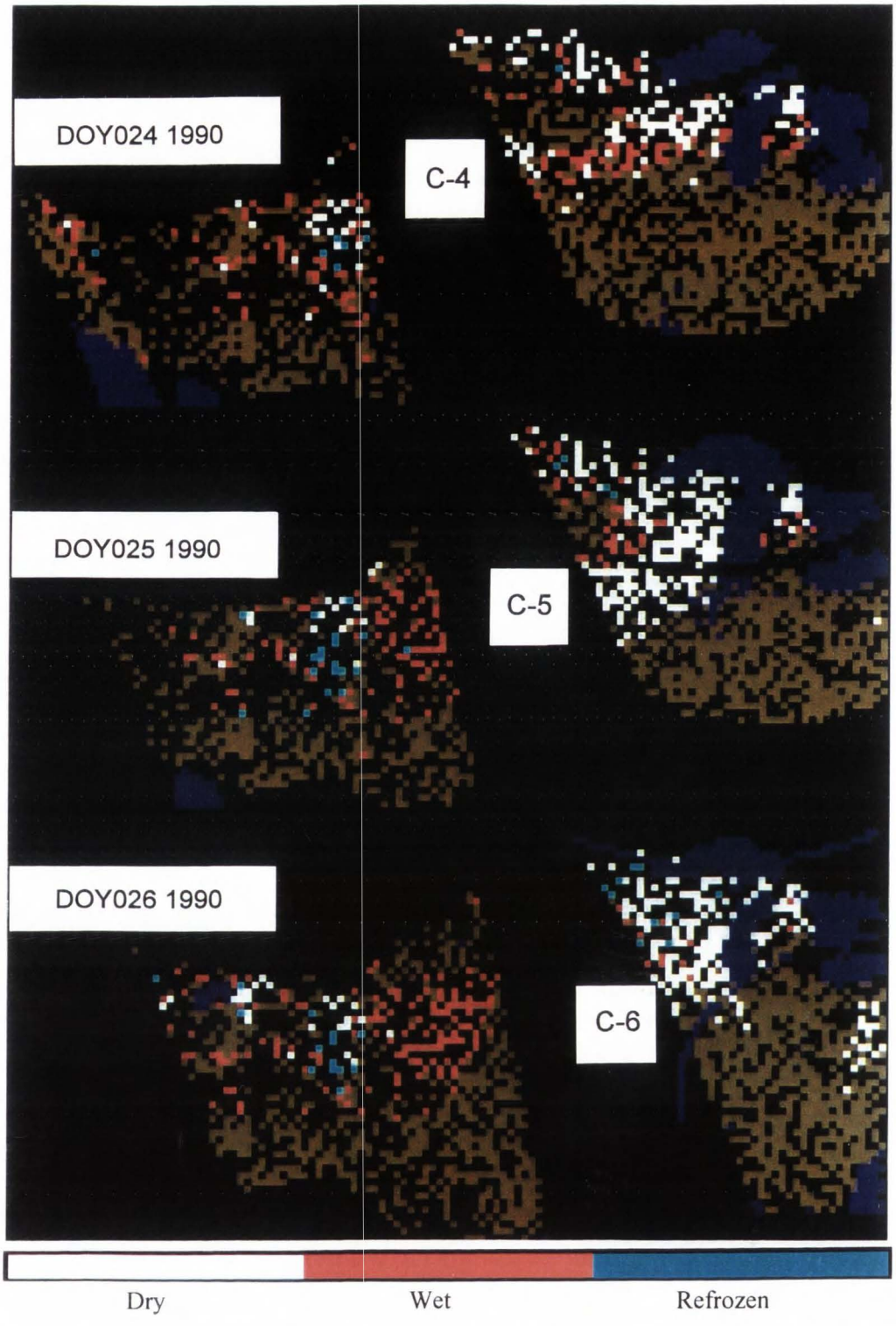

Figure 3.8. Images of ground-based snow conditions at NOAA weather stations with respect to SSM/I footprints on DOY 24-26, 1990.

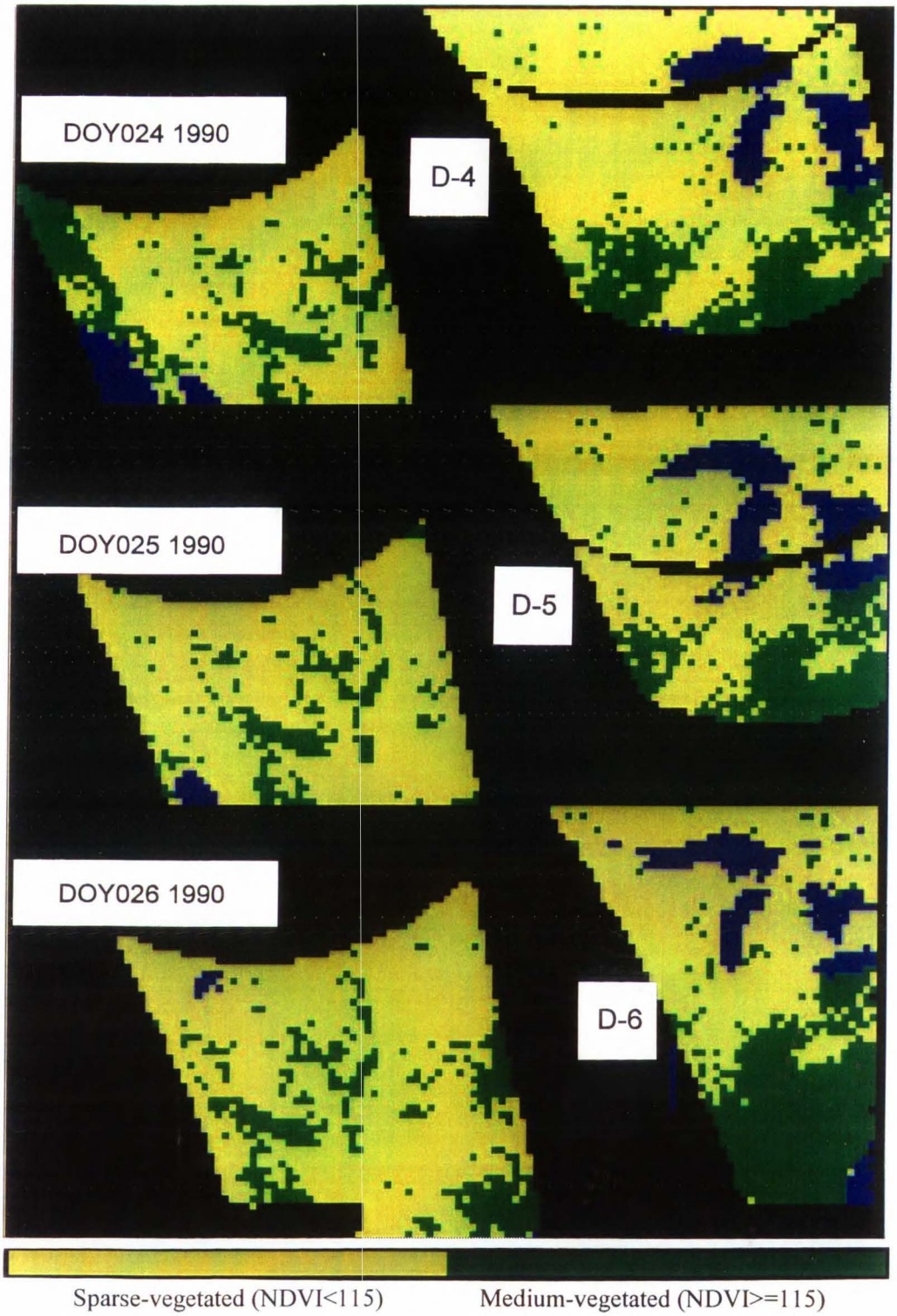

Figure 3.9. Images of monthly NDVI (Jan. 1990) with respect to SSM/I footprints on DOY 24-26, 1990.

In general, both ANN-based and rules-based methods showed similar snow geographical distribution patterns; i.e., the higher the latitude the more the snow cover, and the lower the latitude the more the wet snow. However, the ANN method revealed snow conditions in more detail. It is evident that the ANN-based snow classification outlined the medium-vegetated dry snow (DsMv) at mountainous areas and the sparse-vegetated dry snow (DsSv) at the central plains (Figure 3.6), whereas the rules-based method indicated only dry snow cover at those areas (Figure 3.7).

The main difference between the two classification methods was found in the identification of wet snow conditions. Results showed that most of the SSM/I footprints at northern areas classified as medium-vegetated wet snow (WsMv) by the ANN were defined as snow-free by the snow classification rules (Figures 3.5 to 3.7). Such disagreement could be due to the depolarization effect of the vegetation, making the snow classification rules, which were developed based on data over plains with sparse-vegetated snow cover, difficult to interpret medium-vegetated snow conditions.

Moreover, certain footprints in the southern areas were seen as snow-free condition by the ANN (Figure 3.6) but as wet snow by the rules-based method (Figure 3.7). This finding indicated that frozen ground could be misinterpreted as wet snow by the rules-based method since there are no particular rules for the discrimination of those two land surface conditions as defined in the post-treatment (i.e., rules C in Figure 3.4) by the ANN-based method.

In reference to the images of ground-based data (Figure 3.8), no snow shown in the southern areas confirmed that the SSM/I Tb patterns of frozen ground could be misclassified as wet snow conditions in both ANN and rules-based classification methods. Accordingly, the cutoff point of SWI at 13 or 12 for the frozen ground conditions in posttreatment of the ANN method (Figure 3.4) may not be appropriate.

The ANN-based snow distribution of dry and refrozen snow (Figure 3.6) agreed with the ground-based snow extent (Figure 3.8). However, most sparse-vegetated dry snow (DsSv) by the

ANN was classified as wet snow at ground weather stations. Since the images were from the SSM/I ascending portion, which was at 6 am local time, the ground-based wet snow could result from an error in the ground-based snow classification, due to a relatively high concurrent air temperature over a dry snow condition.

For the NDVI images (Figure 3.9), most of the sparse- and medium-vegetated areas were matched with the ANN-based sparse- and medium-vegetated snow conditions (Figure 3.6). However, disagreement was seen in the medium-vegetated wet snow (Figure 3.6 A-5) over a sparse-vegetated area (Figure 3.9 D-5). Possible explanation could be that the frozen ground was misclassified by the ANN as a wet snow condition. This finding further confirms that the Tb signatures of frozen ground should be examined and taken into account in the ANN training for land-surface snow classification.

E. Conclusions

To date, no single existing SSM/I classification algorithm has been able to identify land-surface snow conditions over varied terrain. This study presented a nonlinear retrieval method that overcomes the drawbacks and limitations of the existing classification methods for SSM/I land-surface snow classification.

Rather than relying on ground-based measurements, knowledge of passive microwave physics of typical SSM/I Tb signatures provides a more meaningful way to identify land surface types derived from an unsupervised cluster analysis. This study demonstrated the importance of cluster analysis in the identification of typical SSM/I Tb signatures of snow conditions using cluster means, by which a reliable ANN mapping performance was achieved.

The ANN supervised learning appears to be a useful method for the classification of snow conditions from satellite data over varied terrain. In ANN training, however, no particular rules can

be drawn for the selection of a number of hidden nodes and learning factors (learning rate, momentum, and RMS tolerance). Accordingly, the best ANN is more likely to be derived from a number of different training runs by trial and error. This study showed that the ANN has the potential to learn typical SSM/I Tb signatures.

Nevertheless, application of the SSM/I ANN classifier requires pre- and posttreatment procedures to classify certain snow-free surfaces. Ultimately, an ANN trained from Tb patterns of all land surface types is expected. Therefore, further research should focus on the identification of more land surface types, especially the heavy vegetation and frozen ground, over different terrains to improve the ANN classification efficiency by training ANN with all possible SSM/I Tb signatures and surface types.

F. References

[1] J. P. Hollinger, "DMSP Special Sensor Microwave/Imager calibration/validation," Naval Research Laboratory, Washington, DC, Final Report, vol. I, 1989.

[2] C. M. U. Neale, M. J. McFarland, and K. Chang, "Land-surface-type classification using microwave brightness temperatures from the Special Sensor Microwave/Imager," *IEEE Trans. Geosci. Remote Sens.*, vol. 28, no. 5, pp. 829-838, 1990.

[3] M. J. McFarland and C. M. U. Neale, "Land parameter algorithms validation and calibration," in "DMSP Special Sensor Microwave/Imager calibration/validation," J. P. Hollinger, Ed. Naval Research Laboratory, Washington, DC, Final Report, vol. II, 1991, pp. 1-108.

[4] J. V. Fiore, Jr. and N. C. Grody, "Classification of snow cover and precipitation using SSM/I measurements: case studies," *Int. J. Remote Sens.*, vol. 13, no. 17, pp. 3349-3361, 1992.

[5] D. K. Hall, M. Sturm, C. S. Benson, A. T. C. Chang, J. L. Foster, H. Garbeil, and E. Chacho,

"Passive microwave remote and in-situ measurements of Arctic and Subarctic snow cover in Alaska," *Remote Sens. Environ.*, vol. 38, no. 3, pp. 161-172, 1991.

[6] D. H. Staelin, "Progress in passive microwave remote sensing: nonlinear retrieval techniques," in *Remote Sensing of Atmospheres and Oceans*, A. Deepak, Ed. San Diego, CA: Academic Press, 19980, pp. 259-274.

[7] S. R. Rotman, A. D. Fisher, and D. H. Staelin, "Analysis of multiple-angle microwave observations of snow and ice using cluster-analysis techniques," *J. Glaciology*, vol. 27, no. 95, pp. 89-97, 1981.

[8] J. Key, J. A. Maslanik, and A. J. Schweiger, "Classification of merged AVHRR and SMMR Arctic data with neural networks," *Photogramm. Eng. Remote Sens.*, vol. 55, no. 9, pp. 1331-1338, 1989.

[9] Y. M. F. Lure, N. C. Grody, H. Y. M. Yeh, and J. S. J. Lin, "Neural network approaches to classification of snow cover and precipitation from spectral sensor microwave/imager (SSM/I)," presented at *8th Int'l Conf. Interactive Info. Proces. Sys. (IIPS) Meteorol., Oceano., and Hydrol.*, Atlanta, GA, 1992.

[10] C. Sun, H. D. Cheng, J. J. McDonnell, and C. M. U. Neale, "Identification of mountain snow cover using SSM/I and artificial neural network," in *Proc. 1995 International Conference on Acoustics, Speech and Signal Processing*, 1995, pp. 3451-3454.

[11] J. M. Zurada, *Introduction to Artificial Neural Systems*. St. Paul, MN: West Publishing Co., 1992.

[12] C. Sun and H. Cheng, "The use of class means in error backpropagation training for species identification of iris data," in *Proc. Joint Conference on Information Sciences*, 1995, pp. 556-559.

[13] G. G. Gutman, "Vegetation indices from AVHRR: an update and future prospects," *Remote*

Sens. Environ., vol. 35, no. 2&3, pp. 121-136, 1991.

[14] K. B. Kidwell, *Global Vegetation Index User's Guide*. Washington, DC: NOAA National Geophysical Data Center, Satellite Data Services Division, 1994.

[15] A. M. Hittelman, L. W. Row, J. J. Kineman, R. E. Habrmann, and D. A. Hastings, *Global View CD-ROMs and User's Manual*. Boulder, CO: NOAA National Geophysical Data Center, 1994.

[16] SCS, *Snow Survey and Water Supply Products Reference*. Portland, OR: USDA SCS West National Technical Center, 1988.

[17] NOAA, *Surface Land Daily Cooperative Summary of the Day TD-3200*. Asheville, NC: NOAA National Environmental Satellite Data and Information Service, 1989.

[18] C. Sun, C. M. U. Neale, and J. J. McDonnell, "Relationship between snow wetness and air temperature and its use in the development of an SSM/I snow wetness algorithm," in *Proc. AGU 15th Annual Hydrology Days*, 1995, pp. 271-280.

[19] SAS Institute Inc., *SAS/STAT Users Guide, Release 6.03 Edition*. Cary, NC: SAS Institute Inc., 1988.

[20] W. S. Sarle, "Cubic clustering criterion," SAS Institute Inc., Cary, NC, Technical Report A-108, 1983.

[21] G. W. Milligan and M. C. Cooper, "An examination of procedures for determining the number of clusters in a data set," *Psychometrika*, vol. 50, no. 2, pp. 159-179, 1985.

[22] SAS Institute Inc., *SAS Procedures Guide, Release 6.03 Edition*. Cary, NC: SAS Institute Inc., 1988.

[23] NeuralWare Technical Publications Group, *Using NWorks: an Extended Tutorial for NeuralWorks Professional II/PLUS and NeuralWorks Explorer*. Pittsburgh, PA: NeuralWare Inc., 1991.

[24] D. E. Rumelhart, G. E. Hinton, and R. J. Williams, "Learning internal representations by error propagation," in *Parallel Distributed Processing: Explorations in the Microstructure of Cognition*, Vol. 1, *Foundations*, J. A. Feldman, P. J. Hayes, and D. E. Rumelhart, Eds. Cambridge, MA: MIT Press, 1986, pp. 318-362.

[25] L. Prechelt, "PROBEN1 - a set of neural network benchmark problems and benchmarking rules," Karlsruhe University, Karlsruhe, Germany, Technical Report 21/94, 1994.

[26] N. C. Grody and A. Basist, "SSM/I Snow Cover Maps of the U.S.," anonymous FTP: ftp.nohrsc.nws.gov in /pub/bbs/ssmi/ssmi.txt, 1995.

[27] J. Hollinger, R. Lo, G. Poe, R. Savage, and J. Peirce, *Special Sensor Microwave/Imager User's Guide*, Washington, DC: Naval Research Laboratory, 1987.

[28] F. T. Ulaby, R. K. Moore, and A. K. Fung, *Microwave Remote Sensing: Active and Passive*, Vol. III, *from Theory to Applications*. Norwood, MA: Artech House, 1986.

[29] T. Masters, *Practical Neural Network Recipes in C++*. San Diego, CA: Academic Press, 1993.

CHAPTER 4

ON THE RETRIEVAL OF SNOW WATER EQUIVALENT AND WETNESS FORM SSM/I DATA USING A NEURAL NETWORK APPROXIMATOR

A. Abstract

The Special Sensor Microwave/Imager (SSM/I) is a useful tool for estimating snow properties because it is sensitive to the changes in snow physical and dielectric properties. To date, SSM/I snow water equivalent and snow wetness algorithms have been developed using regression techniques for a specific region and applied only to those similar geographic areas. In this study, we linked SSM/I observations [i.e., brightness temperatures (Tb's)] with concurrent ground-based snow water equivalent (SWE) and snow wetness (WETNESS) measurements as the input/output relations over a variety of geographical areas with different snow conditions. The data were used to develop an SSM/I ANN snow parameter approximator by which the SWE and WETNESS over different areas were simultaneously estimated from SSM/I observations. A single-hidden-layer ANN was designed to learn the input/output relations. The error backpropagation (backprop) training algorithm was applied to train the ANN. Agreement was found between the ANN-estimated and ground-based snow data. This study indicated that the ANN may overcome the limitations of the existing regression models in the estimation of SWE and WETNESS from SSM/I data over varied terrain. Further improvement is expected as more representative input/output relations between SSM/I observations and ground truth data over varied terrain and different snow conditions are established.

B. Introduction

Measurement of snow accumulation and melt during the snow season is important for water resources management and planning. Conventional snow measurements are made typically via a number of snow courses in the area of interest. Ground snow surveys, however, are point data

measurements and provide only a rough index of the spatial snowpack properties. In order to characterize seasonal snowpack parameters at the large scale, ground snow survey measurements are often supplemented by remotely sensed data [1].

Studies have shown that passive microwave radiometry has significant promise in the remote sensing of snow parameters, because its observed brightness temperatures (Tb's) are sensitive to the changes in snow physical and dielectric properties [2], [3], [4]. Recently, the Special Sensor Microwave/Imager (SSM/I) radiometers, flown on the Defense Meteorological Satellite Program (DMSP) F8, F10, and F11 satellites, have been used to produce global hydrologic data [5]. The SSM/I is a seven-channel, four-frequency, linearly polarized, passive microwave radiometric system, which measures both vertically (V) and horizontally (H) linearly polarized Tb's, at 19.35, 37.0, and 85.5 GHz and only vertical polarization at 22.235 GHz [6].

Unlike in situ methods, the SSM/I provides an indirect estimate by using parameter retrieval algorithms, with Tb's as inputs, to derive information about snow properties. In order to develop the algorithm, either empirical or theoretical interpretations of Tb observations along with ground truth data are required. In the application of the algorithm, the Tb observations are known, and the state of variables is inferred. Thus, conventional snow measurements have always played an important role in the development of SSM/I snow parameter retrieval algorithms.

The basic hydrological measure of a snowpack is the snow water equivalent (SWE), which is the amount of water that would be obtained if the snow column was melted completely. In most operational snow surveys, however, only the snow depth (SD) is measured and is converted to SWE by assuming a snow density of 0.10 [7]. In the United States, daily SD over plains areas is measured by the National Oceanic and Atmospheric Administration (NOAA) weather observing network [8]. Manual measurements of NOAA weather observing network are not practical in deep mountain snowpacks. Consequently, the Soil Conservation Service (SCS) has established an automatic SWE

measurement network system, called SNOTEL (SNOwpack TELemetry) [9], to complement the NOAA snow course data over high-mountain areas in the western United States.

Measurement of snow wetness (snowpack free water content) is essential for determining the onset of melt. Conventional observation of snow wetness through ground-based networks has not yet been established in the United States. Therefore, spatial snow wetness data are often obtained by estimation using empirical equations (e.g., [10]).

To date, SSM/I algorithms for retrieving snow wetness, SWE, and SD have been developed [10], [11], [12]. These algorithms have been based mostly on statistical regression analysis to quantify the relationship between one or more SSM/I Tb variables and a single snow parameter in flat, nonforested areas. Since SSM/I Tb increases as the vegetation density over the snowpack increases [13], the existing algorithms often overestimate snow wetness and underestimate SD or SWE in areas with evergreen forest cover. In addition, the SD and SWE algorithms are typically restricted to dry snow conditions. Since SSM/I Tb increases as the snow wetness increases, an underestimated SD or SWE is expected in areas where the snowpack is wet. Accordingly, existing SSM/I snow parameter algorithms are limitated as general approaches for snow parameter retrieval over different complex cover areas and snow conditions.

Recently, artificial neural networks (ANNs) have been used to retrieve snow parameters from passive microwave data [14], [15], [16]. Results show that ANNs have potential to learn Tb patterns whose complexity and nonlinearity make retrieval accuracy by existing regression approaches impossible. According to [17], the artificial neural network can be regarded as a graphic notation for a large class of algorithms or a function represented by the composition of many basic functions. Studies in [14], [15], using an ANN to recall snow parameters simultaneously from Tb observations, have shown that a unified SSM/I snow parameters algorithm can possibly be developed using an ANN.

Most of the previous ANNs have been trained with input/output relations (i.e., SSM/I Tb's and snow parameter values) from simulated data generated from a radiative transfer model (RTM) (e.g., [14], [15]). In this way, snow parameters at an area of interest are then inferred by the ANNs from passive microwave observations. Since snow properties in nature are typically complex, there are many unknown radiative physical characteristics that need to be determined by rather arbitrary assumptions in the RTM simulation. Although the ANN can learn from the input/output of simulated relations, the parameter retrieval behavior of the ANN on real cases often remains unknown, because the coarse resolution of the SSM/I makes microwave responses deviate largely among footprints for a same-snow condition. This causes the input/output relations to be extremely random and difficult to simulate.

For random variables data, the technique for finding a mapping between inputs and outputs is referred to stochastic approximation [18]. Following [19], an ANN with error backpropagation training is equivalent to a form of stochastic approximation. With the assumption that SSM/I observations and ground-based snow parameters are random variables with respect to each other, it is possible that an ANN can be trained with the inputs of SSM/I observations and the outputs of corresponding ground-based snow measurements.

This study sampled the input/output relations between SSM/I observations and concurrent ground-based snow wetness and SWE measurements over a variety of geographical areas. An ANN was trained with the relations to develop an SSM/I ANN snow parameter approximator, by which the snow water equivalent and snow wetness over different areas can be simultaneously estimated from SSM/I observations.

C. Methods

1) SSM/I and Ground Truth Data: A study area bounded by latitude of 40°N to 45°N and

longitude of 100°W and 115°W, which contained both plains and mountainous region in the western United States, was selected to represent a variety of vegetated terrain. SSM/I Tb's and ground-based snow measurements were obtained from Oct. 1, 1989 to May 30, 1990.

Seven SSM/I Tb's from the DMSP-F8 satellite were obtained from the Naval Research Laboratory. Due to the increase in noise level of both SSM/I 85.5 GHz channels on DMSP-F8 satellite during 1988, only five Tb's of the lower frequency channels, denoted as T19V, T19H, T22V, T37V, and T37H, were used in this study.

Ground-based measurements of daily SWE, and maximum, minimum, and average air temperature over mountainous terrain were obtained from the SCS SNOTEL system [9]. Daily SD, maximum and minimum air temperature, and air temperature at the observing time in the plains were derived from the NOAA weather-observing network [8].

2) Ground-Based Snow Classification and Snow Parameter Estimation: Daily snow condition of each SNOTEL or NOAA weather station at DMSP-F8 local crossing time, either 6 am or 6 pm, was flagged as: (1) snow-free (if SWE or SD was equal to zero), (2) dry snow (while SWE or SD was accumulated from previous time and the concurrent air temperature was below 3.5°C by which the snow wetness was assumed to be less than 3% by volume according to the linear regression model of snow wetness as a function of concurrent air temperature in [10]), (3) wet snow (as SWE or SD was not equal to zero and the concurrent air temperature was large than or equal to 3.5°C), or (4) refrozen snow (if the concurrent air temperature was below freezing point and the snow condition of previous time was either wet or refrozen). For SNOTEL stations, the concurrent air temperature at 6 am and 6 pm were set to be the daily minimum and average air temperature, respectively. For NOAA weather stations, the concurrent air temperature at 6 am or 6 pm was set to be the air temperature at observing time if the time was between 4 am and 7 am or between 4 pm and 7 pm, respectively; otherwise, the concurrent air temperature at 6 am was equal to the minimum air

temperature and that at 6 pm was extrapolated by assuming the maximum air temperature was at 2 pm and linearly decreased to the temperature at observing time, which was after 2 pm or the maximum air temperature of the previous day decreased to the air temperature at observing time which was before 2 pm. Because of the lack of SWE data, SD data at NOAA stations were converted to SWE by assuming a snow density of 0.2 for dry snow, 0.3 for wet, and 0.4 for refrozen.

Since the latitude/longitude coordinates of the SSM/I footprints change with each overpass, a neighborhood merging method was employed to integrate the SSM/I and in situ data into one database. The database was built by searching the ground weather stations that fell within a 15-km search radius around a particular SSM/I latitude/longitude location (i.e., approximately the size of a 37.0 GHz footprint). Values of SWE, and air temperature were then averaged for that SSM/I footprint, respectively. Based on the linear relationship between snow wetness and air temperature in [10], snow wetness (WETNESS) at each footprint was also estimated.

3) ANN-Based Snow Classification and Input/output Data Pair Preparation: Since the ground-based snow conditions (i.e., dry, wet, and refrozen snow) were determined in part by arbitrary assumptions in the estimation of concurrent air temperature, error could be introduced due to the temporal variability of air temperature. This could result in different ground-based snow conditions being related to SSM/I footprints of similar Tb signatures. The SSM/I ANN snow classifier [20] was used to classify SSM/I Tb's in the database. Only data of those SSM/I footprints classified as snow-covered [i.e., dry snow with sparse (DsSv) or medium (DsMv) vegetation, wet snow with sparse (WsSv) or medium (WsMv) vegetation, or refrozen snow with sparse (RsSv) or medium (RsMv) vegetation] with matched ground-based snow conditions and meaningful ground-based snow data (i.e., SWE great than zero) were taken into account for the input/output (i.e, input of five Tb's and output of SWE and WETNESS) data pairs. By doing so, the error in estimation of SWE or WETNESS with respect to a possible true snow condition was reduced. Thus, a subset database of

input/output data pairs was created.

4) Interpretation of Relationships Between Input and Output Data: Correlation analysis was performed to measure the strength of the linear associations between the input (i.e., SSM/I Tb) and output (i.e., SWE or WETNESS) variables in each snow class. Due to the sensitivity of Tb at 37.0 and 19.35 GHz to snow properties [2], scatterplots were used to plot data of each pairs of T37V and SWE for each of the six snow conditions, and T19V−T37H and WETNESS for each of the two wet snow conditions as points in two-dimensional space to observe if there is any pattern in the data.

5) ANN Training, Validation, and Test Data Sets: As indicated in [21], the proportional representation of classes in the entire training data can have a profound influence on the ANN performance. Moreover, based on a prior study [22], the frequency distributions of data elements in each snow class may also be important to the ANN training. Consequently, data elements in the subset database were sorted by snow condition and by values of SWE if snow was dry or refrozen or by values of WETNESS if snow was wet. According to the number of the smallest data elements in the frequency distributions (Table 4-I), 180 data elements of each snow condition with same data size (i.e., 30 elements) for each frequency from the subset database were selected to form the training data set. Duplication was applied to those elements selected from the frequency with fewer than 30 elements. The rationale was to make the data sets as representative for the whole data and as balanced in size for each frequency distribution of the three classes as possible. From the remaining elements, validation and test data sets were created as per the training set selection.

6) ANN Training and Testing: A single-hidden-layer ANN was created. It consisted of an input layer of five nodes representing the inputs of five Tb's, and an output layer of two nodes representing the desired SWE and WETNESS snow parameters. For the hidden layer, the number of nodes was selected at 5, 10, 20, 30, 40, and 50. Given the number of nodes in each layer from input to output as a sequence, the ANN topology was represented as 5-N-2, where N is the number

TABLE 4-1
ELEMENTS SELECTED FOR ANN TRAINING AND TESTING

Snow Condition	Frequency Distributions of SWE or WETNESS	Number of Elements in Data Set			
		Subset	Training (×m)[§]	Validation	Test
Dry	0-100 mm	824	30	5	5
	100-200 mm	481	30	5	5
	200-300 mm	255	30	5	5
	300-400 mm	128	30	5	5
	400-500 mm	87	30	5	5
	500-800 mm	60	30	5	5
Wet	0-1 %	52	30	5	5
	1-2 %	23	15×2	4	4
	2-3 %	25	15×2	5	5
	3-4 %	17	15×2	1	1
	4-5 %	14	10×3	2	2
	5- %	17	15×2	1	1
Refrozen	0-100 mm	69	30	5	5
	100-200 mm	64	30	5	5
	200-300 mm	80	30	5	5
	300-400 mm	45	30	5	5
	400-500 mm	23	15×2	4	4
	500-800 mm	19	15×2	2	2
Total Elements		2283	540	74	74

[§] m: multiplier for data duplication.

of hidden nodes. In addition, a bias node, functioning similar to a constant in a regression, was connected to the nodes in the hidden and output layers.

The error backpropagation training algorithm [23] was applied to train the ANN. This method allows forward feeding node outputs through layers and backward propagating mapping errors to adjust connection weights between layers. According to [24], having a larger learning rate at the hidden layer than that at the output layer can decrease learning time. Learning rate at the hidden layer was set at twice the rate of the output layer. Learning rates were 0.05 and 0.025, for hidden layer and output layer, respectively. The momentum method [25] (i.e., adding the current weight adjustment with a proportion of the previous weight change) was applied to accelerate the learning process. The momentum term was set at 0.90 in this study.

The activation function applied to the net input of nodes in the hidden and output layers was a logistic [24], which maps the net output into the range between 0 and 1. Accordingly, the input were scaled between 0 and 1 with respect to a Tb range from 180 to 280 K to represent the input attributes in the ANN. The desired output data of SWE and WETNESS were also scaled between 0 and 1 with respect to a SWE range from 0 to 800 mm and a WETNESS range from 0 to 10 % by volume, respectively.

The training process started by randomly initializing all connection weights between -0.1 and 0.1. After each training epoch (i.e., the time as all the input/output pairs in the training data set were processed by the ANN), a root-mean-squared (RMS) error was computed on the validation data to examine the training performance of the ANN. The training process was repeated until the minimum RMS error was reached.

After training, the test data set was used to evaluate the approximation performance of the resulting ANNs. The closeness of linear relationship between ANN-estimated and ground-based values was measured by the correlation coefficient (r). The ANN with the best overall r value

became the ANN approximator.

7) Comparison Between ANN and Regression Models: SSM/I data for sparse-vegetated dry snow condition in the subset database, which were not used in ANN training and testing, were selected to evaluate the ANN approximator performance on SWE estimation. The SWEs estimated by the ANN from the SSM/I data were first compared to the ground-based SWEs. Data elements with incompatible ANN-estimated and ground-based SWEs were treated as possible noise patterns and eliminated in the model comparison. The remaining ANN-estimated SWEs were then compared to those estimated by the existing SSM/I SWE retrieval algorithm [26]:

$$SWE = -20.7 - 49.27(T37V - T19V)/18.0 \quad (1)$$

and by the SSM/I SD retrieval algorithm [11]:

$$SD = 444.5 - 1.795(T37V) \quad (2)$$

where SD was further converted to SWE under the assumption that the average density of dry snow is 0.2.

In addition, data of SSM/I Tb's of a footprint with concurrent snow wetness estimations during field work at Snowville, Utah [10] were used to evaluate the ANN approximator on WETNESS estimation. Results were compared to those estimated by the existing SSM/I WETNESS algorithm [10]:

$$WETNESS = -4.75 + 339.53(TD)^{-1} - 6159.53(TD)^{-2} + 40112.00(TD)^{-3} \quad (3)$$

where TD = T19V - T37H.

D. Results and Discussion

1) Interpretation of Linear Relationship: Figures 4.1 to 4.3 show similar proportion of observations in each of the four quadrants divided by the reference lines at the variable means (i.e., $\bar{x}$ for SWE and $\bar{y}$ for T37V). This reflects the fact that there was no significant relationship between

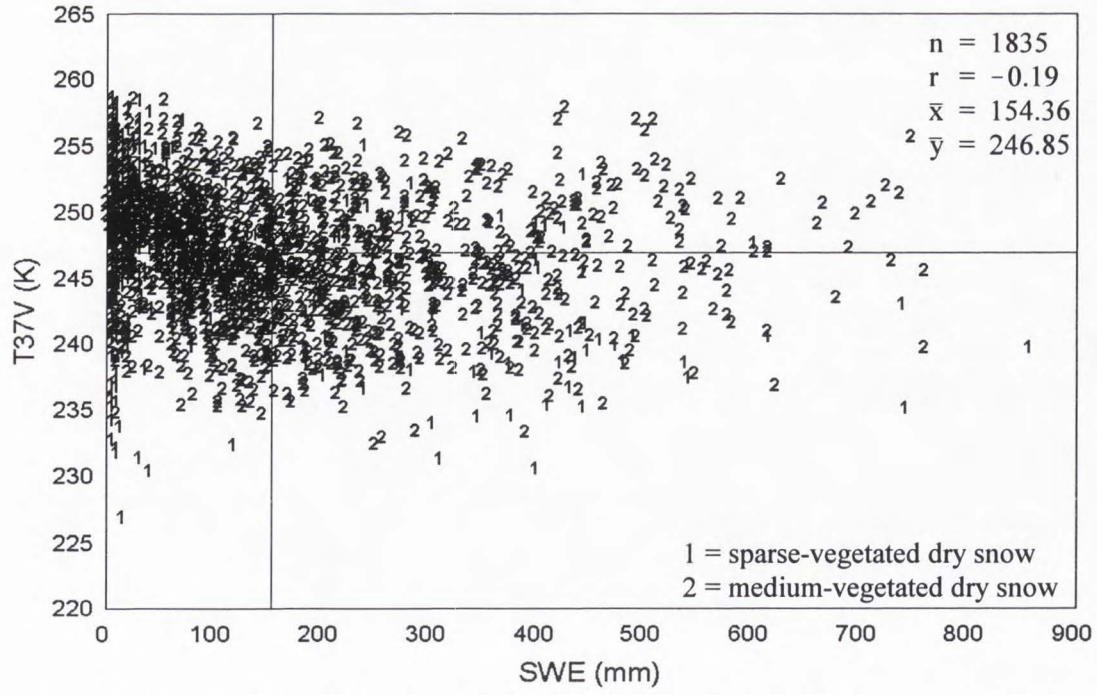

Figure 4.1. SSM/I Tb at 37.0 GHz versus snow water equivalent for dry snow conditions.

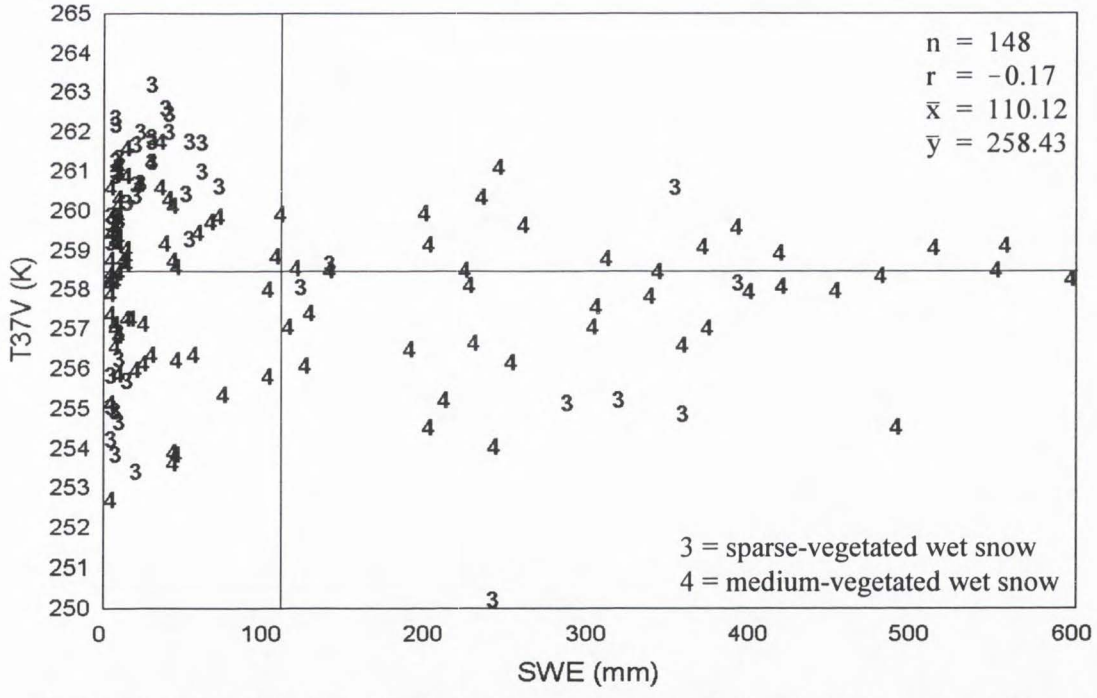

Figure 4.2. SSM/I Tb at 37.0 GHz versus snow water equivalent for wet snow conditions.

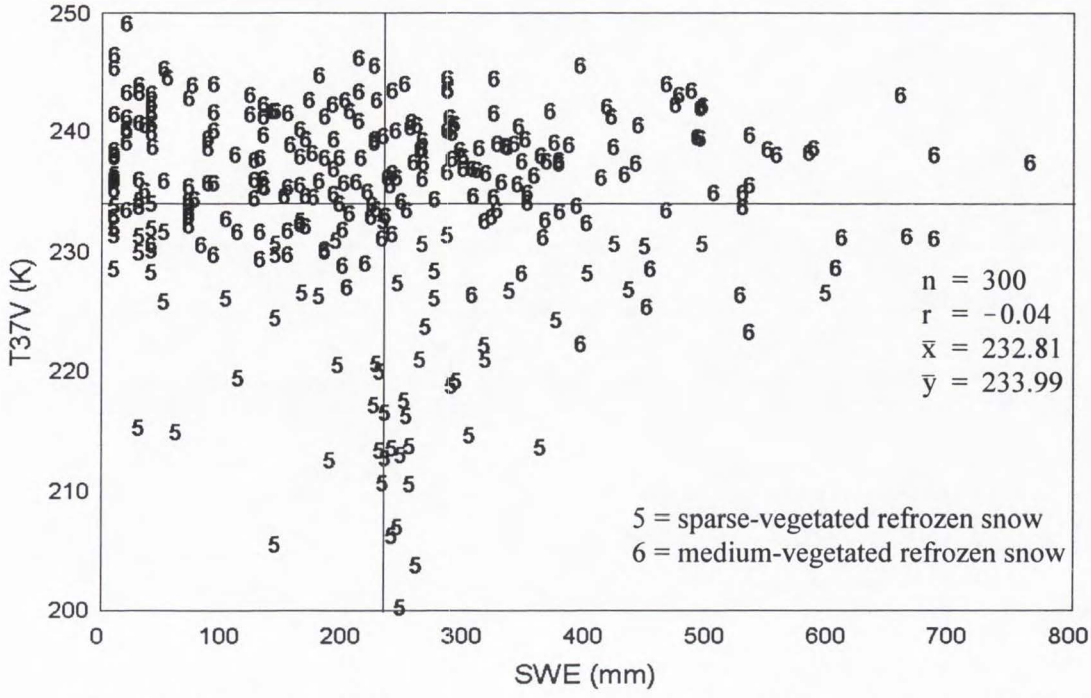

Figure 4.3. SSM/I Tb at 37.0 GHz versus snow water equivalent for refrozen snow conditions.

T37V and SWE for each snow class. On the average, Tb observed at the footprint of snow with medium vegetation was higher than that of snow with sparse vegetation. It is evident that the effect of vegetation cover may mask the microwave emission from the underlying snow and raise the Tb by the emission from the vegetation.

Table 4-II summarizes the correlation coefficient (r) between different pairs of input and output variables in each snow class defined by the ANN-based snow classification. No strong linear relationships were found based on data for each SSM/I single-channel variable. This is because the r values were all close to zero. The nonlinearity found in the data may imply that different geographic areas may have different snowpack conditions, vegetation cover, underlying soil conditions, and surface temperatures, making the extrapolation of relationships between Tb observations and SWE from one area to another more difficult [27]. In addition, the melting and

freezing process in spring may cause increased heterogeneity in grain size, ice layer, and surface crust. As a result, the development of a linear regression model for retrieving SWE over different geographical regions from any SSM/I single-channel observations is likely impossible.

For snow wetness, the relatively lower values of Tb difference (i.e., T19V−T37H) in wet snow with medium vegetation (Figure 4.4) could be a sign of depolarization effects due to the vegetation. In addition, the previously developed regression model [10] was not able to explain the variations in both sparse- and medium-vegetated wet snow conditions. According to [10], the snow wetness regression model was based on single point estimates of WETNESS in relation to the Tb difference of a corresponding sparse-vegetated SSM/I footprint. Thus, the predicted line by the regression model certainly was not in agreement with the ground-based data that were integrated from different point data measurements at corresponding SSM/I footprints over varied terrain.

TABLE 4-II
CORRELATION (R) BETWEEN INPUT AND OUTPUT VARIABLES

Snow Class	Sample Size	Output Variable	Input Variable				
			T37V	T37H	T22V	T19V	T19H
Dry	1835	SWE	−0.19	0.05	−0.07	−0.03	0.13
Wet	148	SWE	−0.17	0.22	0.15	0.17	0.28
Refrozen	300	SWE	−0.04	0.05	−0.10	−0.05	−0.01
Wet	148	WETNESS	0.17	−0.05	−0.01	−0.04	−0.16

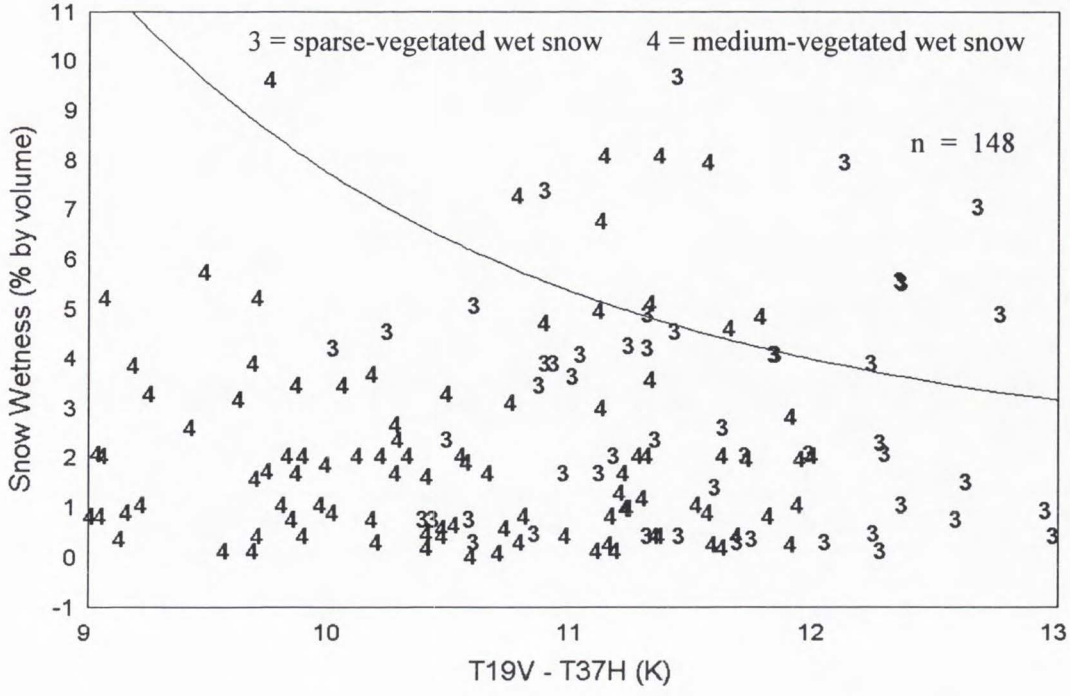

Figure 4.4. Snow wetness versus SSM/I T19V−T37H difference for wet snow conditions and the regression line according to [10].

2) ANN Training and Approximation Performances: Table 4-III summarizes the training performance of the ANN with different topologies. For each ANN topology, there was no evidence to show that a smaller or a higher learning rate may ensure a better ANN performance (i.e., a smaller minimum RMS error). The relatively higher minimum RMS error that resulted in each ANN topology could be the sign that the ANN was trapped in local minimum during training [21]. Overall, better training performance was derived from a number of training runs at different learning rates by trail and error.

Table 4-IV shows the result of the approximation performance of the trained ANN on a test data set. Generally, for most ANN topologies, the estimation of SWE was in agreement with the ground truth at correlation coefficients of around 0.6. The most significant correlation ($r = 0.668$)

TABLE 4-III
RESULTS OF ANN TRAINING AND VALIDATION

ANN Topology	Learning Rate	Training Epochs	Minimum RMS Error	
			SWE	WETNESS
5-10-2	0.1	12439	0.18917	0.09225
	0.2	14014	0.19274	0.09149
	0.3	2684	0.19756	0.09118
	0.4	2044	0.19940	0.08988
	0.5	1499	0.20790	0.08987
5-20-2	0.1	9278	0.19266	0.09097
	0.2	9846	0.18661	0.08880
	0.3	8199	0.18956	0.08646
	0.4	6317	0.19414	0.08632
	0.5	3422	0.19271	0.08661
5-30-2	0.1	10356	0.18901	0.09212
	0.2	9573	0.19465	0.08898
	0.3	7783	0.18858	0.08546
	0.4	6801	0.18699	0.08433
	0.5	3639	0.19285	0.08640
5-40-2	0.1	11438	0.18956	0.08939
	0.2	11571	0.18941	0.09025
	0.3	18961	0.19701	0.08893
	0.4	17544	0.19360	0.08512
	0.5	3102	0.20859	0.09125
5-50-2	0.1	11111	0.19412	0.09149
	0.2	13348	0.19039	0.08968
	0.3	14384	0.18923	0.08466
	0.4	11166	0.21394	0.09078
	0.5	33149	0.19626	0.08266

TABLE 4-IV
RESULTS OF ANN APPROXIMATION ON TEST DATA SET

ANN Topology	Learning Rate	Correlation Coefficient (r)	
		SWE	WETNESS
5-10-2	0.1	0.664	0.128
	0.2	0.631	0.112
	0.3	0.644	0.060
	0.4	0.668	0.073
	0.5	0.629	0.042
5-20-2	0.1	0.653	0.168
	0.2	0.647	0.263
	0.3	0.655	0.212
	0.4	0.610	0.188
	0.5	0.598	0.139
5-30-2	0.1	0.658	0.125
	0.2	0.648	0.198
	0.3	0.645	0.261
	0.4	0.629	0.382
	0.5	0.595	0.164
5-40-2	0.1	0.652	0.185
	0.2	0.639	0.150
	0.3	0.556	0.222
	0.4	0.564	0.205
	0.5	0.526	0.074
5-50-2	0.1	0.636	0.157
	0.2	0.628	0.162
	0.3	0.626	0.257
	0.4	0.468	0.107
	0.5	0.614	0.052

between the ground-based and the ANN-estimated SWEs (i.e., by the 5-10-2 ANN at learning rate of 0.4) in test data set is shown in Figure 4.5. Results show an underestimated SWE in the range over 400 mm. The underestimates could be due to the limitations of the effective passive microwave penetration depth of snow [28] or the effect of overlying vegetation [13] by which the microwave emission of snow above 400 mm may similar to that of snow under 400 mm or less, causing a confusion in the ANN approximation.

No significant correlation was found between ANN-estimated and ground-based snow wetness data (Table 4-IV). One possible reason could be that the total sample size of wet snow was small (i.e., 148 data elements compared to 300 in refrozen and 1835 in dry snow as shown in Table

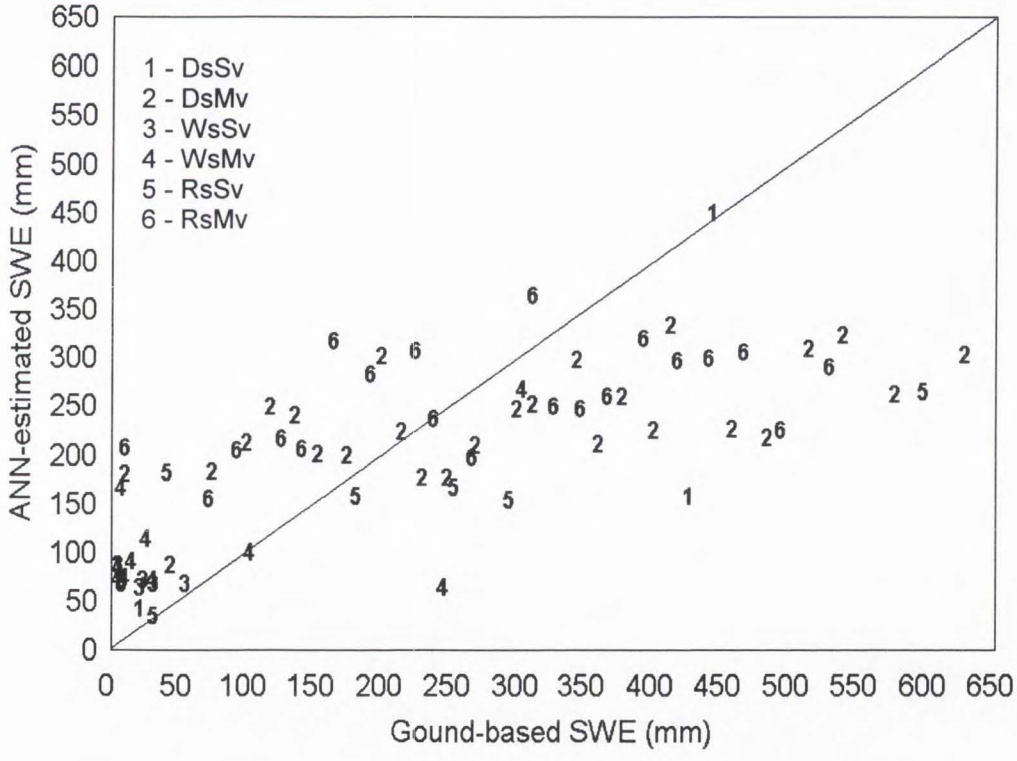

Figure 4.5. Scatterplot of ground-based versus ANN-estimated SWEs in test data set.

4-I) and contaminated by noise patterns at certain levels due to the estimation from uncertain air temperature, resulting in a nonrepresentative snow wetness data in the test set by which the noise patterns were new to the trained ANN. This explanation was confirmed by evaluating the ANN approximation from SSM/I data at a footprint in Snowville, Utah and comparing the ANN-estimated WENTESS values to the concurrent estimations of snow wetness during field work in [10]. As seen in Table 4-V, better agreements ($r > 0.6$) were found between ANN-estimated and ground-based WETNESS values using the Snowville footprint data. This result may also imply that the ANN has the potential to learn the prototypical input/output patterns from samples that are contaminated by noisy data at certain allowable levels.

Overall, in consideration of the optimal correlation between ANN-estimated and ground-based values in both SWE and WETNESS parameters (Table 4-IV and 4-V), the 5-20-2 ANN trained at a learning rate of 0.3 was eligible for inclusion as the ANN approximator.

3) Algorithm Comparison: Figure 4.6 illustrates the comparison between the SWE estimations by the ANN approximator and those by the existing regression models in the sparse-vegetated dry snow condition. Regardless of variation of ground-based SWEs, the SD retrieval algorithm (Eq. 2) formed a linear regression line with respect to the T37V. Although the SWE algorithm (Eq. 1) was a better predictor than the SD algorithm, both models showed an underestimation of SWEs in the high range, with respect to the ground-based SWEs. Since the SWE model was developed based on data from the western prairie region [26], it may not be suited for use in other regions, such as this study area, where a variety of terrain and vegetation is present. On the other hand, since the higher SWE values in the study area were mostly related to mountainous areas, a poor prediction by the SD algorithm is expected because it was developed based on data from the central plains in the United States [11]. Consequently, the ANN approximator seems to be better than the two regression models in SWE estimation over varied terrain from SSM/I data.

TABLE 4-V
COMPARISON BETWEEN ANN WETNESS APPROXIMATION FROM DATA IN AN SSM/I FOOTPRINT AND FROM TEST DATA SET WITH RESPECT TO CORRELATION BETWEEN ANN-ESTIMATED AND GROUND-BASED VALUES

ANN Topology	Learning Rate	Correlation Coefficient (r)	
		Footprint Data in [10]	Test Data (Table 4-IV)
5-10-2	0.1	0.644	0.128
	0.2	0.668	0.112
	0.3	0.421	0.060
	0.4	0.518	0.073
	0.5	0.803	0.042
5-20-2	0.1	0.650	0.168
	0.2	0.486	0.263
	0.3	0.816	0.212
	0.4	0.565	0.188
	0.5	0.553	0.139
5-30-2	0.1	0.504	0.125
	0.2	0.820	0.198
	0.3	0.493	0.261
	0.4	0.502	0.382
	0.5	0.504	0.164
5-40-2	0.1	0.834	0.185
	0.2	0.491	0.150
	0.3	0.493	0.222
	0.4	0.256	0.205
	0.5	0.499	0.074
5-50-2	0.1	0.738	0.157
	0.2	0.449	0.162
	0.3	0.730	0.257
	0.4	0.723	0.107
	0.5	0.286	0.052

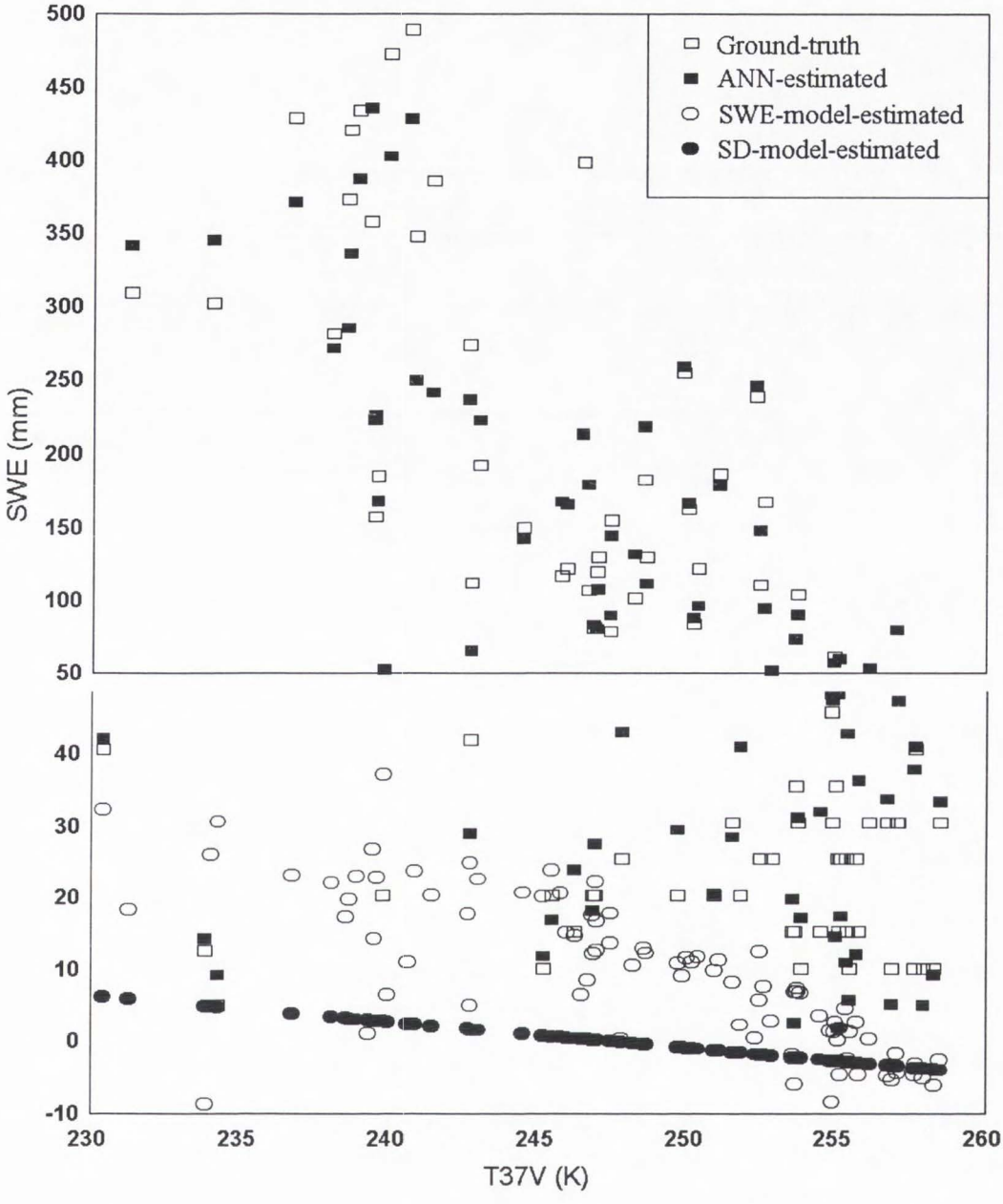

Figure 4.6. Comparison between SWEs estimated by the ANN approximator, the SWE retrieval algorithm (Eq. 1), and the SD retrieval algorithm (Eq. 2) from SSM/I Tb's with respect to ground-based SWEs in sparse-vegetated dry snow condition.

Figure 4.7 shows that the WETNESS estimated by the ANN approximator followed not only the trend of ground-based data but also the prediction line by the WETNESS retrieval algorithm (Eq. 3). Since the ANN was trained by the SSM/I observations from the DMSP-F8 satellite in 1990 and the regression model was derived based on the SSM/I data from the DMSP-F11 satellite in 1993 [10], the agreement (r = 0.816 in Table 4-V) between the ANN-estimated and the model-estimated WETNESS values may suggest that the ANN approach has the potential to find a mapping between SSM/I Tb observations and ground-based snow properties.

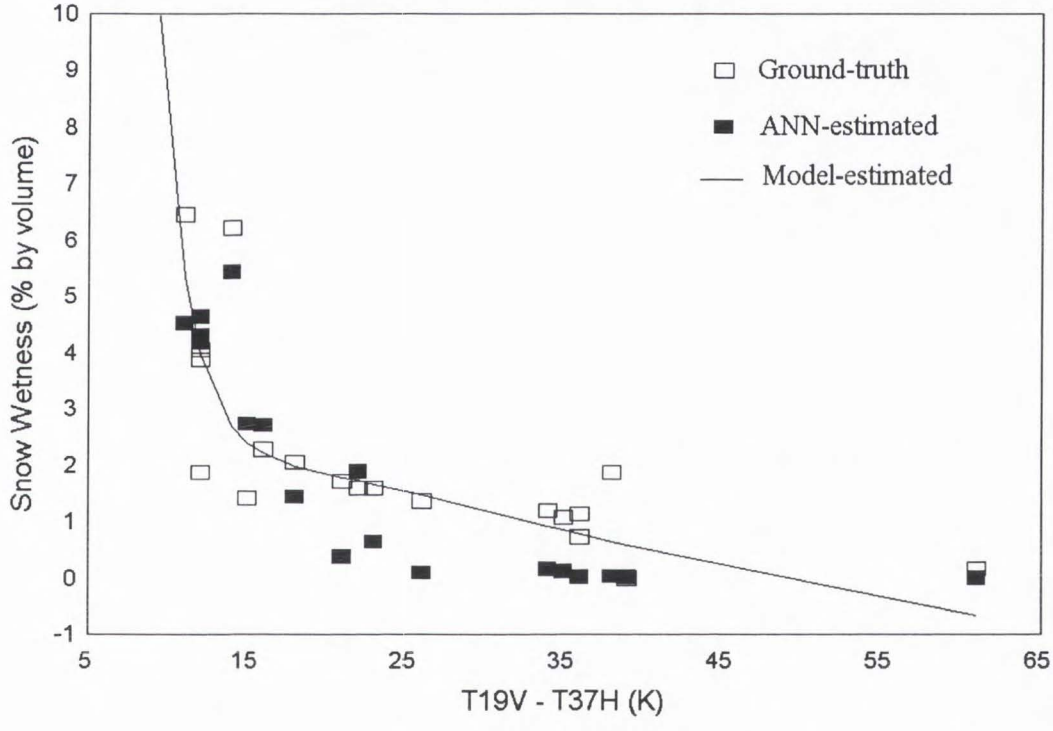

Figure 4.7. Comparison between WETNESS estimated by the ANN approximator and the regression model (Eq. 3) from SSM/I Tb's observed at the Snowville footprint [10] with respect to ground-based data.

E. Conclusions

With the assumption that the SSM/I Tb's and ground-based snow parameters are random variables, this study has successfully demonstrated a backprop ANN approach to find a mapping between inputs of SSM/I data and outputs of SWE and WETNESS data. Results show that an ANN may overcome the limitations of the existing regression models in the estimation of SWE and WETNESS from SSM/I data over varied terrain.

Some of the uncertainties found in the ANN performances could be explained by the same emission behavior of snow cover resulting from different surface conditions and depths. Therefore, the ANN approach might be limited to certain snow depth range.

Although the ANN has the potential to retrieve different snow parameters simultaneously from SSM/I data, the best estimation of each snow parameter was derived from different ANN topologies. Therefore, the development of an individual ANN approximator for each snow parameter estimation seems to be more practical.

This study indicated that the ANN has the ability to learn input/output relations from noisy samples. However, in order to ensure the ANNs have learned from the prototypes, a sufficient number of samples of representative input/output patterns should be available during training. Further improvement is expected as more representative input/output relations between SSM/I observations and ground truth data over varied terrain and different snow conditions are established.

F. References

[1] J. L. Foster, D. K. Hall, A. T. C. Chang, and A. Rango, "An overview of passive microwave snow research and results," *Rev. Geophys. Space Phys.*, vol. 22, no. 2, pp. 195-208, 1984.

[2] F. T. Ulaby, R. K. Moore, and A. K. Fung, *Microwave Remote Sensing: Active and Passive*, Vol. III, *from Theory to Applications*. Norwood, MA: Artech House, 1986.

[3] A. T. C. Chang, J. L. Foster, P. Gloersen, W. J. Campbell, E. G. Josberger, A. Rango, and Z. F. Danes, "Estimating snowpack parameters in the Colorado River basin," in *Large Scale Effects of Seasonal Snow Cover (Proceedings of the Vancouver Symposium, August 1987)*, IAHS publ. no. 166, Wallingford, Oxfordshire, UK: IAHS Press, 1987, pp. 343-352.

[4] A. Rango, "Snow hydrology processes and remote sensing," *Hydrol. Proc.*, vol. 7, no. 2, pp. 121-138, 1993.

[5] R. Ferraro, N. Grody, D. Forsyth, R. Garey, A. Basist, J. Janowiak, F. Weng, G. F. Marks, and R. Yanamandra, "Microwave measurements produce global climatic, hydrologic data," *Eos Trans., AGU*, vol. 75, no. 30, pp. 337-338, 1994.

[6] J. P. Hollinger, "DMSP Special Sensor Microwave/Imager calibration/validation," Naval Research Laboratory, Washington, DC, Final Report, vol. I, 1989.

[7] T. Dunne and L. B. Leopold, *Water in environmental planning*. New York: W. H. Freeman and Company, 1978.

[8] NOAA, *Surface Land Daily Cooperative Summary of the Day TD-3200*. Asheville, NC: NOAA National Environmental Satellite Data and Information Service, 1989.

[9] SCS, *Snow Survey and Water Supply Products Reference*. Portland, OR: USDA SCS West National Technical Center, 1988.

[10] C. Sun, C. M. U. Neale, and J. J. McDonnell, "Relationship between snow wetness and air temperature and its use in the development of an SSM/I snow wetness algorithm," in *Proc. Amer. Geophys. Union 15th Ann. Hydrology Days*, 1995, pp. 271-180.

[11] M. J. McFarland and C. M. U. Neale, "Land parameter algorithms validation and calibration," in "DMSP Special Sensor Microwave/Imager calibration/validation," J. P. Hollinger, Ed. Naval Research Laboratory, Washington, DC, Final Report, vol. II, 1991, pp. 1-108.

[12] B. E. Goodison, A. E. Walker, and F. W. Thirkettle, "Determination of snow water equivalent on the Canadian Prairies using near real-time passive microwave data," in *Proc. Workshop on Application of Remote Sensing in Hydrology*, 1990, pp. 297-316.

[13] D. K. Hall, M. Sturm, C. S. Benson, A. T. C. Chang, J. L. Foster, H. Garbeil, and E. Chacho, "Passive microwave remote and in situ measurements of Arctic and Subarctic snow cover in Alaska," *Remote Sens. Environ.*, vol. 38, no. 3, pp. 161-172, 1991.

[14] A. T. C. Chang and L. Tsang, "A neural network approach to inversion of snow water equivalent from passive microwave measurements," *Nordic Hydrol.*, vol. 23, no. 3, pp. 173-182, 1992.

[15] L. Tsang, Z. Chen, S. Oh, R. H. Marks II, and A. T. C. Chang, "Inversion of snow parameters from passive microwave remote sensing measurements by a neural network trained with a multiple scattering model," *IEEE Trans. Geosci. Remote Sens.*, vol. 30, no. 5, pp. 1015-1024, 1992.

[16] D. T. Davis, Z. Chen, L. Tsang, J. Hwang, and A.T.C. Chang, "Retrieval of snow parameters by iterative inversion of a neural network," *IEEE Trans. Geosci. Remote Sens.*, vol. 31, no. 4, pp. 842-852, 1993.

[17] T. Poggio and F. Girosi, "Networks for approximation and learning," *Proc. IEEE*, vol. 78, no. 9, pp. 1481-1497, 1990.

[18] H. Robbins and S. Monro, "A stochastic approximation method," *Ann. Math. Statist.*, vol. 22, pp. 400-407, 1951.

[19] H. White, "Learning in artificial neural networks: a statistical perspective," *Neural Computation*, vol. 1, no. 4, pp. 425-469, 1989.

[20] C. Sun, C. M. U. Neale, J. J. McDonnell, and H. D. Cheng, "Snow classification from SSM/I data over varied terrain using an artificial neural network classifier," in *Proc. International*

Geoscience and Remote Sensing Symposium, 1996, pp. 133-135.

[21] T. Masters, *Practical Neural Network Recipes in C++*. San Diego, CA: Academic Press, 1993.

[22] C. Sun, C. M. U. Neale, and J. J. McDonnell, "The potential of using artificial neural network in estimation of snow water equivalent from SSM/I data," in *Proc. AGU 16th Annual Hydrology Days*, 1996, pp. 499-509.

[23] J. M. Zurada, *Introduction to Artificial Neural Systems*. St. Paul, MN: West Publishing Co., 1992.

[24] NeuarlWare Technical Publications Group, *Using NWorks: an Extended Tutorial for NeuralWorks Professional II/PLUS and NeuralWorks Explorer*. Pittsburgh, PA: NeuralWare, Inc., 1991.

[25] D. E. Rumelhart, G. E. Hinton, and R. J. Williams, "Learning internal representations by error propagation," in *Parallel Distributed Processing: Explorations in the Microstructure of Cognition*, Vol. 1, *Foundations*, J. A. Feldman, P. J. Hayes, and D. E. Rumelhart, Eds. Cambridge, MA: MIT Press, 1986, pp. 318-362.

[26] A. E. Walker, and B. E. Goodison, "Development and operational application of a Canadian snow water equivalent algorithm using SSM/I data," presented at *1st Shared Processing Network DMSP SSM/I Algorithm Symposium*, Monterey, CA, June 1993.

[27] J. L. Foster, A. Rango, D. K. Hall, A. T. C. Chang, L. J. Allison, and B. C. Diesen, III, "Snowpack monitoring in North America and Eurasia using passive microwave satellite data," *Remote Sens. Environ.*, vol. 10, no. 4, pp. 285-298, 1980.

[28] F. T. Ulaby, R. K. Moore, and A. K. Fung, *Microwave Remote Sensing: Active and Passive*, Vol. II, *Radar Remote Sensing and Surface Scattering and Emission theory*. Norwood, MA: Artech House, 1982.

CHAPTER 5

GENERAL CONCLUSIONS

The overall objective of this study was to improve and further develop SSM/I snow-related algorithms. Improvements were accomplished by: (1) proposing the neighborhood merging method to integrate SSM/I Tb observations and ground-based data with respect to SSM/I ground footprints instead of fixed quarter-degree latitude/longitude cells, (2) conducting field work to establish the relationship between snow wetness and concurrent air temperature to estimate the extensive ground-based snow wetness data needed in the development of SSM/I algorithms, and (3) using cluster analysis to define the typical SSM/I Tb signatures, in terms of cluster means, of six snow classes including both sparse- and medium-vegetated region scenes for each of the dry, wet, and refrozen snow conditions.

Developments were made via: (1) monitoring SSM/I Tb difference (i.e., T19V−T37H) at the sparse-vegetated Snowville, Utah site throughout two snow seasons to develop an empirical SSM/I snow wetness retrieval algorithm based on modeling snow wetness as a function of Tb difference, (2) training an artificial neural network (ANN) with the six defined snow cluster means to develop an SSM/I ANN snow classifier for monitoring land surface snow conditions over varied terrain, and (3) training an ANN with the inputs of SSM/I Tb observations and corresponding outputs of ground-based snow water equivalent (SWE) and snow wetness data to develop an SSM/I ANN snow approximator capable for retrieving both SWE and snow wetness simultaneously from SSM/I data over varied terrain.

Research findings showed that: (1) the empirical SSM/I snow wetness model may overestimate the wetness at footprints where evergreen forests overlie the snowpack, (2) the ANN with best performance only resulted from a number of training runs by trial and error, (3) the ANN

has the potential to find a mapping between SSM/I Tb observations and corresponding snow conditions or parameter estimations, (4) the developed ANN snow classifier might misclassify frozen ground and dense-vegetated surface as wet snow condition due the similar Tb signatures, and (5) although the ANN approximator can retrieve both SWE and snow wetness from SSM/I data, the best estimation of each parameter was derived from different ANN topologies.

It is concluded that: (1) empirical regression models can be developed for a specific region and applied only to those similar geographic areas, (2) the use of ANN approach seems to overcome the drawbacks and limitations of the existing methods for snow classification and estimation from SSM/I data over varied terrain, and (3) the development of an individual ANN approximator for each snow parameter estimation could be more practical than a unified ANN for all parameters.

This study successfully demonstrated a nonlinear snow retrieval approach can make inferences about snow properties from SSM/I data over varied terrain operational. Further improvement of the ANN approach is expected as: (1) more SSM/I Tb signatures of different land surface types are defined and learned by the ANN and (2) more representative input/output relations between SSM/I observations and ground truth data over varied terrain and different snow conditions are established for the ANN training.

APPENDICES

APPENDIX A. C Code for Training an ANN Classifier

```
/*********************************************************************************
* PROGRAM: nnclstrn.c        by  Changyi Sun  email: csun@indigo.ecob.usu.edu *
* ------------------------------------------------------------------------------ *
* COMPILE: cc -O -o nnclstrn nnclstrn.c -lm                                      *
* ------------------------------------------------------------------------------ *
* PURPOSE: To build a multi-hidden-layer backprop ANN classifier.                *
* INPUT  : <nnclstrn.dat>, input/output data pairs of training data set.         *
* OUTPUT : <nnclswts.dat>, updated connection weights of the ANN.                *
*          <nnclstrn.out>, training results of the ANN.                          *
* ------------------------------------------------------------------------------ *
* DATE   : 04-18-1994                        revised and debugged : 06-02-1995 *
* ------------------------------------------------------------------------------ *
* NO COPYRIGHT BUT THE AUTHOR WILL APPRECIATE IF YOU DISTRIBUTE THIS PGOGRAM  *
* IN ITS ORIGINAL CODE.  COMMENTS FOR REVISION AND IMPROVEMENT ARE WELCOME.   *
*********************************************************************************/
# include <math.h>
# include <stdio.h>
# include <stdlib.h>
# include <string.h>
# include <time.h>

/* define the following parameters to your taste -------------------------- */
# define   p  5  /* number of neurons in input layer */
# define   q  6  /* number of neurons in output layer */
# define  h1  10 /* number of neurons in 1st hidden layer */
# define  h2  0  /* number of neurons in 2nd hidden layer */
# define  h3  0  /* number of neurons in 3rd hidden layer */
# define lyr  1  /* number of hidden layer */
# define fnc  2  /* <1>: logistic  <2>: TanH function */
# define lrn  0.05  /* learning rate */
# define mmt  0.9  /* momentum constant */
# define tol  0.100  /* tolerant global RMS error */

/* define the following parameters to fit the requires -------------------- */
# define max  13  /* 3 + the largest number of p, q, h1, h2, h3 */
# define iop  6  /*  total # of input/output pairs in training data */

main()
{  FILE  *fptrn, *fpwts, *fpout;
   int   i, j, k, l, r, s, t, idx, count, num[7], ctrl, flg, fcnt, iocnt, dum;
   float norm, net, Esum, MSE, RMS, Best, tmp;
   float mtrx[iop+1][p+q+2], wt[lyr+2][max][max], adj[lyr+2][max][max];
   float out[lyr+2][max], err[lyr+2][max], dlt[lyr+2][max], df[lyr+2][max];
   char  ans;
   time_t timer; time(&timer); srand(timer);
   num[1] = p; num[2] = h1; num[3] = h2; num[4] = h3; num[5] = q; idx = fnc;
/* Initialize weight matrix in the range of [-0.1, 0.1] ------------------- */
   for(i=1; i<lyr+2; i++)
   {  for(j=1; j<max+1; j++)
      {  for(k=1; k<max+1; k++)
         {  wt[i][j][k] = -0.1 + 0.2*rand()/(RAND_MAX+1.0);
            adj[i][j][k] = 0.0;
         }
      }
   }
/* Read in training data set ---------------------------------------------- */
   fptrn = fopen("nnclstrn.dat","r"); if(fptrn==NULL) exit(0);
   for(i=1; i<iop+1; i++)
   {  for(j=1; j<p+q+2; j++)
      {  if(j==p+1)                                    /* add bias to input */
         {  mtrx[i][j] = 1.0; if(idx==2) mtrx[i][j] = -1.0;
         }
         else fscanf(fptrn,"%f",&mtrx[i][j]);
      }
      if(feof(fptrn)) break;
   }  fclose(fptrn); iocnt = i - 1;  /* the exact input/output pairs read in */
   if(iocnt!=iop)
```

```
   {  printf(" Warning!!!  Data reading is not complete.  Check data size.\n");
      printf(" Contine the training process anyway (y/n)?"); scanf("%s",&ans);
      if(ans!='y' && ans!='Y') exit(0);
   }
/* Normalize input data to the closed interval [0,1] ---------------------- */
   for(i=1; i<iocnt+1; i++)
   {  norm = 0.0;
      for(j=1; j<p+1; j++) norm = norm + mtrx[i][j]*mtrx[i][j];
      for(j=1; j<p+1; j++) mtrx[i][j] = sqrt(mtrx[i][j]*mtrx[i][j]/norm);
   }
/* Scale input data in [0,1] to closed interval [-1,1] --------------------- */
   if(idx==2)
   {  for(i=1; i<iocnt+1; i++)
      {  for(j=1; j<p+1; j++) mtrx[i][j] = 2.0*mtrx[i][j] - 1.0;
      }
   }
/* Scale output data in [0,1] to interval [0.2,0.8] or [-0.8,0.8] ---------- */
   if(idx==1)
   {  for(i=1; i<iocnt+1; i++)
      {  for(j=p+2; j<p+q+2; j++) mtrx[i][j] = 0.6*mtrx[i][j] + 0.2;
      }
   }
   if(idx==2)
   {  for(i=1; i<iocnt+1; i++)
      {  for(j=p+2; j<p+q+2; j++) mtrx[i][j] = 1.6*mtrx[i][j] - 0.8;
      }
   }
/* Feedforward and error calculation at output layer ---------------------- */
   count = 1; fcnt = 0; net = Esum = Best = 0.0;
   while(1)
   {  for(i=1; i<iocnt+1; i++)
      {  for(j=1; j<2; j++)          /* calculate mapping output at 1st hidden */
         {  for(k=1; k<num[j+1]+1; k++)
            {  for(l=1; l<num[j]+2; l++) net = net + mtrx[i][l]*wt[j][l][k];
               if(idx==1)                  /* net squashed by logistic function */
               {  out[j][k] = 1.0/(1.0+exp(-net));
                  df[j][k] = out[j][k]*(1.0-out[j][k]);
               }
               if(idx==2)                  /* net squashed by TanH function */
               {  out[j][k] = (exp(net)-exp(-net))/(exp(net)+exp(-net));
                  df[j][k] = (1+out[j][k])*(1.0-out[j][k]);
               }  net = 0.0;
            }  out[j][k] = 1.0;                          /* add bias to hidden */
            if(idx==2) out[j][k] = -1.0;
         }
         for(j=2; j<lyr+1; j++)  /* calculate mapping output at other hidden */
         {  for(k=1; k<num[j+1]+1; k++)
            {  for(l=1; l<num[j]+2; l++) net = net + out[j-1][l]*wt[j][l][k];
               if(idx==1)                  /* net squashed by logistic function */
               {  out[j][k] = 1.0/(1.0+exp(-net));
                  df[j][k] = out[j][k]*(1.0-out[j][k]);
               }
               if(idx==2)                  /* net squashed by TanH function */
               {  out[j][k] = (exp(net)-exp(-net))/(exp(net)+exp(-net));
                  df[j][k] = (1+out[j][k])*(1.0-out[j][k]);
               }  net = 0.0;
            }  out[j][k] = 1.0;                          /* add bias to hidden */
            if(idx==2) out[j][k] = -1.0;
         }  dum = 3 - j + 1;
         for(j=lyr+1; j<lyr+2; j++)     /* calculate mapping output at output */
         {  for(k=1; k<num[j+dum+1]+1; k++)
            {  for(l=1; l<num[j]+2; l++) net = net + out[j-1][l]*wt[j][l][k];
               if(idx==1)                  /* net squashed by logistic function */
               {  out[j][k] = 1.0/(1.0+exp(-net));
                  df[j][k] = out[j][k]*(1.0-out[j][k]);
               }
               if(idx==2)                  /* net squashed by TanH function */
```

```
                {  out[j][k] = (exp(net)-exp(-net))/(exp(net)+exp(-net));
                   df[j][k] = (1+out[j][k])*(1.0-out[j][k]);
                }
                err[j][k] = mtrx[i][p+k+1] - out[j][k];      /* mapping error */
                dlt[j][k] = err[j][k]*df[j][k];               /* error rates */
                Esum = Esum + pow(err[j][k],2.0)*0.5;         /* total error */
                if(i==iocnt && k==q)
/* ----------- Output the best weights ------------------------------------ */
                {  MSE = Esum/iocnt/q; RMS = sqrt(MSE);
                   if(Best==0.0 || RMS<Best) { Best = RMS; ctrl = 1; flg = 0; }
                   else { ctrl = 0; flg = 1; fcnt = fcnt + 1; }
                   printf(" Epoch=%8d  CurrentRMS=%9.6f",count,RMS);
                   printf(" BestRMS=%9.6f  TargetRMS=%6.3f",Best,tol);
                   printf(" flg=%1d\n",flg);
                   if(RMS<tol || ctrl==1)
                   {  fpwts = fopen("nnclswts.dat","w");
                      for(r=1; r<5+1; r++) fprintf(fpwts,"%5d",num[r]);
                      fprintf(fpwts,"%5d%5d\n",lyr,idx);
                      for(r=1; r<lyr+2; r++)
                      {  for(s=1; s<num[r]+2; s++)
                         {  if((r-lyr)==1)
                            {  for(t=1; t<num[r+dum+1]+1; t++)
                               {  fprintf(fpwts,"%5d%5d%5d",r,s,t);
                                  fprintf(fpwts,"  %10.6f\n",wt[r][s][t]);
                               }
                            }
                            else
                            {  for(t=1; t<num[r+1]+1; t++)
                               {  fprintf(fpwts,"%5d%5d%5d",r,s,t);
                                  fprintf(fpwts,"  %10.6f\n",wt[r][s][t]);
                               }
                            }
                         }
                      }  fclose(fpwts);
                      fpout = fopen("nnclstrn.out","w");
                      fprintf(fpout,"Tplgy=%d-%d-%d Epoch=%8d ",p,h1,q,count);
                      fprintf(fpout,"RMS=%6.3f tol=%6.3f ",Best,tol);
                      fprintf(fpout,"lrn=%6.3f mmt=%6.3f\n",lrn,mmt);
                      fclose(fpout);
                   }
                   if(RMS<tol)
                   {  printf("\n     BKP training is done :)\n"); exit(0);
                   }
                }  net = 0.0;
             }
          }
/* ----- Error bkp and wts adjustment ------------------------------------- */
          for(j=1; j<lyr+2; j++) for(k=1; k<max+1; k++) err[j][k] = 0.0;
          for(j=lyr+1; j>lyr; j--)            /* err bkp from output to hidden */
          {  for(k=1; k<num[j]+2; k++)
             {  for(l=1; l<num[j+dum+1]+1; l++)
                {  tmp = wt[j][k][l];
                   err[j][k] = err[j][k] + dlt[j][l]*wt[j][k][l];
                   wt[j][k][l] = wt[j][k][l]+0.5*lrn*dlt[j][l]*out[j-1][k]
                                 +mmt*adj[j][k][l];
                   adj[j][k][l] = wt[j][k][l] - tmp;
                }  dlt[j-1][k] = df[j-1][k]*err[j][k];
             }
          }
          for(j=3-dum; j>1; j--)                    /* err bkp between hiddens */
          {  for(k=1; k<num[j]+2; k++)
             {  for(l=1; l<num[j+1]+1; l++)
                {  tmp = wt[j][k][l];
                   err[j][k] = err[j][k] + dlt[j][l]*wt[j][k][l];
                   wt[j][k][l] = wt[j][k][l]+lrn*dlt[j][l]*out[j-1][k]
                                 +mmt*adj[j][k][l];
                   adj[j][k][l] = wt[j][k][l] - tmp;
```

```
                }  dlt[j-1][k] = df[j-1][k]*err[j][k];
             }
          }
          for(j=1; j>0; j--)                    /* err bkp from hidden to input */
          {  for(k=1; k<num[j]+2; k++)
             {  for(l=1; l<num[j+1]+1; l++)
                {  tmp = wt[j][k][l];
            wt[j][k][l] = wt[j][k][l]+lrn*dlt[j][l]*mtrx[i][k]+mmt*adj[j][k][l];
                   adj[j][k][l] = wt[j][k][l] - tmp;
                }
             }
          }
       }  Esum = 0.0; count = count + 1;
    }
}
```

APPENDIX B. C Code of the SSM/I ANN Snow Classifier

```
/*****************************************************************************
* PROGRAM: sminncls.c        by  Changyi Sun  email: csun@indigo.ecob.usu.edu *
* ------------------------------------------------------------------------- *
* COMPILE: cc -O -o sminncls sminncls.c -lm                                  *
* ------------------------------------------------------------------------- *
* PURPOSE: To use the ANN classifier for snow classificaion on SSM/I data.   *
* INPUT  : <filename.din>, lat/lon and ssmi 7 Tb's data.                     *
*          <sminnwts.dat>, connection weights used in the ANN classifier.   *
* OUTPUT : <filename.llc>, lat/lon coordinates and the classes by ANN.       *
* NOTE   : the pre-process of snow-free condition is based on Neale's rules. *
* ------------------------------------------------------------------------- *
* date   : 08-08-1995                                                        *
* ------------------------------------------------------------------------- *
* NO COPYRIGHT BUT THE AUTHOR WILL APPRECIATE IF YOU DISTRIBUTE THIS PGOGRAM  *
* IN ITS ORIGINAL CODE.  COMMENTS FOR REVISION AND IMPROVEMENT ARE WELCOME.  *
*****************************************************************************/
# include <math.h>
# include <stdio.h>
# include <stdlib.h>
# include <string.h>
int  num[6];
char line[79], filename[20], outfile[20];
void nncls(int p, int q, int lyr, int max, int idx);
main()
{  FILE *fpin;
   int  i, p, h1, h2, h3, q, lyr, max, ele, idx;
   ele = 0;
   if((fpin=fopen("sminnwts.dat","r")) == NULL)
   {  printf("\nFile < sminnwts.dat > is not ready for read.\n\n"); exit(0);
   }  fscanf(fpin,"%d%d%d%d%d%d%d",&p,&h1,&h2,&h3,&q,&lyr,&idx); fclose(fpin);
   num[1] = p; num[2] = h1; num[3] = h2; num[4] = h3; num[5] = q;
   max = p; for(i=2; i<6; i++) if(max<num[i]) max = num[i]; max = max + 3;
   printf("\nEnter the *.din filename to be processed.\n\n");
   scanf("%s",filename);
   if((fpin=fopen(filename,"r")) == NULL)
   {  printf("\nFile < %s > is not ready for read.\n\n",filename); exit(0);
   }  fclose(fpin);
   for(i=0;i<=20;i++) if(strncmp(filename+i,".",1)==0) break;
   strncpy(outfile,filename,i); strncpy(outfile+i,".llc\0",5);
   nncls(p,q,lyr,max,idx);
}
void nncls(int p, int q, int lyr, int max, int idx)
{  FILE  *fpwts, *fpdin, *fpout;
   int   i, j, k, l, r, s, t, bkpcls, dum;
   float lat, lon, t85v, t85h, t37v, t37h, t22v, t19v, t19h, gvi, pd;
   float Norm, net, tmp, *vctr, ***wt, **out;
   vctr = (float *)malloc((p+q+2)*sizeof(float));
   wt = (float ***)malloc((lyr+2)*sizeof(float));
     for(i=0;i<max+1;i++) wt[i]=(float **)malloc((max+1)*sizeof(float));
     for(i=0;i<max+1;i++)
       for(j=0;j<max+1;j++) wt[i][j]=(float *)malloc((max+1)*sizeof(float));
   out = (float **)malloc((lyr+2)*sizeof(float));
     for(i=0;i<max+1;i++) out[i]=(float *)malloc((max+1)*sizeof(float));
/* Initialize weight matrix ------------------------------------------------ */
   for(i=1; i<lyr+2; i++)
   {  for(j=1; j<max+1; j++)
      {  for(k=1; k<max+1; k++) wt[i][j][k] = 0.0;
      }
   }
/* Read in weights data ---------------------------------------------------- */
   fpwts = fopen("sminnwts.dat","r"); fgets(line,79,fpwts);
   while(!feof(fpwts))
   {  fscanf(fpwts,"%d%d%d%f",&i,&j,&k,&tmp);
      wt[i][j][k] = tmp;
   }  fclose(fpwts);
/* Read in data & classify the data ---------------------------------------- */
   fpdin = fopen(filename,"r"); fpout = fopen(outfile,"w");
```

```
   while(!feof(fpdin))
   {  fscanf(fpdin,"%f%f%f%f%f%f",&lat,&lon,&t19v,&t19h,&t22v,&t37v);
      fscanf(fpdin,"%f%f%f",&t37h,&t85v,&t85h); if(feof(fpdin)) break;
      vctr[1]=t37v; vctr[2]=t37h; vctr[3]=t22v; vctr[4]=t19v; vctr[5]=t19h;
      pd = (t37v+t19v)/2.0 - (t37h+t19h)/2.0;
      if((t22v-t19v)>4.0||(t19v-t19h)>40.0)
      {  bkpcls = 7;                        /* water body or flooding condition */
         fprintf(fpout,"%6.2f%8.2f%4d\n",lat,lon,bkpcls);
      }
      else if(t19v>268.0&&(t37v-t19v)<-6.4)
      {  bkpcls = 8;                                /* precipitation condition */
         fprintf(fpout,"%6.2f%8.2f%4d\n",lat,lon,bkpcls);
      }
      else if(t19v<t37v||t22v>265.0)
      {  bkpcls = 9;                          /* snow-free condition or rain */
         fprintf(fpout,"%6.2f%8.2f%4d\n",lat,lon,bkpcls);
      }
      else
      {  vctr[p+1] = 1.0; if(idx==2) vctr[p+1] = -1.0;  /* add bias to input */
/* Normalize input data to the closed interval [0,1] ----------------------- */
         Norm = 0.0;
         for(i=1; i<p+1; i++) Norm = Norm + vctr[i]*vctr[i];
         for(i=1; i<p+1; i++) vctr[i] = vctr[i]/sqrt(Norm);
/* Scale input data in [0,1] to closed interval [-1,1] --------------------- */
         if(idx==2) for(i=1; i<p+1; i++) vctr[i] = 2.0*vctr[i] - 1.0;
/* Recall the outputs ------------------------------------------------------ */
         for(i=1; i<2; i++)              /* calculate mapping output at hidden */
         {  for(j=1; j<num[i+1]+1; j++)
            {  for(k=1; k<num[i]+2; k++) net = net + vctr[k]*wt[i][k][j];
               if(idx==1) out[i][j]=1.0/(1.0+exp(-net));
               if(idx==2) out[i][j]=(exp(net)-exp(-net))/(exp(net)+exp(-net));
               net = 0.0;
            }  out[i][j] = 1.0;                          /* add bias to hidden */
            if(idx==2) out[i][j] = -1.0;
         }
         for(i=2; i<lyr+1; i++)  /* calculate mapping output at other hidden */
         {  for(j=1; j<num[i+1]+1; j++)
            {  for(k=1; k<num[i]+2; k++) net = net + vctr[k]*wt[i][k][j];
               if(idx==1) out[i][j]=1.0/(1.0+exp(-net));
               if(idx==2) out[i][j]=(exp(net)-exp(-net))/(exp(net)+exp(-net));
               net = 0.0;
            }  out[i][j] = 1.0;                          /* add bias to hidden */
            if(idx==2) out[i][j] = -1.0;
         }  dum = 3 - i + 1;
         for(i=lyr+1; i<lyr+2; i++)     /* calculate mapping output at output */
         {  for(j=1; j<num[i+dum+1]+1; j++)
            {  for(k=1; k<num[i]+2; k++) net = net + out[i-1][k]*wt[i][k][j];
               if(idx==1) out[i][j]=1.0/(1.0+exp(-net));
               if(idx==2) out[i][j]=(exp(net)-exp(-net))/(exp(net)+exp(-net));
               net = 0.0;
            }
         }  tmp = 0.0; if(idx==2) tmp = -1.0;
         for(i=lyr+1; i<lyr+2; i++)
         {  for(j=1; j<q+1; j++)
            {  if(out[i][j]>tmp)
               {  bkpcls = j; tmp = out[i][j];
               }
            }
         }  if(tmp<0.0) bkpcls = 9; if(idx==1&&tmp<0.5) bkpcls = 9;
         if(bkpcls==3&&((t19v-t37h)<10.0||(t19v-t37h)>13.0)) bkpcls = 9;
         if(bkpcls==4&&((t19v-t37h)<9.0||(t19v-t37h)>12.0)) bkpcls = 9;
         fprintf(fpout,"%6.2f%8.2f%4d\n",lat,lon,bkpcls);
      }
   }  fclose(fpdin); fclose(fpout); printf("\n%s file is created.\n",outfile);
}
```

APPENDIX C. Connection Weights Used in the ANN Classifier

```
5   10    0    0    6    1    2
1    1    1     0.533392
1    1    2    -1.691874
1    1    3    -0.123502
1    1    4     4.715361
1    1    5    -5.498882
1    1    6    -2.275994
1    1    7    -0.381456
1    1    8   -22.467062
1    1    9     1.145030
1    1   10    28.343935
1    2    1    -5.882782
1    2    2     4.098454
1    2    3     2.818522
1    2    4     1.785758
1    2    5    -0.369015
1    2    6   -13.381873
1    2    7     1.227129
1    2    8     5.056935
1    2    9     0.635918
1    2   10    27.552616
1    3    1     4.228578
1    3    2    -4.507759
1    3    3     4.047563
1    3    4    -0.656226
1    3    5     0.482231
1    3    6    10.579752
1    3    7    -1.699688
1    3    8    -4.887167
1    3    9    -0.430137
1    3   10   -13.051486
1    4    1     4.068871
1    4    2    -1.943128
1    4    3    -1.905251
1    4    4     0.367727
1    4    5     2.281353
1    4    6    48.854050
1    4    7     1.048660
1    4    8    -2.981371
1    4    9     0.111341
1    4   10   -19.931734
1    5    1    -1.632250
1    5    2     5.249955
1    5    3    14.633612
1    5    4     1.481441
1    5    5     1.472808
1    5    6   -15.582770
1    5    7     0.079386
1    5    8    25.985779
1    5    9    -0.471199
1    5   10   -26.378248
1    6    1     0.062529
1    6    2    -0.309254
1    6    3    -0.854062
1    6    4     1.153583
1    6    5     0.420109
1    6    6     0.078662
1    6    7    -0.051283
1    6    8    -0.507071
1    6    9     1.931241
1    6   10    -0.925133
2    1    1     0.370048
2    1    2    -0.026684
2    1    3     0.073312
2    1    4    -0.584975
2    1    5     1.047015
2    1    6    -0.816871
```

```
2     2     1    -0.516609
2     2     2     0.090769
2     2     3    -0.254353
2     2     4     0.571239
2     2     5    -0.433611
2     2     6     0.641372
2     3     1    -2.402897
2     3     2     3.170993
2     3     3    -0.380947
2     3     4     3.176313
2     3     5     0.841334
2     3     6     2.111204
2     4     1     0.088350
2     4     2     1.505019
2     4     3     1.315729
2     4     4     3.163557
2     4     5    -0.704886
2     4     6     4.150781
2     5     1    -0.353697
2     5     2    -0.016950
2     5     3    -0.191638
2     5     4    -0.063515
2     5     5     0.712272
2     5     6    -0.358231
2     6     1     0.659895
2     6     2    -6.468255
2     6     3     1.466521
2     6     4   -13.023128
2     6     5     1.550192
2     6     6    -1.758168
2     7     1    -0.058418
2     7     2     0.005207
2     7     3    -0.019963
2     7     4     0.078694
2     7     5    -0.080512
2     7     6     0.083504
2     8     1    -3.584871
2     8     2     0.526618
2     8     3    -1.328818
2     8     4     1.238860
2     8     5     0.017738
2     8     6     1.659197
2     9     1     2.957447
2     9     2     0.227078
2     9     3    -1.372164
2     9     4     2.131042
2     9     5     0.519247
2     9     6     2.992964
2    10     1    -2.464011
2    10     2    -3.541936
2    10     3     1.972966
2    10     4     1.176235
2    10     5     1.098366
2    10     6   -11.218157
2    11     1     0.435696
2    11     2     1.175610
2    11     3     0.738388
2    11     4     3.983303
2    11     5    -0.031991
2    11     6     2.143615
```

NOTE: This is the printout of the "sminnwts.dat" data file used in the ANN classifier (sminncls.c).

APPENDIX D. C Code for Training an ANN Approximator

```
/*****************************************************************************
* PROGRAM: nnapxtrn.c        by  Changyi Sun  email: csun@indigo.ecob.usu.edu *
* ------------------------------------------------------------------------- *
* COMPILE: cc -O -o nnapxtrn nnapxtrn.c -lm                                  *
* ------------------------------------------------------------------------- *
* PURPOSE: To build a multi-hidden-layer BKP ANN approximator.               *
* INPUT  : <nnapxtrn.dat>, input/output data pairs of training data set.     *
* OUTPUT : <nnapxwts.dat>, updated connection weights of the ANN.            *
*          <nnapxtrn.out>, training results of the ANN.                      *
* ------------------------------------------------------------------------- *
* DATE   : 09-05-1995                        revised and debugged : 12-14-1995 *
* ------------------------------------------------------------------------- *
* NO COPYRIGHT BUT THE AUTHOR WILL APPRECIATE IF YOU DISTRIBUTE THIS PGOGRAM  *
* IN ITS ORIGINAL CODE.  COMMENTS FOR REVISION AND IMPROVEMENT ARE WELCOME.   *
*****************************************************************************/
# include <math.h>
# include <stdio.h>
# include <stdlib.h>
# include <string.h>
# include <time.h>

/* define the ANN topology and learning factors to your taste -------------- */
# define   p  5  /* number of neurons in input layer */
# define   q  2  /* number of neurons in output layer */
# define  h1  30  /* number of neurons in 1st hidden layer */
# define  h2  0  /* number of neurons in 2nd hidden layer */
# define  h3  0  /* number of neurons in 3rd hidden layer */
# define lyr  1  /* number of hidden layer */
# define fnc  1  /* <1>: logistic  <2>: TanH function */
# define lrn  0.4  /* learning rate */
# define mmt  0.9  /* momentum constant */
# define tol  0.15  /* tolerant global RMS error */

/* define the following parameters to fit the requires ---------------------- */
# define max  33  /* 3 + the largest number of p, q, h1, h2, h3 */
# define iop  540  /*  total # of input/output pairs in training data */

/* define the ranges of [a,b] for each input parameters --------------------- */
# define tba  180.0 /* min. for all Tb's */
# define tbb  280.0 /* max. for all Tb's */

main()
{  FILE  *fptrn, *fpvld, *fpwts, *fpout;
   int   i, j, k, l, r, s, t, idx, count, num[7], ctrl, flg, iocnt, dum, cls;
   float norm, net, Esum, MSE, RMS, Best, tmp, rng[q+1][3];
   float mtrx[iop+1][p+q+2], wt[lyr+2][max][max], adj[lyr+2][max][max];
   float out[lyr+2][max], err[lyr+2][max], dlt[lyr+2][max], df[lyr+2][max];
   char  ans;
   time_t timer; time(&timer); srand(timer);
   num[1] = p; num[2] = h1; num[3] = h2; num[4] = h3; num[5] = q; idx = fnc;
   for(i=1; i<q+1; i++) for(j=1; j<3; j++) rng[i][j] = 0.0;
   rng[1][1] = 0.0; rng[1][2] = 800.0;                  /* min and max of swe */
   rng[2][1] = 0.0; rng[2][2] = 10.0;                /* min and max of wetness */
/* Initialize weight matrix in the range of [-0.1, 0.1] --------------------- */
   for(i=1; i<lyr+2; i++)
   {  for(j=1; j<max+1; j++)
      {  for(k=1; k<max+1; k++)
         {  wt[i][j][k] = -0.01 + 0.02*rand()/(RAND_MAX+1.0);
            adj[i][j][k] = 0.0;
         }
      }
   }
/* Read in training data set ------------------------------------------------ */
   fptrn = fopen("nnapxtrn.dat","r"); if(fptrn==NULL) exit(0);
   for(i=1; i<iop+1; i++)
   {  for(j=1; j<p+q+2; j++)
      {  if(j==p+1)                                     /* add bias to input */
```

```
         {  mtrx[i][j] = 1.0; if(idx==2) mtrx[i][j] = -1.0;
         }
         else fscanf(fptrn,"%f",&mtrx[i][j]);
         if(j>p+1)
         {  if(rng[j-p-1][1]>mtrx[i][j]) rng[j-p-1][1] = mtrx[i][j];
            if(rng[j-p-1][2]<mtrx[i][j]) rng[j-p-1][2] = mtrx[i][j];
         }
      }  fscanf(fptrn,"%d",&cls);
      if(feof(fptrn)) break;
   }  fclose(fptrn); iocnt = i - 1;  /* the exact input/output pairs read in */
   if(iocnt!=iop)
   {  printf(" Warning!!!  Data reading is not complete.  Check data size.\n");
      printf(" Contine the training process anyway (y/n)?"); scanf("%s",&ans);
      if(ans!='y' && ans!='Y') exit(0);
   }
/* Scale input data to the closed interval of [0,1] ----------------------- */
   for(i=1; i<iocnt+1; i++)
   {  for(j=1; j<p+1; j++) mtrx[i][j] = (mtrx[i][j]-tba)/(tbb-tba);
   }
/* Scale input data in [0,1] to closed interval of [-1,1] ----------------- */
   if(idx==2)
   {  for(i=1; i<iocnt+1; i++)
      {  for(j=1; j<p+1; j++) mtrx[i][j] = 2.0*mtrx[i][j] - 1.0;
      }
   }
/* Scale output data to the closed interval of [0,1] ---------------------- */
   for(i=1; i<iocnt+1; i++)
   {  for(j=p+2; j<p+q+2; j++)
         mtrx[i][j]=(mtrx[i][j]-rng[j-p-1][1])/(rng[j-p-1][2]-rng[j-p-1][1]);
   }
/* Scale output data in [0,1] to interval of [-1.0,1.0] ------------------- */
   if(idx==2)
   {  for(i=1; i<iocnt+1; i++)
      {  for(j=p+2; j<p+q+2; j++) mtrx[i][j] = 2.0*mtrx[i][j] - 1.0;
      }
   }
/* Feedforward and error calculation at output layer ---------------------- */
   count = 1; net = Esum = Best = 0.0;
   while(1)
   {  for(i=1; i<iocnt+1; i++)
      {  for(j=1; j<2; j++)        /* calculate mapping output at 1st hidden */
         {  for(k=1; k<num[j+1]+1; k++)
            {  for(l=1; l<num[j]+2; l++) net = net + mtrx[i][l]*wt[j][l][k];
               if(idx==1)                /* net squashed by logistic function */
               {  out[j][k] = 1.0/(1.0+exp(-net));
                  df[j][k] = out[j][k]*(1.0-out[j][k]);
               }
               if(idx==2)                    /* net squashed by TanH function */
               {  out[j][k] = (exp(net)-exp(-net))/(exp(net)+exp(-net));
                  df[j][k] = (1+out[j][k])*(1.0-out[j][k]);
               }  net = 0.0;
            }  out[j][k] = 1.0;                          /* add bias to hidden */
            if(idx==2) out[j][k] = -1.0;
         }
         for(j=2; j<lyr+1; j++)  /* calculate mapping output at other hidden */
         {  for(k=1; k<num[j+1]+1; k++)
            {  for(l=1; l<num[j]+2; l++) net = net + out[j-1][l]*wt[j][l][k];
               if(idx==1)                /* net squashed by logistic function */
               {  out[j][k] = 1.0/(1.0+exp(-net));
                  df[j][k] = out[j][k]*(1.0-out[j][k]);
               }
               if(idx==2)                    /* net squashed by TanH function */
               {  out[j][k] = (exp(net)-exp(-net))/(exp(net)+exp(-net));
                  df[j][k] = (1+out[j][k])*(1.0-out[j][k]);
               }  net = 0.0;
            }  out[j][k] = 1.0;                          /* add bias to hidden */
            if(idx==2) out[j][k] = -1.0;
```

```
         }  dum = 3 - j + 1;
         for(j=lyr+1; j<lyr+2; j++)    /* calculate mapping output at output */
         {  for(k=1; k<num[j+dum+1]+1; k++)
            {  for(l=1; l<num[j]+2; l++) net = net + out[j-1][l]*wt[j][l][k];
               if(idx==1)                /* net squashed by logistic function */
               {  out[j][k] = 1.0/(1.0+exp(-net));
                  df[j][k] = out[j][k]*(1.0-out[j][k]);
               }
               if(idx==2)                    /* net squashed by TanH function */
               {  out[j][k] = (exp(net)-exp(-net))/(exp(net)+exp(-net));
                  df[j][k] = (1+out[j][k])*(1.0-out[j][k]);
               }
               err[j][k] = mtrx[i][p+k+1] - out[j][k];      /* mapping error */
               dlt[j][k] = err[j][k]*df[j][k];               /* error rates */
               Esum = Esum + pow(err[j][k],2.0);             /* total error */
               if(i==iocnt && k==q)
/* ----------- Output the best weights ------------------------------------ */
               {  MSE = Esum/iocnt/q; RMS = sqrt(MSE);
                  if(Best==0.0 || RMS<Best) { Best = RMS; ctrl = 1; flg = 0; }
                  else { ctrl = 0; flg = 1; }
                  printf(" Epoch=%8d  CurrentRMS=%9.6f",count,RMS);
                  printf(" BestRMS=%9.6f  TargetRMS=%6.3f",Best,tol);
                  printf(" flg=%1d\n",flg);
                  if(RMS<tol || ctrl==1)
                  {  fpwts = fopen("nnapxwts.dat","w");
                     for(r=1; r<5+1; r++) fprintf(fpwts,"%5d",num[r]);
                     fprintf(fpwts,"%5d%5d\n",lyr,idx);
                     for(r=1; r<lyr+2; r++)
                     {  for(s=1; s<num[r]+2; s++)
                        {  if((r-lyr)==1)
                           {  for(t=1; t<num[r+dum+1]+1; t++)
                              {  fprintf(fpwts,"%5d%5d%5d",r,s,t);
                                 fprintf(fpwts,"  %10.6f\n",wt[r][s][t]);
                              }
                           }
                           else
                           {  for(t=1; t<num[r+1]+1; t++)
                              {  fprintf(fpwts,"%5d%5d%5d",r,s,t);
                                 fprintf(fpwts,"  %10.6f\n",wt[r][s][t]);
                              }
                           }
                        }
                     }  fclose(fpwts);
                     fpout = fopen("nnapxtrn.out","w");
                     fprintf(fpout,"Tplgy=%d-%d-%d Epoch=%8d ",p,h1,q,count);
                     fprintf(fpout,"RMS=%6.3f tol=%6.3f ",Best,tol);
                     fprintf(fpout,"lrn=%9.5f mmt=%6.3f\n",lrn,mmt);
                     fclose(fpout);
                  }
                  if(RMS<tol)
                  {  printf("\n     BKP training is done :)\n"); exit(0);
                  }
               }  net = 0.0;
            }
         }
/* ----- Error bkp and wts adjustment ------------------------------------- */
         for(j=1; j<lyr+2; j++) for(k=1; k<max+1; k++) err[j][k] = 0.0;
         for(j=lyr+1; j>lyr; j--)           /* err bkp from output to hidden */
         {  for(k=1; k<num[j]+2; k++)
            {  for(l=1; l<num[j+dum+1]+1; l++)
               {  tmp = wt[j][k][l];
                  err[j][k] = err[j][k] + dlt[j][l]*wt[j][k][l];
      wt[j][k][l] = wt[j][k][l]+0.5*lrn*dlt[j][l]*out[j-1][k]+mmt*adj[j][k][l];
                  adj[j][k][l] = wt[j][k][l] - tmp;
               }  dlt[j-1][k] = df[j-1][k]*err[j][k];
            }
         }
```

```
            for(j=3-dum; j>1; j--)                    /* err bkp between hiddens */
            {  for(k=1; k<num[j]+2; k++)
               {  for(l=1; l<num[j+1]+1; l++)
                  {  tmp = wt[j][k][l];
                     err[j][k] = err[j][k] + dlt[j][l]*wt[j][k][l];
             wt[j][k][l] = wt[j][k][l]+lrn*dlt[j][l]*out[j-1][k]+mmt*adj[j][k][l];
                     adj[j][k][l] = wt[j][k][l] - tmp;
                  }  dlt[j-1][k] = df[j-1][k]*err[j][k];
               }
            }
            for(j=1; j>0; j--)                    /* err bkp from hidden to input */
            {  for(k=1; k<num[j]+2; k++)
               {  for(l=1; l<num[j+1]+1; l++)
                  {  tmp = wt[j][k][l];
              wt[j][k][l] = wt[j][k][l]+lrn*dlt[j][l]*mtrx[i][k]+mmt*adj[j][k][l];
                     adj[j][k][l] = wt[j][k][l] - tmp;
                  }
               }
            }
         }  Esum = 0.0; count = count + 1;
      }
   }
```

CURRICULUM VITAE

Changyi Sun
(August 1996)

OBJECTIVE:

A research position in global moisture studies from satellite and airborne remote sensing.

EDUCATION:

Utah State University, Logan, Utah, USA.
Ph.D. in Watershed Science, 1996.
Best Student Ph.D. Poster Presentation at the AGU 16th Annual Hydrology Days, 1996

Utah State University, Logan, Utah, USA.
M.S. in Watershed Science, December 1992.

Colorado State University, Fort Collins, Colorado, USA.
B.S. in Watershed Science, May 1988.
Delano F. Scott Scholarship for 1987-1988.

EXPERIENCE:

RESEARCH ASSISTANT, Biological & Irrigation Engineering, Utah State University, Logan, Utah, USA, (9/91 - present).

Developed and improved the SSM/I snow retrieval algorithms by proposing a new data merging method to improve the accuracy in integration of SSM/I and ground-truth data, conducting a field experiment to develop a relationship between snow wetness and air temperature and base on that relationship to develop an SSM/I snow wetness retrieval algorithm, and designing artificial neural networks to classify land surface snow conditions and estimate snow parameters over varied terrain. Designed a dynamic database using running average of SSM/I observations to implement land surface soil moisture retrieval.

RESEARCH ASSISTANT, Range Science, Utah State University, Logan, Utah, USA, (09/88 - 03/91).

Examined the physical and chemical properties of soil surface crust layers in semiarid region. Designed and built an instrument for laboratory measurement of soil saturated hydraulic conductivity.

TECHNICIAN, Taipei Water Resources Management Bureau, Taipei, Taiwan, ROC, (7/84 - 10/85).

Collected field water samples and performed chemical analysis of water to monitor water quality. Designed and conducted a questionnaire survey to evaluate the possibility and cost of removing the piggery pollution sources.

PUBLICATIONS

1 C. Sun, "Vesicular porosity development related to saturated hydraulic conductivity and sodic soil conditions in some semiarid soils," M.S. Thesis, Utah State University, Logan, UT, 1992.

2 C. Sun, H. D. Cheng, J. J. McDonnell, and C. M. U. Neale, "Identification of mountain snow cover using SSM/I and artificial neural network," in *Proc. 1995 International Conference on Acoustics, Speech and Signal Processing,* 1995, pp. 3451-3454.

3 C. Sun and H. D. Cheng, "The use of class means in error backpropagation training for species identification of iris data," in *Proc. 2nd Annual Joint Conference on Information Sciences*, 1995, pp. 556-559.

4 C. Sun, H. D. Cheng, C. M. U. Neale, and J. J. McDonnell, "SSM/I land surface snow classification using a neural network," in *Proc. IASTED International Conference on Signal and Image Processing-SIP-95*, 1995, pp. 155-158.

5 C. Sun, C. M. U. Neale, and J. J. McDonnell, "Relationship between snow wetness and air temperature and its use in the development of an SSM/I snow wetness algorithm," in *Proc. AGU 15th Annual Hydrology Days,* 1995, pp. 271-280.

6 C. M. U. Neale, X. Qiu, C. Sun, K. P. Gallo, R. M. Rabin, and G. R. Diak, "Monitoring surface moisture and flooding in the central plains with the Special Sensor Microwave/Imager (SSM/I)," in *2nd International Scientific Conference on the Global Energy and Water Cycle*, Preprint Volume, 1996, pp. 217-218.

7 C. Sun, C. M. U. Neale, and J. J. McDonnell, "The potential of using artificial neural network in estimation of snow water equivalent from SSM/I data," in *Proc. AGU 16th Annual Hydrology Days*, 1996, pp. 499-509.

8 C. Sun, C. M. U. Neale, and J. J. McDonnell, "Snow wetness estimation from SSM/I data over varied terrain using an artificial neural network," in *Proc. Eastern Snow Conference*, 1996, in press.

9 C. Sun, C. M. U. Neale, J. J. McDonnell, and H. D. Cheng, "Snow classification from SSM/I data over varied terrain using an artificial neural network classifier," in *Proc. International Geoscience and Remote Sensing Symposium (IGARSS'96)*, 1996, pp. 133-135.